Barrel Vibrations in Small Arms using Combined Experimental/Computational Methods

A thesis

submitted in partial fulfilment

of the requirements for the Degree

of

Doctor of Philosophy in Mechanical Engineering

at

The University of Canterbury

by

David Leonhardt

2021

Abstract

Small arms are used on a global scale by militaries, hunters, competitive shooters, recreational shooters, and others. Despite this widespread use, the design and development of these tools depends heavily on prototyping and iterative testing. Additionally, the open literature concerning small arms is limited, especially in regard to those types of firearms in common use by civilians. The goal of this research was to develop a high fidelity finite element model that would enable a detailed look into the factors governing the vibration of rifle barrels. Such a model can serve as a valuable research and development tool, reducing the high cost of prototyping. This thesis first addresses the degree of detail required in such a model to adequately capture the behavior of a sporting firearm. Experimental testing was performed in order to validate the model and lend additional insight into the factors at play. The validated model is then used to examine the influenced of curved barrel centerlines on projectile trajectories. Finally, the validity of a method of predicting shot dispersion from a single simulation is investigated.

UNIVERSITY OF CANTERBURY
Te Whare Wānanga o Waitaha
CHRISTCHURCH NEW ZEALAND

Deputy Vice-Chancellor's Office
Postgraduate Research Office

Co-Authorship Form

This form is to accompany the submission of any thesis that contains research reported in co-authored work that has been published, accepted for publication, or submitted for publication. A copy of this form should be included for each co-authored work that is included in the thesis. Completed forms should be included at the front (after the thesis abstract) of each copy of the thesis submitted for examination and library deposit.

Please indicate the chapter/section/pages of this thesis that are extracted from co-authored work and provide details of the publication or submission from the extract comes:

Parts of this work are included in Chapters 2, 4, and 5.

Leonhardt, D., and Garnich, M., 2019. "A Finite Element Model to Predict the Influence of Asymmetries on Barrel Dynamics in Small Arms". 31st International Symposium on Ballistics, 1015-1026.

Please detail the nature and extent (%) of contribution by the candidate:

Modeling work described and all writing was done by the candidate. Co-author offered directional guidance and manuscript editing. Candidate contribution estimated at 90%.

Certification by Co-authors:

If there is more than one co-author then a single co-author can sign on behalf of all

The undersigned certifies that:

- The above statement correctly reflects the nature and extent of the Doctoral candidate's contribution to this co-authored work
- In cases where the candidate was the lead author of the co-authored work he or she wrote the text

Name: *Mark Garnich* Signature:  Date: *24/06/2021*

UNIVERSITY OF CANTERBURY
Te Whare Wānanga o Waitaha
CHRISTCHURCH NEW ZEALAND

Deputy Vice-Chancellor's Office
Postgraduate Research Office

Co-Authorship Form

This form is to accompany the submission of any thesis that contains research reported in co-authored work that has been published, accepted for publication, or submitted for publication. A copy of this form should be included for each co-authored work that is included in the thesis. Completed forms should be included at the front (after the thesis abstract) of each copy of the thesis submitted for examination and library deposit.

Please indicate the chapter/section/pages of this thesis that are extracted from co-authored work and provide details of the publication or submission from the extract comes:

Parts of this work are included in Chapters 2-5.

Leonhardt, D., and Garnich, M., Combined Experimental/Finite Element Investigation of Transverse Barrel Movement, Submitted to Journal of Pressure Vessel Technology – in review, 2021

Please detail the nature and extent (%) of contribution by the candidate:

Modelling work described and all writing done by the candidate. Experimental testing performed in conjunction with co-author. Co-author also offered directional guidance and manuscript editing. Candidate contribution estimated at 85%.

Certification by Co-authors:

If there is more than one co-author then a single co-author can sign on behalf of all

The undersigned certifies that:

- The above statement correctly reflects the nature and extent of the Doctoral candidate's contribution to this co-authored work
- In cases where the candidate was the lead author of the co-authored work he or she wrote the text

Name: *Mark Garnich* Signature:  Date: *24/06/2021*

UNIVERSITY OF CANTERBURY
Te Whare Wānanga o Waitaha
CHRISTCHURCH NEW ZEALAND

Deputy Vice-Chancellor's Office
Postgraduate Research Office

Co-Authorship Form

This form is to accompany the submission of any thesis that contains research reported in co-authored work that has been published, accepted for publication, or submitted for publication. A copy of this form should be included for each co-authored work that is included in the thesis. Completed forms should be included at the front (after the thesis abstract) of each copy of the thesis submitted for examination and library deposit.

Please indicate the chapter/section/pages of this thesis that are extracted from co-authored work and provide details of the publication or submission from the extract comes:

Parts of this work are included in Chapters 2-5.

Leonhardt, D., Lucic, M., and Garnich, M., Analysis of the Effect of Bore Centerline on Projectile Exit Conditions in Small Arms, Submitted to Defence Technology – in review, 2021

Please detail the nature and extent (%) of contribution by the candidate:

Modeling work described and all writing done by the candidate. Centerline measurements conducted by Lucic. Garnich facilitated centerline measurements, offered directional guidance, and edited the manuscript. Candidate contribution estimated at 75%.

Certification by Co-authors:

If there is more than one co-author then a single co-author can sign on behalf of all

The undersigned certifies that:

- The above statement correctly reflects the nature and extent of the Doctoral candidate's contribution to this co-authored work
- In cases where the candidate was the lead author of the co-authored work he or she wrote the text

Name: *Mark Garnich* Signature: Date: *24/06/2021*

Acknowledgements

I would like to thank Dr. Mark Garnich for valuable guidance, support, and input throughout the project. From helping with experimental testing to offering direction on modeling questions Mark was there every step of the way. Not to mention, I quite literally wouldn't be in New Zealand without his offer of study.

I would like to thank Elliot, Tim, Henry, and Otis for their help with assorted experimentally related tasks. They made the experimental aspects of this project possible.

I would like to thank Hardy Rifle Engineering Ltd., and Dan Hardy specifically, for supplying test equipment.

I would like to thank Novacam Technologies Inc. of Pointe-Claire, Quebec, Canada for their assistance in conducting barrel measurements.

Finally, I would like to thank my wife Amelia for love and support throughout the course of my post-graduate study.

Contents

List of Figures

List of Tables

Chapter 1

Introduction

1.1 Motivation

Much of the development of small arms is still conducted through the use of trial-and-error methods. Such methods often prove costly in terms of both materials and time. Additionally, isolation of the many variables that can affect ballistic performance can be extremely difficult. These factors make the small arms design problem a prime candidate for improvement through the addition of computer modeling. Proper application of finite element analysis (FEA) offers the opportunity to iterate on design features in a manner that is faster and more cost effective than traditional prototyping methods. For this reason, government labs and some larger companies have increasingly used such methods in their research and development process. A sophisticated finite element model additionally allows investigation of sources of vibration and variability through its ability to isolate or remove factors in ways that cannot be achieved experimentally.

1.2 Background

Ballistic modeling is largely the purview of government labs and private companies, leading to minimal presence of this niche subject in the open literature. Consequently, there are a number of terms and concepts that bear defining.

1.2.1 Ruger Precision Rifle

The firearm used in this research effort, shown in Figure 1.1, is called the Ruger Precision Rifle (RPR). Manufactured by Sturm, Ruger & Co., Inc., the RPR is bolt-action precision rifle primarily designed for long range target shooting. It was selected for use in this project due to a combination of availability and the capability to easily change barrels. While the RPR is made up of a large number of individual components, only the following subgroups need be defined for the purposes of this thesis:

- **Barrel**: The barrel is a rifled metal tube which contains and directs the pressure and projectile during the firing process. It is attached via threaded connection to both the upper receiver and the handguard. The end which attaches to the receiver contains the chamber, the interior portion of the barrel which has been machined to hold a cartridge during firing. The transition between the chamber and the bore is known as the throat or leade. The opposite end, through which the bullet exits, is known as the muzzle. Barrel muzzles may be threaded for various attachments, but this feature was omitted from the model. The shape which defines the profile of the barrel outer diameter is called the profile or contour. Barrels are almost always manufactured from steel, with 416R stainless and 4140 chrome-moly being prominent examples.

- **Handguard**: The handguard is the tube which covers a portion of the barrel. This allows the rifle to be held or rested on an object without touching the barrel directly. Typically constructed of aluminum, this style of handguard is designed to isolate the barrel from user interference. The handguard attaches at the barrel/receiver junction via threaded connection using a component called a "barrel nut".

- **Upper receiver**: Also referred to as the "action", the upper receiver is an aluminum component that contains the bolt, attaches to the barrel, attaches to the lower receiver, and provides a mounting location for

Figure 1.1: Ruger Precision Rifle, the firearm studied in this research effort. Image used with permission of Sturm, Ruger & Co., Inc.

optics.

- **Lower receiver**: The lower receiver attaches to the stock, the upper receiver, and the grip. This aluminum component also contains the magazine well and the associated release mechanism. In the context of this research the combination of the lower receiver and stock is occasionally referred to as the "chassis".

- **Bolt**: The bolt, which rides within the upper receiver, is the component responsible for inserting and extracting ammunition during the firing cycle. Though consisting of multiple parts, only the bolt face and firing pin assembly bear special mention. When the bolt is closed and firearm fired, the bolt face is the surface which bears a portion of the longitudinal pressure loading. In the context of this thesis the bolt face is also referred to as the breech or breechface. Contained within the body of the bolt, the firing pin assembly uses a spring to drive a rod, called the firing pin, forward (when released by the trigger) to strike the primer and initiate combustion.

- **Stock**: The stock is the portion of the firearm extending rearward from the rear upper/lower receiver joint. It is used to steady the firearm, align the user's eye with the scope or other sighting device, and transfer recoil force during firing.

1.2.2 Ammunition

Modern firearms are designed to fire individual ammunition cartridges (Figure 1.2). A typical loaded cartridge is comprised of four components, listed below.

- **Projectile**: The projectile is the component of ammunition which is accelerated down the barrel to be launched at the target. In the context of this research the term "projectile" is interchangable with "bullet". Modern bullets are typically made of a gilding metal (copper) jacket stretched over a lead-antimony core. Bullet mass is given in grains (gr), with a grain defined as 1/7000 of a pound ($\approx$ 6.48E-02 grams).

- **Propellant**: The propellant is the substance which undergoes combustion and provides the gasses/pressure to propel the projectile. Modern firearms typically use "smokeless gunpowder", often referred to as simply "powder". The powder comes in the form of small kernels, the burn rate of which is controlled by a combination of coatings, composition, and geometry. As with bullets, powder mass is commonly given in grains. An aggregate of propellant kernels is referred to as a "charge".

- **Primer**: The primer is a metallic structure that is mounted in the end of the cartridge case opposite the bullet. The primer contains a chemical composition that reacts when subjected to a sufficient impact. This reaction, which propels a small amount of high temperature particles into the body of the cartridge, is responsible for ignition of the main powder charge.

- **Cartridge case**: The cartridge case is responsible for containing the other three components and is most commonly made of brass. During firing, the case acts as the pressure vessel containing the combustion process and stretches until it is supported radially by the chamber walls and longitudinally by the chamber throat in the front and the bolt face in the rear.

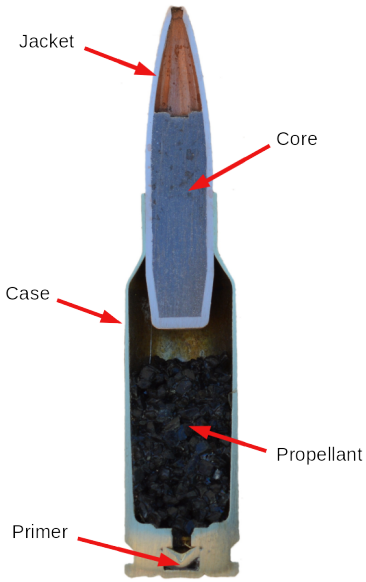

Figure 1.2: Cross-sectioned and labeled cartridge case. Image used with permission of Kevin Gross.

1.2.3 Internal Ballistics

Internal ballistics is the portion of the ballistic cycle that takes place prior to the exit of the projectile from the barrel. This portion of the firing cycle begins with the impact of the firing pin on the primer. In general terms, the internal ballistic cycle is as follows.

1. The firing pin impacts the primer, igniting it.

2. The primer sends a pressure pulse and high temperature particles into the propellant bed.

3. The pressure impulse compresses the propellant against the base of the projectile, dislodging it from the case. Simultaneously, the particles begin ignition of the propellant.

4. The propellant burns, creating gases which expand and rapidly increase the pressure inside the cartridge case.

5. The increase in pressure stretches the brass to fill the confines of the

chamber and simultaneously begins to accelerate the projectile down the barrel. This is resisted by the engraving pressure (forcing the bullet into the rifling), friction with the barrel walls, and the compression of air in front of the projectile. The equal and opposite reaction to this takes the form of recoil.

6. This process continues until bullet exit, after which the pressure and temperature drop rapidly. The exit of the projectile marks the transition to the exterior ballistic regime.

1.2.4 External Ballistics

External ballistics is the study of the portion of the ballistic cycle which takes place after the exit of the projectile from the barrel. This is relevant when considering the effects of projectile exit conditions on downrange performance, e.g. when investigating the effects of different barrel centerline profiles. Terms of importance include the following:

- **Exit time**: It is convenient to define the *exit time* as the moment the projectile no longer makes contact with the bore surface. The state of the barrel/projectile system at that point will be referred to as the *exit state*. Note however, that projectile exit is not actually a discrete event. Rather, as the bearing surface of the projectile emerges from the barrel the relative stiffness of the connection is progressively reduced until full separation occurs.

- **Pitch**: Pitch refers to an angle in the vertical plane, and may be applied to both the projectile and the muzzle face.

- **Yaw**: Yaw refers to an angle in the horizontal plane, and may be applied to both the projectile and the muzzle face.

- **Line-of-sight**: Line-of-sight (LOS) is defined as a direct horizontal line from the bolt face to a target downrange. This neglects any curva-

ture of the bore due to manufacturing defect or gravity droop. Worded differently, LOS is defined by the nominal bore axis of a non-warped, non-drooped barrel prior to firing.

- **Jump**: Jump refers to the angle between the projectile trajectory and the LOS to a given point-of-aim (POA). If gravity drop is neglected, the actual point-of-impact (POI) may be calculated given the distance to the target.

- **Dispersion**: In this context, dispersion refers to the variability in POI for some number of shots. Common measures of firing dispersion include extreme spread (the furthest distance between any impacts) and average-to-center (the average distance from the mathematical center of the group to each impact location).

1.2.5 Miscellaneous Terminology

There are also a number of terms used that do not fall neatly into the above categories.

- **Large gun**: In the context of this research and the associated literature, *large gun* refers to a class of weapon generally only found in military use. Examples include, but are not limited to: tank guns, artillery pieces, and ship-mounted weapons. This class of weapon usually fires either a shell containing an explosive payload, or a projectile consisting of a finned rod supported during the in-bore period with a sabot.

- **Small arms**: Small arms refers to firearms which are man-portable and typically fired from the shoulder, usually firing solid projectiles with a diameter between 4.3 and 12.7 millimeters.

- **Lock Time**: Lock time is defined as the period of time between the pull of the trigger and the impact of the firing pin on the primer. This quantity is controlled by trigger/firing pin assembly design, depending

on spring stiffnesses and travel distances. Shorter lock time is associated with increased precision, as it provides a shorter period of time during which external forces (typically the shooter) can disturb the aim point.

- **Accuracy**: In the context of firearms, accuracy refers to deviation of POI from POA. This can be used in reference to a single impact or an entire group. This is generally not a concern for firearms with adjustable sighting devices. Accuracy is often erroneously used as a synonym for precision.

- **Precision**: In the context of firearms, precision refers to the degree of dispersion in POI for a group of shots. Minimizing dispersion is often a focus of firearms research.

1.3 Explicit Finite Element Analysis

This thesis is written under the assumption that the reader is at least passingly familiar with finite element analysis. However, dynamic modeling and explicit solvers are not as commonly used as static modeling and implicit solvers. Therefore, this section will outline some key differences and point out key factors to consider when using explicit solution methods to analyze highly transient behaviors.

The key difference between a static and a dynamic analysis is the presence of the mass matrix in the latter. A dynamic problem involves a calculation of accelerations, and therefore requires density definitions that allow a mass to be associated with each element. Though an implicit solver may be used to solve dynamic problems, an explicit solver is better suited to highly transient scenarios. Features of explicit solvers include the following:

- Use of a central-difference operator to step through time

- Employ an easily invertible lumped mass matrix

- Doesn't require a global stiffness matrix

- Convergence iterations are not required
- Excellent scaling in parallel processing

In terms of model building it is important to understand how mesh density affects model stability and runtime. The central-difference method is conditionally stable, meaning that there exists a maximum time step size beyond which the operator is no longer stable. This stability limit is correlated to the time it takes for a stress wave to propagate across the smallest element in the model (also referred to in this work as the limiting element) and is negatively affected by damping. In general the maximum time step, ΔT, may be estimated using Equation 1.1 where L_{min} is the characteristic length of the smallest element and c_d is the speed of sound in the material assigned to that element.

$$\Delta T \approx \frac{L_{min}}{c_d} \tag{1.1}$$

Equation 1.1 also makes clear two ways in which model computational expense may be decreased: an increase in size of the smallest element(s) or an increase in material density for the smallest element(s). Increasing element size is the most straightforward approach to reducing model runtime. However, given geometry constraints or mesh convergence concerns, it may not be feasible to increase the dimensions of the limiting element(s). In this case it is possible to artificially scale the mass associated with the limiting element(s). If the scaled elements represent a relatively small portion of the full mesh then the change to total model mass will be negligible. This approach is most suitable when a model contains just a few limiting elements that cannot be increased in size. An example of this usage is given in later in Chapter 4.

1.4 Aims and Objectives

The most basic goal of this research effort is the development of a state-of-the-art finite element model capable of simulating the firing cycle of a precision

bolt action rifle. In general, the uses of such a model include, but are not limited to: replacing/supplementing prototyping during the development cycle, giving insight into system sensitivities to assorted input variables, and isolating the contribution of individual firearm components to group dispersion. In order to do so, an investigation into which physical characteristics of the dynamic problem are important to accuracte prediction of firearm behavior must be performed. Specifically, this research investigates mass asymmetries, stiffness characteritics, and loading beyond that of the firing pressure. The final goal of this research is to then demonstrate the capabilities of the model by investigating the influence of model features such as bore centerline curvature.

1.5 Thesis Structure

This thesis is divided into six chapters, beginning with the motivation and background presented here. Chapter 2 presents a review of the open literature that is relevant to the project. Explanation of the experimental methodology is contained in Chapter 3, which details the equipment and techniques used to measure firearm characteristics and barrel vibrations. Explanation of the modeling methodology is contained in Chapter 4, which which focuses on finite element modeling. Chapter 5 examines the key findings of the research effort and contains discussion of their importance. The thesis concludes in Chapter 6 with a summary of conclusions and a list of suggestions for ways in which the work could be continued or expanded.

Chapter 2

Literature Review

As introduced in Chapter 1, furthering understanding of the causes of vibration in small arms barrels and the effect on firing precision is desirable. Full investigation of the subject requires examination and testing of the small arms system in a variety of configurations. Experimental testing is possible, but its feasibility is limited by the fidelity of the data that can be collected along with the expense in both time and equipment. Computer modeling of the system, if sufficiently accurate, represents a powerful tool for simulating small arms of arbitrary design at a potentially lower cost than prototyping and physical testing. Additionally, a model can allow observation of phenomena that are difficult or impossible to observe experimentally and allow isolation of variables that cannot be isolated experimentally. Due to this, a number of efforts have been made in the past to apply computational tools to the analysis of both small and large arms.

This chapter will discuss the open literature as it pertains to small arms modeling. Where appropriate, ways in which the literature directly influenced the direction of this research are detailed. Note that a significant number of the papers discussed here are centered around the modeling of large guns. They have received a larger share of attention, and can offer guidance in small arms modeling, despite the differences in scale and typical projectile construction. Topics of consideration include internal ballistics, barrel structural modeling,

and non-ideal bore centerlines. Brief treatment is given to experimental testing of small arms, thermal modeling, and combined thermo-mechanical modeling.

2.1 Internal Ballistics

Internal ballistics (IB) refers to the portion of the ballistic cycle that occurs before the projectile leaves the bore. This includes the thermo-chemical processes of ignition and combustion, pressure distribution, heat transfer, and balloting (the in-bore lateral movement of the projectile). Internal ballistics computations are used to estimate pressure loading for purposes of barrel/firearm modeling. Modeling of the combustion process is outside the scope of this project, but a certain understanding of internal ballistics processes, and the solvers used to model them, is useful. This section will briefly discuss several approaches to modeling internal ballistics. These approaches are primarily distinguished by the number of dimensions modeled, referred to as the "degree" of the model. They range from lumped parameter models (zero degree) to two-dimensional approaches.

The work by Corner [1] was the definitive text on interior ballistics when it was written, and is still largely relevant to date. He addresses a number of approaches to the interior ballistics problem. Many modern lumped parameter models are based on Corner's method. Note that this style of solver is still in widespread use.

Miner [2] developed a lumped parameter interior ballistics model that compared well to established solvers, including IBHVG2 (Internal Ballistics of High Velocity Guns, version 2) [3], a code developed by the US Army's Ballistic Research Lab. An effort was made to duplicate this solver for the purpose of coupling it directly with the finite element model. Unfortunately, several key equations are rendered illegible and neither the author nor his advisor responded to inquiries. Additionally, the parameters needed for such a model to run are difficult to obtain.

More modern internal ballistics solvers have advanced to include simulation of propellant grains, the combustion products, and their interaction. Mickovic et al. [4] presented a comparison of three separate models: a traditional zero-dimensional code assuming proportionate expansion, a one-dimensional code assuming a two-phase mixture, and a one-dimensional code modeling two-phase flow. When benchmarked against firing data, the code incorporating two-phase flow outperformed the other two methods substantially. These results indicate that there are limitations to the common lumped parameter models, such as the one used in this research. However, such fomulations are ubiquitous due to relative simplicity coupled with acceptable accuracy.

The state of the art has been further advanced by the generalization to multiple dimensions. Bougamra and Lu [5] reported a two-dimensional axisymmetric two-phase approach implemented in the computational fluid dynamics software package Fluent. Comparison to experimental data showed strong agreement.

Development or enhancement of an interior ballistics solver was outside the scope of this project. This meant that advanced couplings between multi-dimensional multi-phase solvers and the finite element model, as demonstrated by Newill [6], was not feasible or possible. However, a small number of packages are available commercially, almost all utilizing a lumped parameter formulation. Most are prohibitively expensive, therefore a package developed for precision reloaders (typically competition shooters who load their own ammunition), QuickLOAD [7], was used to obtain the necessary input data (breech pressure, propellant burn percentages, projectile position, projectile velocity, etc.) for modeling the interaction of the pressure front, projectile, and barrel.

2.2 Primer Effects

Although technically a subset of interior ballistics, the subject of primer behavior has been isolated by a small number of authors. Primer behavior is of

particular interest to this research effort due to the potential for the primer pressure pulse to affect or induce barrel vibrations. While a survey of the literature does not reveal any work directly addressing this interaction with the barrel, research has been done on the primer impulse itself. This includes investigating the relationship between crimp strength (tension holding the projectile in the case) and primer-induced de-bulleting (primer force dislodging of the projectile prior to ignition of the main charge) in mid-sized guns [8], primer-induced de-bulleting and projectile tilt in small arms [9–12], and the coupling of a primer model with an advanced internal ballistics engine [13].

The referenced works show conclusively that the primer alone provides enough energy to the system to displace the projectile a measurable amount. While the internal ballistics software used in this effort is not sophisticated enough to capture this effect or be coupled with a primer model, the possibility exists to directly modify the base pressure curve to capture primer effects. Doing so would make this model the first in the open literature to explore the effects of the primer impulse on barrel vibration.

2.3 Barrel Structural Behavior

A great deal of time and attention has been devoted to the study of the dynamic behavior of gun barrels. The bulk of high-fidelity modeling effort has been focused on the investigation of large guns such as artillery and tank guns. Introduced in Chapter 1, key differences between large guns (artillery, tank guns, anti-aircraft guns) and small arms (handguns, shoulder-fired rifles) bear reiteration. Key differences of small arms include shorter in-bore time, higher stiffness in projectile/bore interaction (relative to projectile assemblies involving a sabot or bore-riders), and (for bolt action firearms) reduced presence of moving parts (recoil system). A general goal of small arms modeling efforts is to better understand how individual variables in the system, such as barrel contour, charge mass, and initial projectile tilt affect the dynamics

of the system, particularly the muzzle exit condition of the projectile. These kinematic variables defining the muzzle exit condition are initial conditions for exterior ballistic calculations and are thus important to precision for direct-fire guns. The most generalized goal of the present effort is to create and validate a model capable of including the above types of individual variables, with bore curvature chosen as the variable used to showcase the capabilities of the model.

Beyond the differences in firearm scale, approaches to modeling either type of gun system differ in other ways. Some researchers have simulated the barrel using a beam formulation, others have used three-dimensional continuum finite elements (the approach taken in this research effort). Each of those approaches can also be differentiated based the level of detail in both included geometry (only the barrel vs additional components) and loading (either pressure or projectile vs both).

2.3.1 Large Guns

Beginning with efforts focused on large guns, several of these modeling efforts have approached barrel modeling through some form of beam formulation. Tawfik [14] used an Euler-Bernoulli formulation to investigate stability boundaries for barrels with a stepped profile. Using beam formulations, researchers have considered loading cases representing the projectile as a moving mass [15], neglecting pressure, and pressure loading (neglecting the projectile) [16]. Others have considered the effects of barrel inclination [17] and the case of multiple firings [17, 18]. Zhao et al. [18] first examined lateral vibration of the rifle barrel as a cantilever beam subjected to a moving mass. They did not consider the effects of the moving pressure front, and assumed uniform projectile acceleration. Under those assumptions they showed a negative correlation between projectile velocity and muzzle deflection, with higher velocities inducing less deflection. Second, the case of multiple firings was considered. It was shown that the amplitude of the muzzle oscillations is additive for shots fired in quick succession. Third, Zhao et al. considered the case of a projectile with mass

eccentricity. Subject to the same assumptions as above, the muzzle deflection occurred at a higher frequency and amplitude. Ruzzene and Baz [19] used a model utilizing a shell formulation to evaluate the presence of stiffening rings placed along the barrel. Bulman [20] reviewed the gun dynamics package SIMBAD, which offers a choice between Euler-Bernoulli and Timoshenko beam elements. He noted that the package accounted for components of the recoil mechanism, something typically neglected by other researchers. Koç et al. used a beam model to train an artificial neural network to predict barrel behavior [21], and to investigate the effect of unbalanced projectiles [22]. It is clear that there exists wide variation in modeling approach, even when considering only beam formulations. In general, these approaches also enjoy the advantage of high computational efficiency. Originally dismissed by the author, the possibility exists that a coupling of a beam and solid modeling approach would offer the optimal blend of accuracy and efficiency.

While beams models can lend valuable insight into the behavior of the barrel, beam models cannot easily incorporate all the physical features and boundary conditions that capture details of projectile-bore interaction and higher frequency behavior associated with increased geometric detail. Researchers have employed three-dimensional finite element analysis with continuum elements in pursuit of greater accuracy.

Focusing still on large guns, Hopkins [23] examined the combination of loading due to both the pressure front and the mechanical loading from the projectile. Prior models used frictionless contact between the projectile and the bore, as the friction was already accounted for in the applied pressure curves. Hopkins' implementation involved the coupling of an internal ballistics code and a finite element model. While unsuccessful, the preliminary work was laid to incorporate feedback from the finite element model into the internal ballistics solver, allowing an iterative solution process. At a basic level, the approach taken by Hopkins is similar to that used in this work. While more sophisticated methods for applying boundary conditions are used in the present

work, the modeling philosophy is the same.

Wilkerson and Hopkins used three-dimensional FEA to examine the effects of a balanced breech system on recoil behavior for the M1A1 main gun. Two models were used: one of the gun in standard configuration, and one with additional mass added to align the gun center-of-gravity with the bore centerline [24]. Individual pressure history curves were assigned to each axial ring of elements along the length of the bore. Though eventially replaced, this method of applying boundary conditions was the first method implemented in the present effort. Earlier experiments found that the balanced breech model exhibited lower muzzle deflections during firing than in the standard configuration. The authors attempted to use FEA to explain these differences. They appeared to be related to the clearances present in the gun assembly. This work directly influenced the course of the present effort as it emphasized the importance of accounting for gun geometry beyond that of the barrel alone. Attempting to account for overall gun geometry is one of the defining aspects of the model presented here.

Wilkerson [25] continued the previous work in examining the influence of the recoil mechanism in the M256 gun system. The model allowed a number of input parameters to be varied and their influence on the muzzle exit condition to be noted. These parameters included chamber pressure and projectile seating. It was found that projectile seating had a much larger effect on muzzle exit than pressure variation. In terms of the goals of this thesis, this study represents an example of using a continuum finite element model to assess the impact of input parameters on barrel behavior. Additionally, the importance of considering overall gun geometry was reinforced.

Tzeng and Hopkins [26] examined the phenomenon of dynamic strain amplification (additional strain induced when the velocity of the pressure front approaches the wave-propagation speed for flexural waves in the barrel) in composite overwrapped barrels. Composite plies were not modeled explicitly. Rather, "smeared" properties based on a rule-of-mixtures approach were used.

The model was further simplified through the use of axisymmetry. Their results showed that the dynamic strain amplification effect was still present in composite overwrapped cylinders. Additionally, the composite-steel interface was near the location of maximum shear stress, leading to concerns about delamination and fatigue.

Laughlin [27] examined balloting, the behavior of the projectile in bore, in the context of the damage it may cause to smart munitions. Projectile behavior is modeled in the proposed project, and two simulation techniques used by Laughlin in the analysis are of interest. First, Laughlin's finite element model incorporated a two-step process where an initial static step was used to apply the effects of gravity to induce barrel droop before simulating the firing cycle in an explicit simulation. This eliminated undesirable underdamped vibrations from polluting the firing results. Second, rifling was not simulated. Rather, a resistive pressure was used in the interior ballistics calculations that included the engraving forces. Rotation of the projectile was induced instead through an applied torque. The two-step approach to the application of gravity was the most efficient and straightforward approach described in the literature, and was subsequently successfully implemented in the present work. Though unique, the no-rifling approach was not tested, as the author did not encounter the same level of difficulty in modeling projectile engraving that Laughlin did.

Axisymmetric formulations have been used to investigate axial waves during firing [28]. While an axisymmetric approach does reduce computational cost, the increased efficiency is not worth the reduction in model capability. When considering barrel dynamics, lateral bending modes are of primary interest. Ahmed, Brown, and Hameed used FEA to show the importance of including off-axis masses in the modeling process, their model included the breech geometry as well as additional masses attached to the gun tube [29,30]. Alexander presented a comparison between experimental data and two different modeling methodologies [31]. The model included the barrel, projectile, mount, and recoil system and accounted for gravity droop, recoil, and friction.

Rifling was not included, but an external torque was applied to the projectile. A well written paper, Alexander highlights the discrepancies that may be present both between different modeling approaches and when attempting to validate said models against experimental data. FE techniques have also been used for analysis of transverse vibration modes [32]. Ding, Liu, and Zhang used the Abaqus Python scripting interface to develop a method for meshing worn barrel geometries [33]. Their method uses a script to adjust nodal coordinates based on a wear variable given as a function of position and allows for the deletion of nodes in the case of extreme wear. A very similar approach (omitting the element deletion capability) was used to generate curved centerlines in this research. A finite element code has also been coupled to an internal ballistics code allowing calculation of pressure for each point in the bore at all points in time, these models did not include geometry beyond the barrel and projectile [34, 35]. Chevalier et al. [36] examined the effects of bore curvature with a model including only barrel and projectile geometry. Burns et al. [37] and Eches et al. [38] recognized the importance of accounting for additional geometry in their models, including mounting/cradle geometry and additional masses attached to the barrel (fume extractor, muzzle reference sight, etc).

2.3.2 Small Arms

Of more direct relevance to this thesis are those research efforts which dealt explicitly with small arms. As with the literature pertaining to large guns, different approaches have been taken to the modeling of small arms, including beam formulations and FEA utilizing continuum elements.

Using a beam formulation, Vitek investigated the effects of shortening the guiding portion of the bore relative to the total length of the barrel in order to time projectile exit with favorable vibration patterns [39], and developed an excitation function for the firing of a sporting rifle [40]. In the case of the bore length study, basic mode shapes and calculated inputs were validated, but not the final calculated barrel displacements. Development of the excitation

function excluded the effects of firearm geometry beyond that of the barrel.

Researchers have applied continuum finite element analysis to small arms as well. Deng, Sun, and Chiu used FEA to simulate the firing process in both a rifle [41] and a pistol [42]. For the 5.56 mm rifle both the projectile and the rifling were included. An empirical method was used to calculate the input loading. The barrel geometry chosen was a simple cylinder with no contouring. Boundary conditions consisted of rigidly fixing the rear face of the barrel. Friction was accounted for, but compressed gases in front of the projectile were not. Muzzle velocity was used as the validation criterion. Projectile spin velocity and stresses were examined. The finite element analysis of the firing of a 9mm handgun was similar to the previous rifle model. A fully three-dimensional model was created, with the barrel geometry reduced to an uncontoured cylinder. Rifling was included. The same empirical models were used to provide pressure data. Frictional effects were taken into account, but air resistance was neglected. Element deletion was used with a failure model to enhance modeling of the deformation of the projectile during the engraving process, a relatively uncommon model enhancement. Only the effects of the projectile were considered, pressure loading of the bore from combustion gases was neglected. A combination of experimentally measured velocity and examination of bullet engraving was used to validate the model.

Štiavnický and Lisý investigated the effects of barrel fixing lengths and various barrel attachments on barrel vibration [43]. The model did not include a breech. They attempted to examine barrel vibrations intrinsic to the system itself, i.e. no imperfections or external influences. Both the 5.56 caliber projectile and the propellant gas pressure were modeled. Barrels of two geometries (varied in profile), and featuring different additional masses (to simulate common attachments) were simulated. The pressure history used was obtained experimentally. Muzzle displacement was recorded at the moment of projectile exit, as was displacement of the bullet base. Recorded muzzle displacements were highest during peak pressure (bullet engraving), and rose

again immediately before bullet exit. Muzzle lateral acceleration was highest at bullet exit. These results do not match qualitatively with either the numerical or experimental results obtained in the present effort, likely due to omitting action/receiver geometry.

Chen [44] presented a process for automating the application of pressure boundary conditions in firing cycle FE simulations. Previous approaches had required manual application of pressure curves to individual elements, and relied on linear interpolation between the bore and breech pressures. The automated process used the IBHVG2 interior ballistics code to generate breech pressure data and interpolated using the more accurate Lagrange gradient to calculate intermediate pressures. The code then wrote an LS-DYNA keyword file which included pressure definitions for each band of elements along the bore. This approach was applied to the modeling of an M4 rifle. A small number of the models described in this thesis used a similar approach to the application of pressure boundary conditions.

By and large, the majority of modeling efforts in the area of small arms do not include geometry beyond the barrel and projectile [39, 41, 42, 45, 46], and those that do [43] neglect factors such as gravity, recoil, and action geometry. Experimental validation of these various models is often limited to matching of muzzle velocities.

This literature review, and thesis as a whole, focus on structural modeling of the firearm. That said, small arms have also be the subject of experimental scientific study. Three examples of such works follow. Sava et al. [47] used high speed photography to track the motion of the muzzle after projectile exit. Experimentally focused efforts have revealed the importance of both firearm geometry [48] and mounting conditions [49] on barrel response. These findings agree with much of the large gun literature in indicating that a high-fidelity model will necessarily include other system components beyond the barrel and projectile.

A review of large gun literature indicates that three-dimensional modeling

with continuum elements where the geometry includes components beyond the barrel provides increased levels of model accuracy. Despite this, models including detailed small arms geometry are essentially absent. Another significant difference between the two bodies of literature is the degree of validation achieved, with large gun papers being generally better validated. This can be explained in large part by the relative ease of measuring the behavior of larger guns. The larger displacements, longer in-bore period, and larger, more easily instrumented components all lend themselves to easier measurement. Consequently, the research described in this thesis aims to fill both of these gaps in the small arms literature by providing a validated model that includes geometry beyond that of the barrel.

2.4 Non-Ideal Centerlines

Bore curvature has the potential to induce projectile movement relative to the barrel (balloting) and affect projectile exit conditions in ways detrimental to precision. While more pronounced in large guns due to the heightened compliance of sabots and obturators relative to solid projectiles, effects are still present in the context of small arms and remain important for direct-fire applications. Discussion of various efforts which have been made to model the effects of barrel curvature in both large guns and small arms are included in this section.

Neglecting thermal effects during repeated firing, curvature of the bore centerline can be attributed to two factors: droop due to gravity and manufacturing variability (hereafter referred to as warp). Droop has been modeled exclusive of warp in the context of both the primary object of study [50] and as a secondary model feature in related research efforts [27, 31, 51]. Warp has also been modeled in the absence of droop [45, 52, 53]. However, it is more common that models incorporate both droop and experimentally measured warp. These efforts include both those where the bore curvature is the object

of study [54, 55] and those where it is treated as an incidental model feature [20, 24, 25, 34, 36–38, 56]. This last method is the most widely used and offers the most realistic approach to capturing actual weapon behavior. For these reasons, this was the method adopted by the author when investigating the effects of curved centerlines.

Chen [44] used measured barrel data to create a parametric model capable of generating a number of centerline variations for a large smooth-bore gun. He showed that bore curvature contributed strongly to lateral projectile movement, with the effect exaggerated for curvature near the muzzle. Eichhorst et al. [45] discussed several methods by which centerline curvature may be included in finite element models. Using a M4 barrel, they showed that a non-ideal bore resulted in increased pitching and yawing of the in-bore projectile. They concluded that the effects were of lesser significance than those induced by off-axis masses attached to the barrel.

Of those efforts mentioned, only one was conducted in the context of small arms [45]. In that case a single centerline was considered. A feature of the present effort is the inclusion of a study of five measured centerlines, as well as a study of the effects of centerline orientation, investigated by rotating a single centerline about the nominal bore axis.

2.5 Barrel Thermal Effects

Strictly speaking, thermal effects are outside the scope of this thesis. However, a short introduction to previous efforts is useful in terms of framing potential future work and is included here. The thermal transient during firing is complex, involving extreme temperatures (≈1500 °C), high thermal gradients, and multiple heat transfer mechanisms.

Chen [52] developed a numerical model for estimating heat flux in multi-layer gun barrels. An inverse method, it depended upon external temperature measurements to predict the heat flux at the inner wall. The model was purely

one-dimensional. The researchers were concerned primarily with chrome lining, but the method is suitable for other materials. By nature, the model cannot predict barrel behavior based on ballistic inputs.

Lee et al. [57] also used an inverse method, solved using the conjugate gradient, to estimate the heat flux at the barrel inner surface. The barrel simulated featured a chrome lined bore, and the contact resistance between the two materials was taken into account. This method requires knowledge of all material properties and heat transfer coefficients, and calculates the heat flux based on temperature measurements. While the method was not tested against true experimental data, it performed well on numerically generated test cases. Like the model developed by Chen, the model cannot predict barrel behavior based solely on knowledge of the internal ballistics.

Hill and Conner [58] numerically investigated the transient heat transfer problem in the context of sequential firing. Convection and radiation were both accounted for, as were temperature dependent material properties. The researchers used a one-dimensional approach, solved using the finite-difference method. Input conditions were obtained using a commercial internal ballistics solver named PRODAS and coupled with the Lagrange gradient assumption (assuming that propellant gas velocity varies linearly from the breech to the projectile base) to obtain pressures as a function of position. The primary advantage of this approach is the speed of execution. Experimental validation showed a small degree of inaccuracy, attributed to the numerous assumptions made to improve computational efficiency.

Akçay and Yükselen [59] examined the transient heat transfer problem in one-dimension, solved via a finite difference method, and extended the solution to calculate cook-off temperature. Of note, they included material temperature dependencies in their modeling.

Qu et al. [60] used finite element techniques to examine barrel heating for the case of sequential firing. A quarter symmetry model was used in conjunction with a number of assumptions about the gas flow.

Sun and Zhang [61] examined the thermal aspect of the internal ballistic cycle, with considerations for chrome lining and water cooling. They used temperature and a convection coefficient as boundary conditions, rather than a simplified heat flux. They concerned themselves only with radial heat transfer, and made use of symmetry conditions.

Işik and Göktaş [62] used both experimental and numerical methods to examine thermal effects in barrels. While they were specifically interested in the cook-off phenomenon (spontaneous firing due to excessive chamber temperature), their methods are applicable to thermal analysis of gun barrels in general. They used thermal imaging to measure the temperature distribution on the exterior of the barrel. This allowed field measurements, rather than point measurements with a thermocouple. Numerically, the boundary conditions were simplified to an iteratively determined heat flux value, rather than a temperature and convection coefficient. The model itself was limited in scope to the chamber area of the barrel.

In the context of the presented work it would be desirable to predict temperature distributions in the barrel and examine the effects (or lack thereof) of any associated thermal distortion on barrel dynamics. This is important for the case of multiple shots in succession.

2.6 Combined Thermo-Mechanical Modeling

Treatment of the coupled problem, i.e. including both thermal and mechanical loading, as well as their interaction, is less common in the literature. Few papers exist on the fully coupled approach to modeling the in-bore process. Those that do exist focus more on stresses within the barrel, with little consideration given to any possible changes in structural dynamics. As with pure thermal modeling, this portion of literature is of most interest in the context of potential future work.

Chang-Wei et al. [63] examined the combined thermo-mechanical prob-

lem using a simple two-dimensional axisymmetric finite element model. An unidentified interior ballistics code was used to calculate temperature, convection coefficients, and pressure for each stage in the firing cycle. The researchers assumed radiation effects on the bore interior could be accounted for by adjustment of the convection coefficient. Both convection and radiation were taken into account for the outer surface. The researchers indicated a strong coupling of temperature and stress, showing greatly increased stresses with the inclusion of the temperature profile. The investigators also concluded that the thermal response, for the single shot case, is a thin-layer phenomenon.

Perhaps the most sophisticated study of this sort was performed by Şentürk et al. [64]. The authors used both experimental and numerical methods to study the combined thermo-mechanical problem during firing. In contrast to [63], the finite element model was fully three-dimensional. Experimental pressure and velocity data was used to develop boundary conditions for the finite element model. The finite element results compared well to thermal measurements from thermal imaging. No projectile was modeled, only the pressure front and concurrent temperature increase.

2.7 Summary

A review of the available literature reveals that modeling of small arms has been limited, particularly in terms of the geometry included in the model. Both beam and continuum element formulations have been employed, but very few models have included geometry beyond that of the barrel and projectile. No model surveyed included receiver geometry; models that included more than a barrel and projectile only introduced small components directly attached to the barrel. This gap in the literature exists despite a robust body of work on larger guns indicating the importance of considering barrel mounting conditions. Additionally, attempts at direct validation of barrel movement have been limited to the point that it is possible to say that no validated capability

to predict projectile muzzle exit conditions for small arms exists.

Accurate modeling of barrel dynamics will require the inclusion of firearm geometry beyond the barrel and projectile. Validation of such a model will require specialized equipment operating at high sampling rates. This thesis describes the development and validation of such a model. The model is then used to explore the subject of curved bore centerlines, another subject of research that has been primarily explored in the context of large guns.

Chapter 3

Experimental Methodology

Physical experiments and measurements were used to inform and validate the finite element model which served as the focus of this research. These efforts can largely be divided into two categories: those focused on the measurement of barrel movement and those focused on measurement of firearm/barrel geometry.

3.1 Barrel Vibration Measurement

High-speed laser vibrometers were utilized during dry- and live-fire experiments in order to measure lateral barrel displacements. Originally intended as basic model validation, the experiments in conjunction with model results also gave rise to new insights on contributions to barrel motion. This section will describe the equipment and methods used to gather data and will list the configurations tested.

3.1.1 Testing Equipment

The experimental testing facility featured a number of components, centered around a testing chamber designed to allow safe live-fire testing.

Testing Chamber A sound-limiting testing chamber was constructed in order to facilitate live-fire testing on campus. Note that a safety plan was estab-

Figure 3.1: Testing chamber during construction.

lished and approval obtained from the Mechanical Engineering Department, Campus Security, and the Christchurch Police prior to design and construction of the facility. Pictured in Figure 3.1, the chamber features double-wall construction, limiting the ability of sound and other vibration to enter or exit. Additionally, the floor is "floating" with the floor holding the experimental equipment separated from the true floor and the rest of the chamber by a vibration dampening polymer layer. Ducting was installed to both serve as an outlet for exhaust gases and allow data cables and tubing for the pneumatic firing system to be routed through the chamber wall.

Though not strictly a part of the chamber, this facility also contained a bullet trap, a construction designed to capture the fired projectiles. The trap was constructed of plywood and filled with sand, with the projectile entering

Figure 3.2: Results of bullet trap testing. The projectile penetrated roughly 190 mm into the sand.

through a single layer of plywood covered with foam to minimize backsplash of splinters or dust. The bullet trap was designed with a nominal factor of safety of 3.0 in regards to projectile stopping distance and was tested off campus prior to use in the test facility. Test results shown in Figure 3.2 verify that the projectile stopped just short of 190 mm, out of an available stopping distance of 609 mm, for a safety factor of 3.2.

Firearm and Mounting The firearm chosen for this study was a Ruger Precision Rifle chambered in 6.5 Creedmoor. The barrel is 609.6 mm (24 in) in length, and features conventional 6-groove rifling with a 1-in-8 inch twist

rate. The handguard was removed during testing to allow measurement access along the length of the barrel. This change was accounted for both in modeling and when measuring the firearm center of mass.

During testing the firearm was only loosely supported. This was done to approximate real, human-shouldered firing conditions. Figure 3.3 shows the experimental apparatus. The firearm mount is constructed primarily of steel, with rubber straps used to support the firearm. The majority of the weight of the firearm is supported by a strap underneath the center-of-mass. A safety strap passes over the top of the firearm at the same axial location, limiting recoil induced motion to protect the measurement equipment. The remaining weight of the firearm is supported by a third strap located at the rear of the firearm. As a safety feature, two upright struts combine with a tether cable on the bolt to prevent the firearm from being removed from the mount while the bolt is installed. The trigger is actuated pneumatically using an inflatable bladder placed within the trigger guard, in order to limit the net force exerted on the firearm during the trigger actuation.

Measurement Equipment Displacement data was gathered using two Keyence LK-H027 sensor heads connected to a Keyence LK-G5001V controller. This combination allows for 0.02 micron repeatability and a 392 kHz sampling rate. At this sampling rate the sensors have a measurement range of ± 0.3 mm at a nominal distance of 20 mm. The high cost of sensor heads precluded simultaneous horizontal and vertical measurements. The two sensor heads are placed directly opposite one another, with the measurement points in a plane with the barrel centerline. The fixture supporting the sensor heads allows for either vertical or horizontal placement of the sensors, as depicted in Figure 3.4. Per manufacturer recommendations for opaque surfaces, measurements are best taken on a diffuse white surface. Therefore, the barrel was wrapped with a thin layer of teflon tape at the chosen measurement locations.

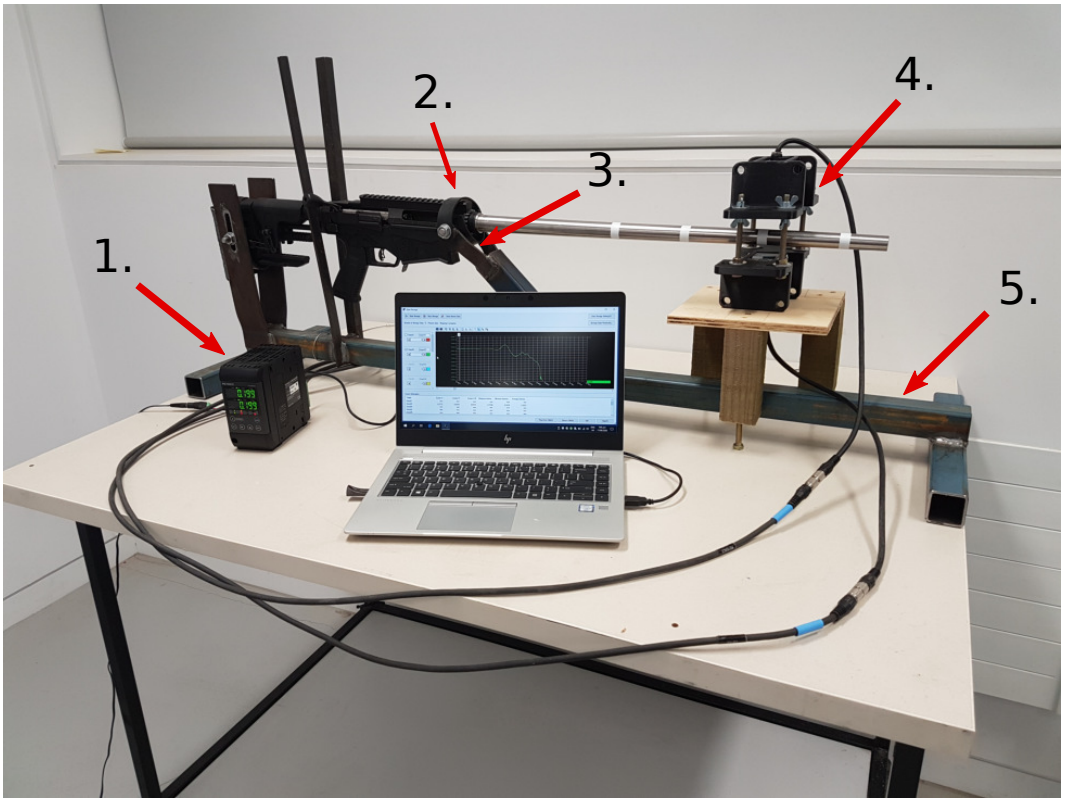

Figure 3.3: Mockup of testing apparatus including firearm, mount, laser vibrometers, and data acquisition equipment. Indicated are the vibrometer controller (1), recoil limiting strap (2), support strap (3), laser vibrometers and mount (4), and support frame (5).

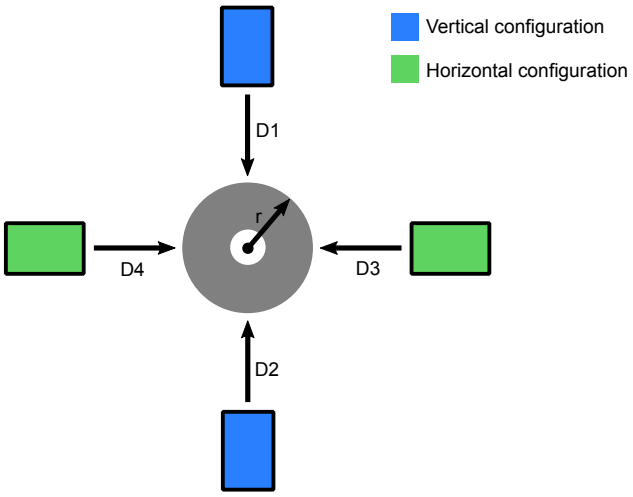

Figure 3.4: Two possible vibrometer configurations (green or blue) allowed by the fixturing. D_1-D_4 are measured distances and r is the barrel radius.

3.1.2 Laser Vibrometry

Data from the vibrometers is processed to convert the distance measurements into barrel center coordinates relative to the initial position. Assumptions are necessary because there are more degrees of freedom than measurements taken. At the point of measurement the barrel can move vertically, horizontally, axially, and undergo radial expansion. Axial movement is assumed to have a negligible effect on the transverse measurements. The amount of axial movement is known to be small during the in-bore transient, such that the lateral movement of the barrel does not vary significantly in that amount of travel. Further, the barrel is assumed to be a perfect cylinder in the vicinity of the measurements.

Under these assumptions, Equations 3.1 and 3.2 can be used to convert the measured vibrometer distances into X-Y coordinates in the plane perpendicular to the barrel cross-section. Here D_{1-4} are the distances denoted in Figure 3.4 and X and Y are the coordinates of the barrel center relative to its initial position. Distances are zeroed relative to their initial value.

$$X = \frac{D_4 - D_3}{2} \tag{3.1}$$

$$Y = \frac{D_2 - D_1}{2} \tag{3.2}$$

In theory it is possible to use measurements from a single orientation to calculate movement in both planes if the barrel radius is known and assumed constant. However, such a calculation depends on the presence of perfectly cylindrical geometry and relies on perfect positioning of the sensors. In practice these requirements render such a calculation impossible.

While acquisition of high quality data was difficult in general, additional difficulty was encountered when attempting to capture barrel movement in the horizontal direction. Despite careful alignment prior to firing, the horizontal sensors consistently failed to capture the barrel movement during the in-bore

period. It was postulated that the greater deflection experienced in the vertical plane meant that a combination of barrel movement and surface curvature resulted in the sensors being unable to acquire a reading.

In an attempt to address this, a polymer sleeve in the shape of a hex-nut was procured. When used as intended, the nut is slid onto the barrel and indexed relative to the sensors such that each sensor is reading a point in the middle of a flat on the nut. The walls near the center were thin in order to minimize the effect of the nut on measured dynamics. The nut then provides a surface which is nominally normal to the sensor regardless of (small) changes in vertical position. This worked, though the nut was prone to coming loose if not tightened after each firing. There is a potential for torsion of the barrel to register as horizontal motion, but calculations of this effect based on the finite element model indicated it to be negligible.

3.1.3 Test Configurations

As discussed previously, the vibrometers chosen for this research are designed to capture very small displacements normal to a surface at high frequency. This ability to detect very small disturbances means that any results obtained have the potential to be polluted or obscured by outside factors acting on the rifle. There are a number of motion/vibration sources not directly related to the pressure and projectile that could be detected. These include:

- Background noise: Despite the use of a specially designed and constructed testing chamber, environmental factors cannot being completely eliminated. Examples of possible factors include air movement through ventilation ducts, vibration from building HVAC systems, and human movement outside the chamber.

- Pneumatic firing system: Although the pneumatic bladder system was chosen as a method to limit the net force exerted on the firearm during firing, the potential to cause small displacements still exists. For

example, uneven bladder expansion or a stiffening of the air line during pressurization could cause minor rigid body movement.

- Firing pin: Two aspects of firing pin behavior have the possibility to affect barrel measurements. The first is inertial force due to acceleration of the firing pin after release by the trigger. The second is the impact of the firing pin, an event involving two separate smaller impacts (first against the primer, second against the portion of the bolt designed to limit total firing pin travel).

- Primer: Though related to the pressure experienced by the barrel during firing, the explosive discharge of the primer provides an impulse separate from that of the main charge.

Given these potential confounding factors, care was taken in choosing configurations to test, some of which were chosen to isolate individual variables described above. Note that an essentially infinite number of test scenarios can be envisioned. The vibrometers can be placed at any point along the barrel, and in any orientation. However, the muzzle is the location of greatest interest. The following experimental tests were performed, with results given in Chapter 5. Data was gathered at a location 50 mm behind the muzzle. This position was chosen as it was close to muzzle, but far enough away to protect the sensitive vibrometers from the muzzle blast during live fire.

1. No loading

2. Pneumatic bladder inflation (PBI), no trigger pull/firing pin

3. PBI, dry-fire on empty chamber

4. PBI, dry-fire on previously used primer

5. PBI, live-fire with only primer, no powder, no projectile

6. PBI, live-fire

Configuration 1 was used to establish a baseline for the noise to be expected in later results and determine the degree of filtering/smoothing necessary. Sources of potential noise included air movement and fan vibration from the room containing the test chamber. Configuration 2 was used to test the degree to which the inflation of the bladder which actuates the trigger effected measurements. Configuration 3 was used to determine the amount of movement caused by the trigger/firing pin mechanism. Configurations 4 and 5 were variations of Configuration 3, testing the degree to which the firing pin impulse was affected by the presence of a primer. Configuration 6 involved firing live ammunition (140 grain Sierra Match King propelled with a standard charge of ADI 2209 propellant).

Though not included in the above firing schedule, a number of live-fire tests were performed with the vibrometers located at 152.4 mm (6 in) and 254.0 mm (10 in) behind the muzzle.

3.2 Geometry/Mass Measurements

Measurements were taken for various aspects of the rifle. The information gathered was used to either more accurately model the firearm (center-of-mass and moment of intertia) or obtain information useful to interpreting test data (lock time).

3.2.1 Center-of-Mass and Moment of Inertia

An important feature of the finite element model and a significant driver of lateral barrel vibration, the firearm center-of-mass location is a quantity of interest. A trifilar pendulum, shown in Figure 3.5, was constructed to enable measurement of both center-of-mass location and moment of inertia. The pendulum consists of a stand which provides attachment points for three cables which support a measurement platform. Noting that each cable has an in-line load gauge, the firearm center-of-mass may be determined by shifting it until

Figure 3.5: Trifilar pendulum used for measurement of center-of-mass location and mass moment of inertia.

the 3 gauges show equal loading. Rotational inertia (I_{zz})is determined using Equation 3.3, where m is mass, g is acceleration due to gravity, L is the cable length, T is the measured period of oscillation, and r is the radius of the measurement platform.

$$I_{zz} = \frac{mg}{L}\left(\frac{Tr}{2\pi}\right)^2 \tag{3.3}$$

Note that both the mass and inertia terms refer to combined quantities that include both the measurement platform and the object to be measured. Therefore, the experiment must first be conducted with the empty platform and that inertia result subtracted from the total obtained when the measurement is repeated with the object of interest.

Here the mass moment of inertia of the RPR in the vertical plane (Ixx), in the as-tested configuration (no handguard, steel barrel), was measured to be 0.301 kg/m$\hat{2}$. Using the breech face as the origin, the center of mass was measured to be 5.4 mm towards the muzzle and 13.6 mm below the barrel axis.

3.2.2 Lock Time Calculation

As detailed in Chapter 5, live-fire results indicated that the trigger/firing pin assembly has a significant effect on barrel vibration. For this reason it was desirable to calculate the lock time associated with the firing mechanism. This was not intended to act as a detailed investigation, but rather provide a reasonable estimate of the time frame during which the firing pin was acting on the system prior to firing. This was accomplished through the following procedure:

The stiffness of the firing pin spring was determined by loading the spring using a known force, measuring the deflection, and repeating the process for a second force. These measurements were taken five times for each load, with the average values used in conjunction with Equation 3.4 which may be rearranged to obtain the stiffness, k. Here the force, F, is the difference in known forces applied and x is the difference in measured displacements. A spring stiffness of 5291 N/m was obtained.

$$F = kx \tag{3.4}$$

Mass measurements were taken for relevant components of the firing pin mechanism, with the spring assumed to contribute only 50% of its mass to the total moving mass. This assumption is a close approximation of the spring behavior, as one end remains fixed while the other travels the full distance with the firing pin. Excluding the spring, the moving mass was 52 g, 35 of which is associated with the firing pin. The spring itself had a mass of 11 g.

Firing pin travel distance and initial compression of the firing pin spring were also measured. The spring is compressed 0.91 mm during assembly and is compressed a further 6.08 mm when cocked. From these values the spring force in both the cocked and fired positions can be calculated from Equation 3.4 and the energy W associated with that change can be calculated from Equation 3.5 where F is the spring force and a and b refer to the compressed and uncompressed spring lengths, respectively. The energy is not needed to

calculate lock time, but is useful for understanding the impulse imparted by the firing pin. In this case the force associated with the cocked position was 135 N and the force for the fired position was 102 N. The total energy associated with this change was 0.72 J.

$$W = \int_a^b F dx \tag{3.5}$$

Calculation of lock time proceeds under two assumptions: that the average spring force may be used to calculate acceleration and that the firing pin undergoes constant acceleration. Under these assumptions firing pin accelaration α may be calculated using Newton's Second Law (Equation 3.6). Here m is the effective moving mass previously described.

$$F = m\alpha \tag{3.6}$$

This value is then used with the firing pin travel distance, d, in Equation 3.7, which may be rearranged to solve for time, t. Here the lock time was calculated to be 2.4 ms.

$$d = \frac{1}{2}\alpha t^2 \tag{3.7}$$

3.2.3 Bore Curvature

Unavoidable variation in manufacturing processes means that rifle barrels are not machined perfectly. One form of defect, hereafter referred to as warp, is a bore centerline that is not concentric with the barrel outer contour for some portion of its length. That is, the as-machined bore centerline is not straight. As discussed in Chapter 2, this form of defect is known to affect barrel/projectile dynamics in large guns but has received relatively little treatment in the context of small arms. In order to facilitate an investigation of the effect of centerline warp in RPR barrels on projectile exit conditions, a small sample of barrels were procured and the bore centerlines measured.

Figure 3.6: Novacam measurement apparatus with barrel clamped vertically to eliminate gravity effects.

Five barrels, nominally manufactured in an identical manner, were provided by Hardy Rifle Engineering Ltd. Centerline measurements for each barrel were conducted by Novacam Technologies, a company specializing in non-contact 3D metrology. Barrels were 609.6 mm (24 in) in length and chambered in 6.5 Creedmoor. An optical measurement technique was used, in which the barrels were fixed in a vertical orientation to eliminate gravity effects and a probe connected to an interferometer was lowered through the bore (Figure 3.6). 89 locations were measured, 6.35 mm apart, and center coordinates calculated for each position. The measurement, like the bore, does not extend the full length of the barrel, starting at the end of the chamber and extending to the muzzle.

The raw data is given relative to the axis of travel of the probe. Whether this axis is parallel to the nominal bore-axis is a matter of fixturing. Rather than rely on positioning during measurement, the data is shifted such that the start and end of the data are on the nominal bore-axis (the centerline of a perfectly straight barrel not subject to gravity). Adjustment of the data is accomplished by application of a linear shift. This assumption ensures that small differences in alignment during the measurement process do not impact

the modeling process. Additionally, this is a reasonable assumption when considering that the barrel contouring process used for these barrels indexes using the bore in such a way that the barrel outer surface is concentric with the bore at both ends.

During manufacture, the cylindrical raw barrel material is drilled using a specialized gun drill which is allowed some degree of runout per unit length. This leads to a bore that wanders (within the given tolerance) from the outer contour. The hole typically exhibits a slight helix superimposed on a dominant curve. The drilled material is then indexed at each end on the center of the drilled hole and the outer diameter is turned on a lathe. This operation means that, regardless of any deviation along the length of the bore, the inner and outer diameters are nominally concentric at each end. While this is only true to within a tolerance, it provides a realistic basis for the assumption.

Figure 3.7 shows the total measured deviation from a straight centerline for each of the five barrels. Centerlines are numbered in order of greatest total deviation to least. Figure 3.8 shows the components of warp in the horizontal and vertical planes. Each data set was rotated about the nominal barrel axis in a way that maximizes deflection in the vertical plane for ease of comparison. This was done through an optimization routine set to maximize the sum of vertical coordinates for all data points through rotation of the data about the nominal axis. The horizontal deviation is on the order of 3% of the vertical. This indicates the warp is nearly planer, something also suggested by the similarity between the total and vertical deviations.

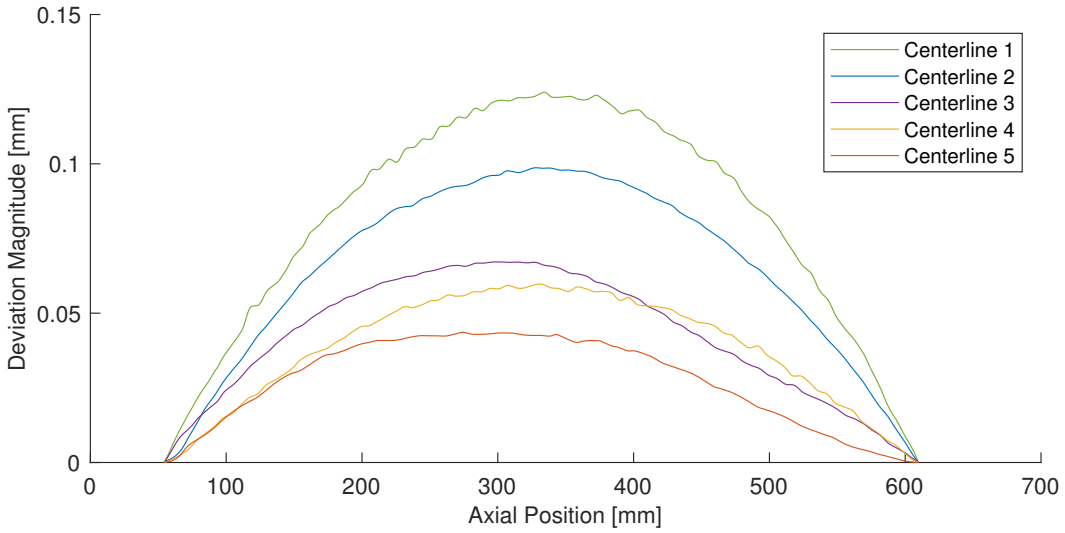

Figure 3.7: Total magnitude of deviation from straight centerline for the five barrels.

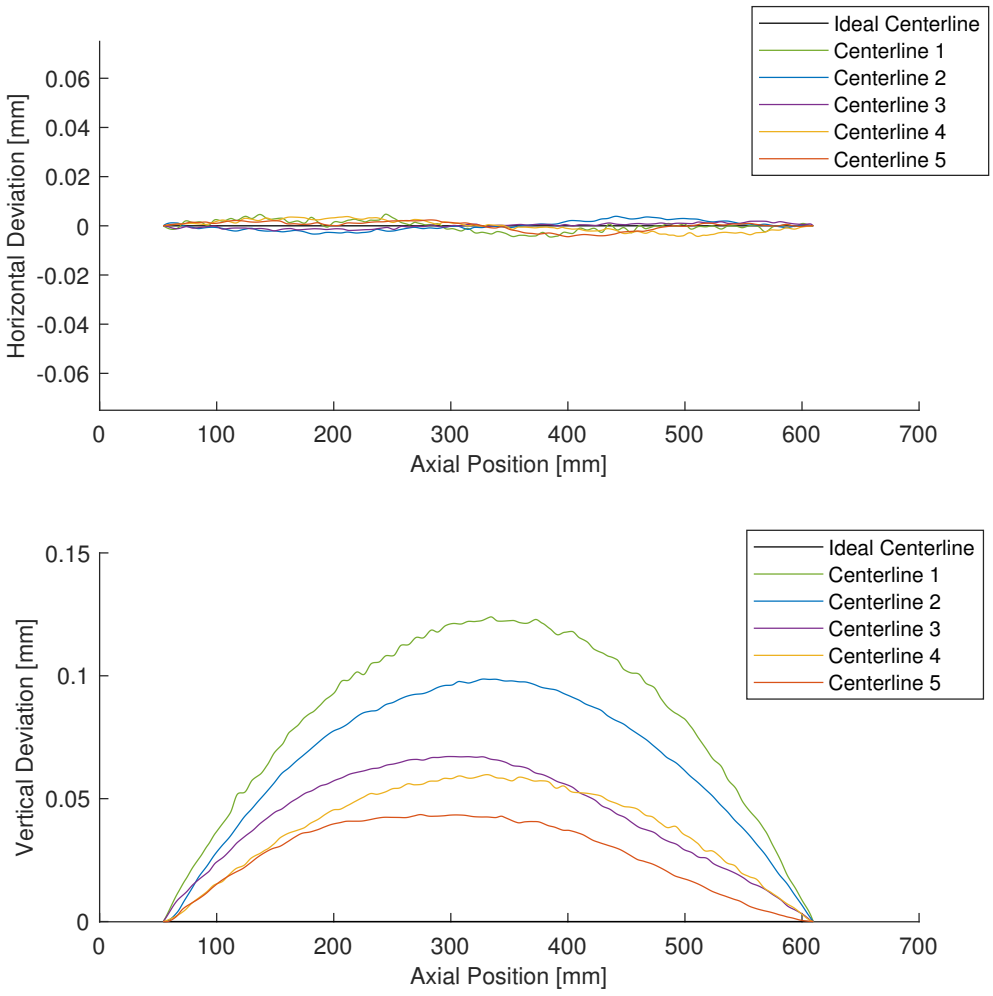

Figure 3.8: Horizontal and vertical deviation from straight centerline for the five barrels.

Chapter 4

Modeling Methodology

Modeling of the Ruger Precision Rifle using finite element analysis was the primary focus of this research effort. This chapter covers the evolution of the model geometry, material properties, the loading applied, and a description of numerical techniques used to extract useful results from the models. Discussion of each aspect of the modeling process includes a summary of iterations during model development and a description of the final model. Where useful, descriptions of unsuccessful or un-utilized model features are included.

4.1 Modeling Philosophy

Parameterization was a central focus of the modeling approach, a choice which added a great deal of complexity to the model building process. A primary goal of the project was to create a robust model with potential for use in a research and development environment, making model adaptability desirable. To this end, the majority of the model construction was accomplished through the use of the Python scripting capabilities present in Abaqus/CAE. Non-barrel components, i.e. projectiles and receiver geometries, were created manually using the Abaqus/CAE graphical user interface (GUI) and stored in "library" files to be imported as needed by the main model generation script. Generating the model by script allows for potential rapid changes in barrel dimensions, material properties, pressure loadings, and overall model configurations.

However, the focus on scripted generation comes with notable downsides. Model development is more complex, and therefore slower than creating a single model configuration using the Abaqus/CAE GUI. Of greater concern, fine control of edge seeds, biases, and other meshing parameters becomes far more difficult. This makes model optimization non-trivial and ultimately resulted in a model with lower computational efficiency than desirable. Note that, in theory, any action which may be accomplished in the Abaqus/CAE GUI may also be accomplished using Python commands. This is also true of mesh controls, but difficulties were encountered in using commands for locating individual edges and vertices. This was almost certainly related to the precision with which Abaqus defines the curves making up the barrel coupled with the tolerances of the feature locating commands.

In retrospect, restricting the modeling to a small number of configurations that could be more easily refined may have yielded better results. Less time would have been spent on model development and more on the application of the model. On the other hand, such an approach would limit the overall number of configurations that could be tested and would not lend itself as well to future expansion.

Alternative approaches were also considered. A common approach, as discussed in Chapter 2, is the use of a beam formulation solved using the finite element method. Beam models offer computational efficiency at the cost of model fidelity, a trade-off that runs counter to the desire to capture both barrel and projectile behavior in detail. A second approach, and perhaps the path that offers the best balance of accuracy and computational efficiency, is a model combining a 3D barrel and breechface geometry with spring elements and point masses representing the rest of the firearm. This was not considered until later in the project, at which point it was judged to be wiser to continue with the existing model.

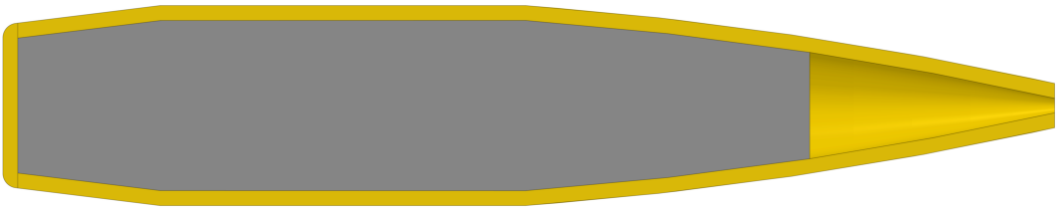

Figure 4.1: Cross-section of Berger 140gr VLD projectile used during the initial stage of modeling.

4.2 Model Geometry and Mesh

The geometry of the model consists of three distinct components: the projectile, the barrel, and the receiver or action. This section details the modeling of each of these individual components, and concludes with a description of the ways in which these components were combined to form complete models.

4.2.1 Projectile Geometry

Initial modeling was conducted with a projectile produced by Berger Bullets, a 140 grain VLD (Very Low Drag), which is depicted in Figure 4.1. Though there are many variants, this basic projectile design is ubiquitous, consisting of a gilding metal jacket stretched over a lead-antimony alloy core. Properties for all model components are given in Section 4.2.4. The model accounts for both materials, but assumes the core and jacket are fully connected. It is known that excessive rates of barrel twist coupled with high projectile velocities may lead to the jacket debonding from the core [65], this was not implemented in this model. This effect may be accounted for by using a contact/friction boundary condition between the jacket and core [42].

The meshed projectile is shown in Figure 4.2, with the mesh having an average seed size of 0.25 mm and consisting of 53,280 C3D8R (reduced integration hexahedral) elements. Mesh sizing was largely determined by the need to interface with the barrel rifling, resulting in a mesh that was already converged relative to a second requirement based on gross barrel movement. A traditional convergence study using many different mesh spacings was not con-

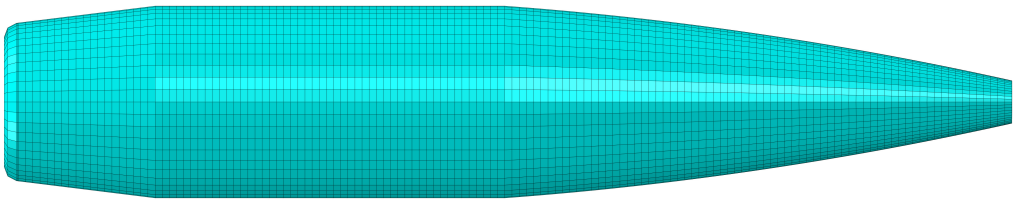

Figure 4.2: Meshed 140gr VLD projectile.

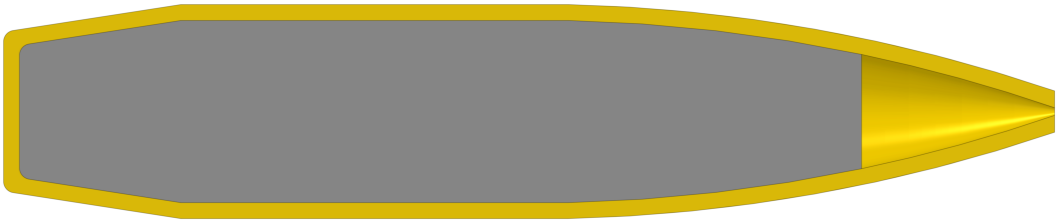

Figure 4.3: Sierra MatchKing (SMK) 140 grain projectile used in modeling and validation efforts.

ducted. Rather, initial element size was based on the characteristic dimension of the rifling elements. A comparison of barrel displacement behavior was then made to a simulation utilizing a projectile with global seed spacing half that of the initial value, without appreciable change. Note that this convergence does not extend to realistic engraving behavior.

When procuring projectiles for experimental testing, the previously modeled Berger projectile was unavailable. This led to the modeling of a second (readily available) projectile design. Produced by Sierra Bullets, the 140 grain BTHP SMK (Boat Tail Hollow Point Sierra MatchKing) is depicted in Figure 4.3. The model again assumes the core and jacket are fully connected, a reasonable assumption for the modeled barrel twist rate and projectile velocity.

The meshed projectile is shown in Figure 4.4, with the mesh again having an average seed size of 0.25 mm and consisting of 52,584 C3D8R elements.

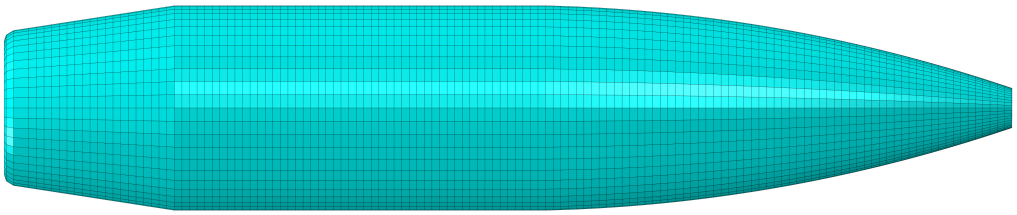

Figure 4.4: Meshed 140gr SMK projectile.

Finally, a third projectile model was used for the simulations involving warped centerlines. Earlier models focused on the overall movement of the barrel (which was not affected significantly by a more detailed projectile), and therefore did not require an especially fine mesh. However, unacceptably high levels of noise in projectile output variables for the centerline simulations indicated that a finer mesh was required in order to better capture projectile engraving and balloting behavior. Additionally, this 140gr SMK was partitioned to facilitate a helical mesh, with a twist rate matching that of the barrel. Chaplin and Gubernat [66] found that helical meshing has the effect of reducing artificial bore resistance. Both local and biased seeds were used, resulting in 277,568 C3D8R elements. This has a large detrimental impact on computational performance, increasing model runtime by roughly a factor of four. The helical meshing is shown in Figure 4.5 and Figure 4.6 depicts the cross-section revealing the internal mesh. Figures 4.7 and 4.8 show the engraved projectiles for the coarse and fine mesh, respectively.

4.2.2 Barrel Geometry

Steel Barrels The parametric nature of the model generation script allowed for essentially infinite variation in barrel characteristics. However, all relevant modeling was done with a barrel model based on the barrel of the Ruger

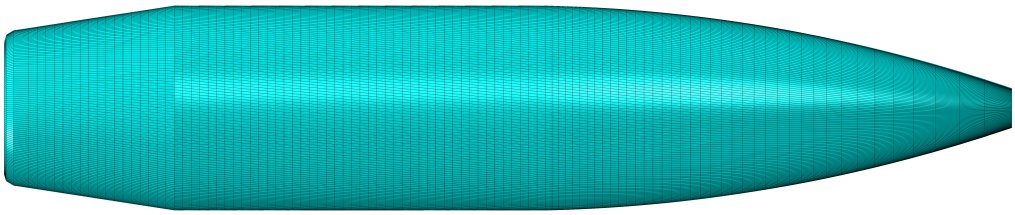

Figure 4.5: Fine helical mesh on 140gr SMK projectile.

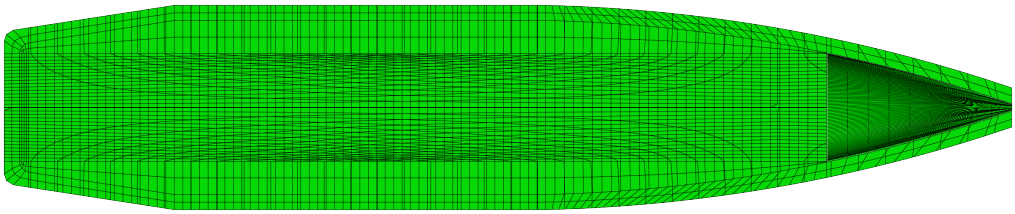

Figure 4.6: Cross-section of the 140gr SMK showing the internal mesh.

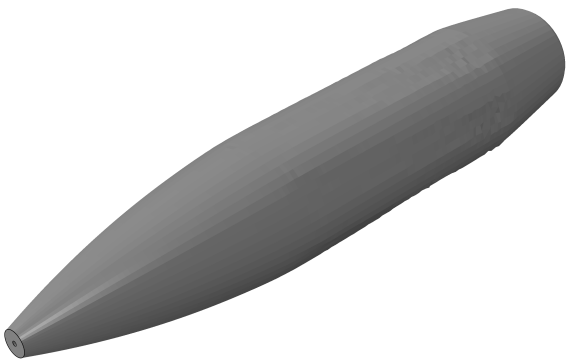

Figure 4.7: Engraved 140gr SMK utilizing a coarse mesh (not shown). Note the lack of defined engraving marks.

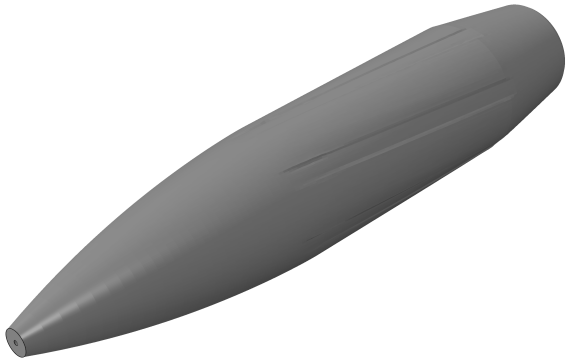

Figure 4.8: Engraved 140gr SMK utilizing a finer mesh (not shown). Note the clear engraving marks.

Precision Rifle used for validation and described in Chapter 3. Apart from the helical rifling, the base barrel is axisymmetric.

The whole geometry was created with a twist and the cyclic symmetry of the barrel was utilized to include the rifling in the geometry. This geometry was created by extruding individual portions of the barrel with a twist (i.e., individual lands, wedges of the barrel) and all merged into a solid model representation. Preserving internal boundaries during the merging process provides the partitions necessary to create a high-quality hexahedral mesh. Figure 4.9 depicts the three portions of the cross-section combining to form a unit of cyclic symmetry, in turn defining the full barrel cross-section. The cross-section geometry is generated by the script based on the number of lands, the land:groove ratio, the land cant angle, bore diameter, and groove diameter. Each of the three cross-sections is extruded based on barrel twist rate, patterned radially a number of times equal to the number of lands, and then merged into a single solid geometry. The resulting rifled tube is shown in Figure 4.10, where the partition lines from the preserved internal boundaries are visible. The unstressed barrel has a perfectly straight centerline.

Adding additional details to the geometry (chamber, outer contour) was accomplished using a series of cut operations, similar to those used in the

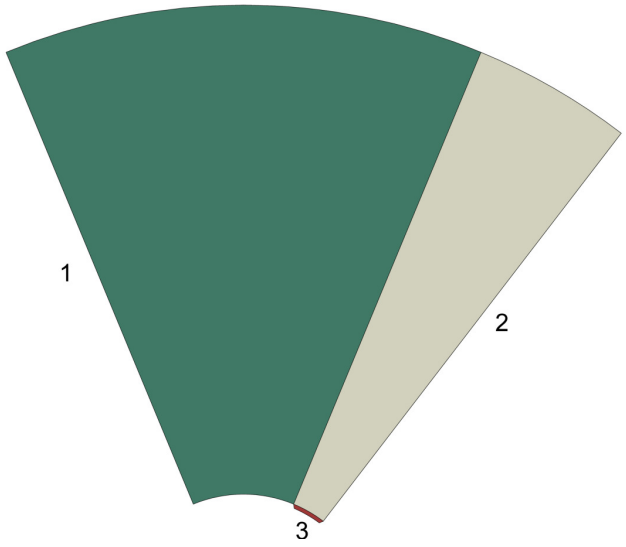

Figure 4.9: The three cross-sectional sub-areas extruded and patterned to create the barrel geometry.

Figure 4.10: Barrel geometry complete with partitions corresponding to the internal rifling pattern.

actual machining of barrels. The barrel was assigned the properties of 416R stainless steel to match the test barrel. Properties for all materials used in the model are found in Section 4.2.4.

Meshing of the barrel geometry was complicated by the nature of scripted model generation, as the partitioning and seeding was required to be parametric in nature. Additionally, the dimensions of the rifling are very small relative to the overall dimensions of the barrel. Consequently, mesh convergence is reached for the barrel just in reducing the mesh size to a density that accommodates the dimensions of the rifling, in this case an average seed size of 0.625 mm. The barrel is made up of 845,154 elements, 844,974 of which are type C3D8R and 180 of which are type C3D6, which is a reduced integration linear wedge element. The wedge elements are used in the chamber leade, shown in Figure 4.11.

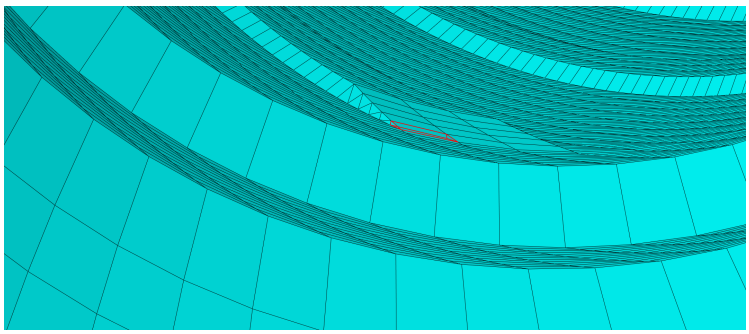

Figure 4.11: Wedge elements used in chamber leade. These are also the limiting elements in terms of time step if using a coarse-meshed projectile model.

Figure 4.12: Depiction of barrel model in the filament-wound configuration. Red represents the composite material.

Composite Barrels Although complex barrel geometries were not pursued, two composite barrel structures were implemented within the model. Both implementations attempt to closely replicate commercially available designs. The first implementation, shown in Figure 4.12, simulates a geometry in which a composite layer is placed directly around a steel core. Such barrels are typically constructed by filament winding or roll-wrapping carbon fiber material around the steel barrel blank, followed by curing and final machining. The second implementation, shown in Figure 4.13, simulates a geometry in which a straight-walled composite sleeve is placed over the top of the barrel. This sleeve contacts the barrel at both ends, but leaves an air gap in-between. As with the first construction, carbon-fiber is the typical composite of choice. No further modeling was conducted using the geometries. Rather, they are presented as examples of the flexibility of the chosen parametric approach.

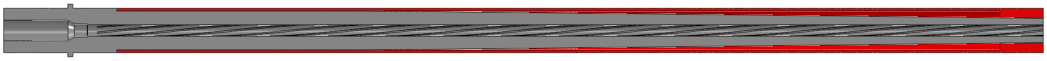

Figure 4.13: Depiction of barrel model in the sleeved configuration. Red represents the composite material.

Bore Curvature Most modeling was done using an idealized straight bore centerline, with gravity loading being the only source of barrel curvature. Later, an effort was made to incorporate the results of the experimental bore centerline measurements described in Chapter 3 into the model.

Due to the nature of the centerline measurements, there is no reference location/orientation relative to the rest of the barrel. Therefore, assumptions regarding data endpoints and centerline orientation were required to establish a basis for implementing the centerline data in the model. First, the data was shifted so that the deviation is zero at both chamber and muzzle. Second, the data is rotated about the nominal axis of the barrel to correspond to the desired barrel installation orientation. The resulting centerline data points are then fit using a Fourier series through the use of the MATLAB Curve Fitting Toolbox. The curve defining coefficients are then used in the parametric Python script used by Abaqus/CAE to generate the model. Figure 4.14 shows the fitted curves used in both the horizontal and vertical directions.

The finite element mesh is initially generated with an ideal linear bore centerline. Nonlinear bore centerlines are then created by editing nodal coordinates for nodes located near the bore surface such that the centerline is shifted onto the nonlinear path. Nodal coordinates are manipulated directly before being written to the solver input file. Specifically, Abaqus keeps an internal version of the input file that may be edited prior to writing to the final file. In this case, nodes within a specified distance (determined dynamically for each centerline based on the degree of curvature to be added, typically about two element thicknesses) of the bore surface are shifted as prescribed by the Fourier series curve fit. Movement of the nodal positions is small enough to cause minimal distortion of associated elements. This is illustrated in Figure 4.15, which shows a section of the bore before and after implementing centerline shift.

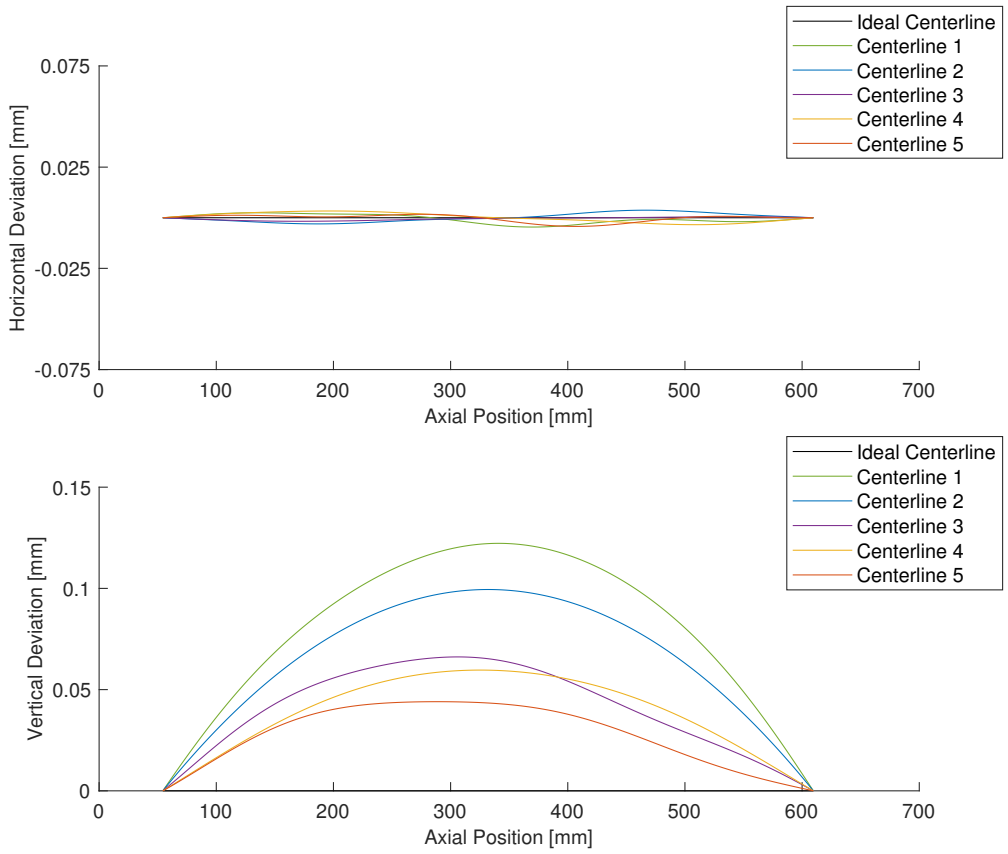

Figure 4.14: Sample centerlines measured and subsequently implemented in the finite element model. Gravity droop is not shown here.

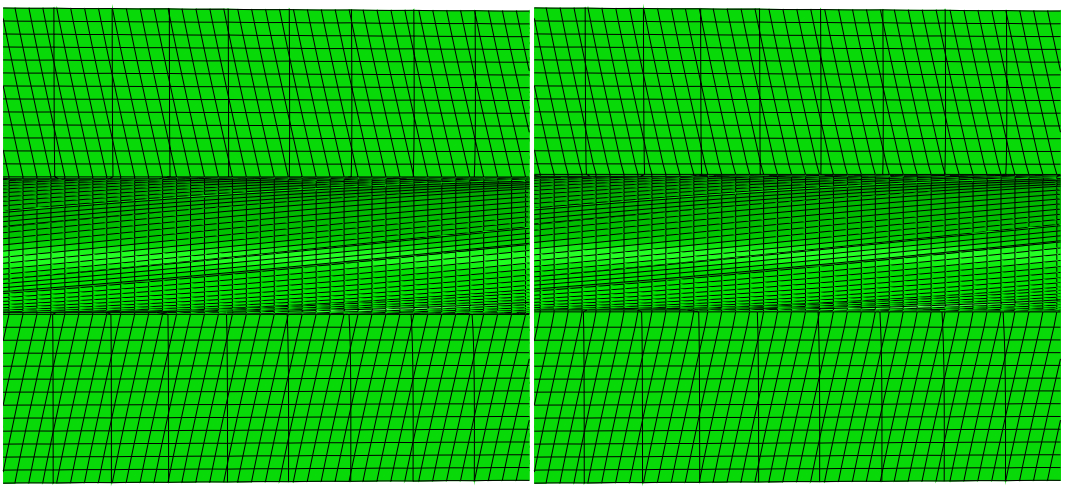

Figure 4.15: Comparison of barrel mesh before (left) and after (right) shifting the centerline.

4.2.3 Receiver Geometry

As discussed in the literature review contained in Chapter 2, many previous investigations of barrel behavior have included only the barrel and projectile. This limits their usefulness as predictive tools, as action/receiver geometry has a significant effect on barrel dynamics. The importance of including barrel support structure in modeling efforts has been known for many years [24]. The ideal approach would be to explicitly include the full geometry of the firearm using continuum finite elements. However, a balance of efficiency and accuracy must always be considered relative to available computational resources. Here we included an accurate representation of the barrel, a good representation of the upper receiver and approximate representations of the remainder of the rifle assembly. The main objective of the remaining components was a reasonable representation of stiffness and an accurate representation of total mass and mass center location.

The first receiver model used in initial modeling is shown in Figure 4.16. As with the barrel, the action models used in this investigation are based on the Ruger Precision Rifle. Two deliberate simplifications have been made to the true geometry. The bolt is not modeled, the bolt face is instead integrated directly into the action geometry to form a pressure boundary surface so that total recoil forces would be accounted for without modeling the entire bolt geometry. Additionally, the ejection port has been shifted 0.89 mm in order to line up precisely with the magazine well to simplify the meshing process. The actions were assigned material properties corresponding to 4140 stainless steel.

The upper receiver adds asymmetry to the model and is the only part of the rifle assembly directly connected to the barrel. Significant additional components are directly or indirectly attached to the receiver. Modeling the upper receiver alone is not sufficient to capture the offset between the center-of-mass (CoM) of the firearm and the line of action of the recoil created by the propellant gas pressure and therefore not sufficient to capture the recoil

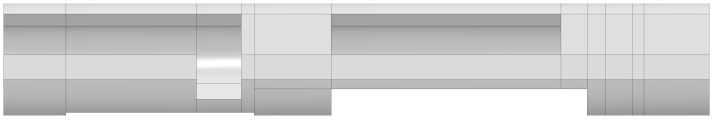

Figure 4.16: Most basic version of the RPR receiver model.

moment generated by that offset. It does however, represent the majority of the small mass asymmetry in the horizontal plane. In this case, the center of mass in the horizontal plane is offset to the left (from the shooter's perspective) by 1.54 millimeters. Note that, given the horizontal symmetry of the base extrusion without ports, this mass imbalance also indicates a lower bending stiffness on the right side of the receiver.

A second receiver model was also created, shown in Figure 4.17. In this model an attempt was made to account for the total mass of the firearm. Two cylindrical model features, hereafter referred to as "pillars", were added at the location of the action screws, which fasten the action to the rest of the firearm. These pillars have density such that they represent the mass of all components not explicitly included in the rest of the geometry. Variation in the length of the pillars and the density of each pillar allow the model center-of-mass to be shifted. This feature accounts for the primary driver of lateral vibration in the vertical plane: the recoil moment created by the distance between the line of action of the recoil force and the firearm center-of-mass. The stiffness of the pillars has a small influence on barrel dynamics. In this case, the stiffness used was that of steel, matching both the fasteners and mating parts.

Finally, a third version of the receiver geometry was created. To account for total mass, allow for simple variation of CoM location, and better capture the way in which recoil forces are transferred to the chassis of the rifle, an additional feature was created. Shown in Figure 4.19, the same two pillars

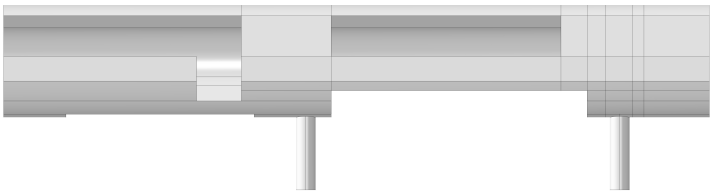

Figure 4.17: RPR receiver model with two additional masses in pillar form.

Table 4.1: Component mass and center-of-gravity details.

	Rear Block	**Rear Pillar**	**Front Pillar**	**Receiver**	**Barrel**
Mass [g]	1180	827	3.86	680	1790
Volume [mm^3]	445000	978	978	85000	228000
Density [g/mm^3]	0.00266	0.846	0.00394	0.00800	0.00785
CG-Z [mm]	-275	-103	-7.43	-88.1	276
CG-Y [mm]	-27	-35.0	-35.0	0.0261	0.00

at the location of the action screws are present, and an additional block of material was added to the rear of the receiver in the location of the stock interface. These features of the model have densities such that they represent the mass of all components not explicitly included in the model. Variation in the size and densities of each part allow the model center-of-mass to be shifted. Table 4.1 contains the mass, volume, density, and CG location for each of the five major model components. The CG dimensions are given relative to the breech end of the barrel. These components combine for a total mass of 4487 grams with a mass center located 5.4 mm above the barrel axis and 13.6 mm behind the barrel breech.

An optimization algorithm was developed in order to determine the assorted densities. Considering both density and size for each mass results in eight possibly variables: three densities, two pillar lengths, and three block dimensions. The pillar diameters are constrained by the geometry of the ac-

tion itself, and were not considered for optimization. However, only three constraint equations exist: one for vertical CG position, one for horizontal CG position, and one for total mass. Consequently, all dimensional variables were fixed and matrix inversion was used to solve the constraint equations for the three remaining density variables. This approach returns the three densities that will produce the correct total mass and CG location for the chosen mass geometries, but does not guarantee that the results will be physical. That is, many choices of pillar and block geometry will require that at least one of the three possess a negative density. At this point, the assumed block and pillar geometries were varied and the simultaneous equations solved in a trial-and-error process until dimensions were found that resulted in three positive densities.

Also contained in Table 4.2 below, the modulus of the block and pillars matches that of 4140 steel, the material the simulated connections are mated to. Models were run in order to assess the degree of influence the pillar/block material stiffness had on model outputs. Figure 4.18 shows the effect of either doubling or halving the material stiffness on predicted vertical muzzle displacement. A small effect is evident, but was judged at the time to be minor enough to continue with the use of nominal steel stiffness.

This eccentric mass is the primary driver of recoil moment and lateral vibration in the vertical plane. This approach effectively changes the model CoM to capture the recoil moment during the firing cycle while deviating <6% from the firearm's mass moment of inertia as measured using a trifilar pendulum. The receiver was meshed with C3D8R reduced integration 8 node hex elements.

A downside of the geometry described is a poor representation of the structural stiffness of the chassis assembly. That is, the ability of the modeled receiver geometry to resist bending in the vertical plane is less than the true geometry. On the actual firearm a Picatinny rail (an aluminum component allowing the attachment of optics) is fastened to the top of the upper re-

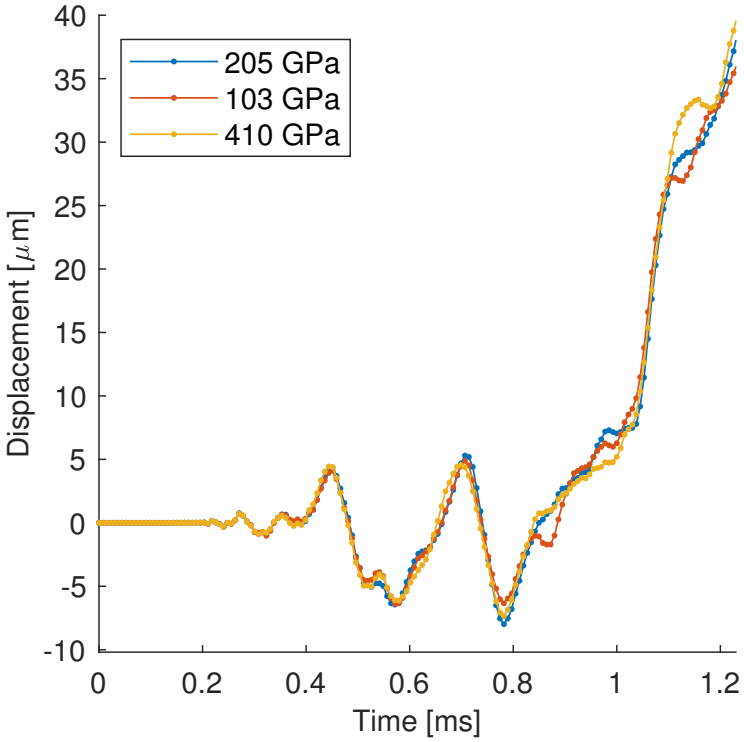

Figure 4.18: Predicted vertical muzzle displacement for three different block/pillar material stiffnesses.

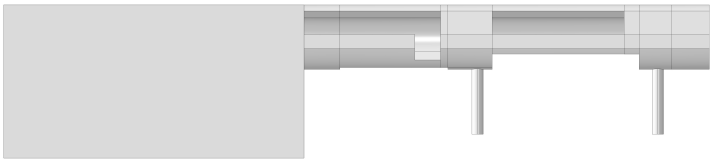

Figure 4.19: RPR receiver model with three additional masses in the form of two pillars and a block.

Table 4.2: Elastic properties for all materials in model.

	4140	**416R**	**Gilding Metal**	**Pb-Sb**	**Front Pillar**	**Rear Pillar**	**Block**
$\boldsymbol{\rho}$ **[g/mm^3]**	0.008	0.00785	0.00886	0.01125	0.0039437	0.8456615	0.00265893
$\boldsymbol{\nu}$ **[-]**	0.29	0.30	0.307	0.44	0.30	0.30	0.30
$\boldsymbol{E}$ **[MPa]**	205000	193000	115000	14000	205000	205000	205000

ceiver and the lower receiver is mated to the upper in such a way as to resist bending. Additional simulations were conducted with an artificially stiffened upper receiver (increased Young's modulus) acting as a proxy for the missing components in order to estimate the effects of those exclusions.

Note that this method does have effects beyond the intended increase in the ability of the model to resist bending. Higher material stiffness leads to a faster wave propagation speed, which also has the effect of reducing the maximum time step for the elements involved. Higher wave speed in particular has the potential to alter high frequency model behavior. This was acceptable, as the model output of interest, peak muzzle deflection, is insensitive to the small amplitude, high frequency vibrations that would be affected.

4.2.4 Material Properties

Properties for all materials used during modeling are contained in Tables 4.2 and 4.3. Non-linear behavior was approximated as piecewise linear, and assumed both monotonic loading and the use of the von Mises yield criterion. It should be noted that 440 MPa is the ultimate tensile strength for gilding metal. The additional data point was used to extend the stress-strain curve and prevent crashes during the model development process. It is no longer necessary, but was left in the material library to maintain compatibility with earlier versions of the code.

Table 4.3: Plastic properties for projectile materials.

Pb-Sb		**Gilding Metal**	
Stress [MPa]	**Plastic Strain [-]**	**Stress [MPa]**	**Plastic Strain [-]**
42	0	400	0
68	0.1	440	0.0365
72	0.2	1495	1
77	0.3	-	-
127	1	-	-

4.3 Model Parameters

This section covers model parameters not covered in more detail elsewhere in the thesis. Examples include contact formulation and mesh convergence.

4.3.1 Contact and Friction

Contact exists in two different regions of the model: between the barrel and action and between the barrel and projectile. Rather than introduce the complexity of modeling the threaded connection between the action and barrel, the two were joined with tie constraints. This should result in a more efficient transfer of energy between the two parts, something that has the potential to affect axial stress waves. However, given the relatively high torque specification for the joint (approximately 90 N-m), the tie constraint was judged to be an acceptable approximation.

Of greater interest is the contact between the barrel and projectile. Normal contact formulations available in Abaqus/Explicit are limited relative to Abaqus/Standard. When using "hard" contact, the desired behavior, the only available pressure-overclosure formulation is the default penalty method. The tangential behavior was modeled as frictionless. While seemingly counterintuitive, doing so is required due to the method by which the internal gas pressure is calculated. To do otherwise would be to essentially "double-count" the re-

sistive force, a known downside to not incorporating a closed-loop internal ballistics solver [23].

4.3.2 Element Formulation, Mesh Size, Time Step, and Convergence

As mentioned in the descriptions of individual components above, nearly the entire model was meshed with C3D8R reduced integration linear hexahedral (hex) elements. The only exception was the sloped beginning of the lands, which were meshed with C3D6 linear wedge elements. Though less flexible than tetrahedral elements, hex elements are attractive from the perspective of computational efficiency. Abaqus/Explicit permits three hex element formulations: a linear brick (C3D8), a reduced integration linear brick (C3D8R), and a linear brick utilizing an incompatible modes formulation (C3D8I).

In general, it would be prudent to perform a mesh convergence study for each element type in order to establish which formulation gives the best balance of accuracy and computational performance. However, in this particular instance, mesh convergence was a secondary consequence of generating a mesh of sufficient density to correctly capture the smallest features of interest (the rifling). Even if rifling were to be omitted from the model, the mesh must still be fine enough to adequately capture the contact between the projectile and bore. In this case, the mesh was fine enough to achieve convergence with any of the three element types and the C3D8R was the most computationally efficient (nearly 100% faster than either the C3D8 or C3D8I). Convergence of the final mesh was verified by comparison with a model wherein the average seed size was halved.

As an additional check, convergence behavior was investigated for a cantilever beam model that approximates the barrel structure. Using beam tip displacement as a convergence criterion, the C3D8 achieved convergence within 5% of the analytical solution at a seed size of approximately 6.5 mm, the C3D8I at approximately 5.5 mm and the C3D8R at approximately 4 mm. For this

geometry, a decrease in average seed size from 6.5 mm to 4 mm results in a 62% increase in number of elements. This indicates that even if mesh size was not dictated by geometric constraints, the efficiency of the C3D8R element in the explicit solver outweighs the higher element count required to obtain convergence.

Already addressed in Section 1.3, the time step used in an explicit solver is directly related to the size and density of the elements. Lower density and smaller elements require smaller time steps. For the models used in this research, the limiting elements in terms of time step were located in the throat of the barrel, where wedge elements are used to represent the beginning of the rifling (Figure 4.11 above). As mentioned in the earlier referenced section, a technique called "mass-scaling" may be used to artificially scale the mass of the limiting elements in order to increase the overall time step. As long as mass-scaling is applied in moderation, i.e. doesn't increase the mass to such a degree as to strongly influence model results, it offers a valuable tool for increase computation effiency.

For the case of this model, mass-scaling was applied only to the 180 wedge elements making up the sloped entry to the rifling. This increased the maximum allowable time step from 1.4E-06 to 2.2E-06, a 57% increase.

4.4 Internal Ballistics

Internal ballistics (IB) refers to the portion of the firing cycle which occurs prior to the projectile leaving the barrel. Primarily relating to the combustion of the propellant (smokeless gunpowder), this also includes the ignition of the primer. In terms of modeling, IB calculations are necessary in order to determine the pressure loading which is applied to the model.

Accurate application of pressure boundary conditions requires the pressure to vary both spatially and temporally. For the purposes of this project it was assumed that the pressure only varies axially. Therefore it is only required

to compute pressure curves for each axial position along the length of the bore. Two different approaches to this problem are common in the literature. Both methods employ a user subroutine to enable accurate spatial application through tracking of the area exposed to pressure at any given instant (wetted surface). The first approach uses an internal ballistics (IB) solver to preformulate a breech pressure history based on assumed ballistic parameters. Pressure distribution based on projectile location is then calculated and applied by the subroutine in each increment. For this approach to work correctly, the assumed parameters must be an accurate match with the ballistic parameters that evolve in the simulation (projectile displacement and velocity). Due to the fact that the coupling is one-way, iteration may be required to obtain acceptable agreement. The second approach is to directly couple an IB solver with the finite element model via user subroutine [6, 34, 67]. This allows the IB code access to model generated ballistic parameters for each increment. In theory, real-time pressure computation ensures the spatial and temporal distributions are always adapted and accurate for the instantaneous IB state. This two-way coupling is based on the combustion volume, as determined from the position of the projectile calculated by the finite element solver.

4.4.1 Pressure Curve

Initial modeling used a variant of the first method described above (one-way coupling). Rather than use a user subroutine to calculate and apply the pressure, a pressure curve was computed for each ring of elements in the bore at the time of model generation. This was computationally inefficient and did not couple the application of pressure to the instantaneous location of the projectile. Therefore, the pressure could outrun or lag behind the projectile if the projectile behaved differently than predicted by the internal ballistics calculations. In practice, this only occurred in very minor fashion, but a user subroutine approach was implemented in later models to preclude the possibility entirely.

In this implementation the pressures were calculated based on the breech pressure history predicted by the IB program QuickLOAD, coupled with the Lagrange approximation to estimate axial pressure variation from the breech to the projectile base.

As discussed in Chapter 2, QuickLOAD is a 0-degree, lumped parameter model. This means that only the chamber pressure is directly calculated; distribution in pressure is not calculated in any given dimension. This should not be construed to mean that the model is inaccurate, lumped parameter models are known to provide good estimates of both chamber pressure and projectile exit velocity [1, 2]. The higher degree models described in the literature review offer advantages when considering pressure waves within the combustion chamber, details of cartridge case expansion, or similar local phenomenon. For the purposes of this model, primarily concerned with macro-scale barrel movement, a lumped parameter model is adequate. However, an assumption must be made to estimate the pressure distribution along the length of the exposed bore surface.

The Lagrange approximation assumes propellant gas density is independent of axial position and that the velocity of the propellant gas varies linearly from zero at the breech to the bullet velocity at the base of the projectile. This approximation is regarded as sufficiently accurate [44, 58, 68] and is one of two pressure gradient options available in the widely used IBHVG2 internal ballistics solver [3]. Equation 4.1 is a representation of the Lagrange approximation, relating the breech pressure, P_{Breech}, to the pressure at the base of the projectile, P_{Base}, for any point in time. Here c is propellant mass, w is the projectile mass, and P_{Loss} is a representation of the resistive forces in the system that include friction on the projectile and pressure of gas in front of the projectile. Derivation and further details are covered by Corner [1] and Carlucci and Jacobson [69].

$$P_{Base}(t) = \frac{P_{Breech}(t) + \frac{c}{2w}P_{Loss}(t)}{1 + \frac{c}{2w}} \tag{4.1}$$

The breech and base pressure can then be used to estimate the pressure of any intermediate point at an arbitrary time, $P(x,t)$, through the use of Equation 4.2. Here x is the location of interest, for $x \leq y(t)$, where $y(t)$ is the time-dependent position of the projectile. Equation 4.2 is sufficient to define the pressure boundary conditions for this investigation when evaluated at the location of each ring of elements along the bore. The chamber was assumed to experience the breech pressure along its entire length.

$$P(x,t) = P_{Breech}(t) - \frac{c}{2w}\left(P_{Base}(t) - P_{Loss}(t)\right) \cdot \left(\frac{x}{y(t)}\right)^2 \tag{4.2}$$

Equation 4.2 is implemented using a combination of the VUAMP and VDLOAD user subroutines offered in Abaqus/Explicit. At each time step, the subroutine checks for element faces belonging to the wetted surface, and calculates the appropriate pressure based on location on an individual basis. As discussed in Section 4.3, friction between the barrel and projectile was excluded from the finite element model. Consequently, P_{Loss} was set to zero in the above equation. Correctly compensating for the resistance pressure requires the ability to feed the resistance directly into the breech pressure calculations, something not possible when using QuickLOAD.

The pressure curve is computed *a priori* and does not take feedback from the actual position of the projectile. Consequently, the simulation neglects the effects variation in the interaction between the projectile and the bore may have on the internal ballistic process. However, the use of a precomputed pressure curve has the advantage of allowing easy modification of the curve, e.g. inclusion of a primer induced pressure pulse.

4.4.2 Primer Impulse

A typical pressure curve, as computed by QuickLoad, is shown in Figure 4.20. This curve is produced by the deflagration of the main charge without consideration for the primer impulse. In this case the curve has also been modified manually in order to reduce numerical noise in the finite element model. Quick-

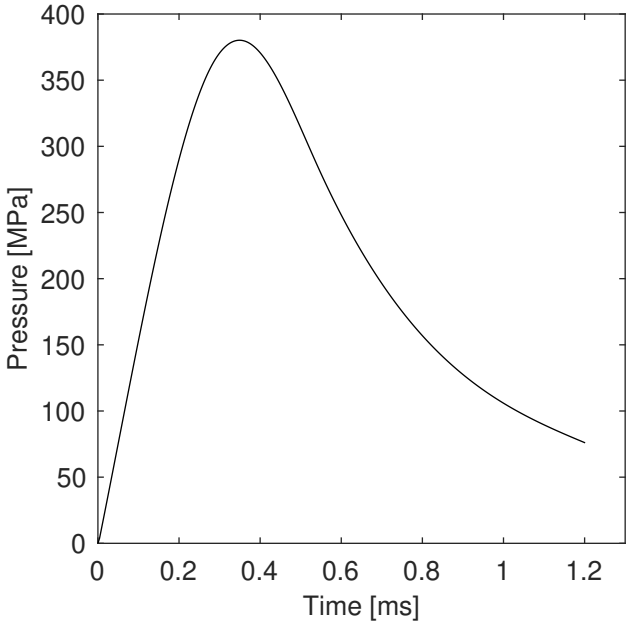

Figure 4.20: Breech pressure curve used as input to the finite element model.

LOAD assumes a non-zero starting pressure based on the force to engrave the projectile. This non-zero initial pressure is seen by the explicit solver as an essentially infinite acceleration which induces high frequency numerical noise. The curve was extended down to zero while maintaining the total energy represented by the curve. Note that the rate of rise in the pressure affects the range of vibration frequencies that are excited, with steeper initial slopes exciting more (higher) frequencies than lower initial slopes.

Minnicino and Ritter [10] used a short test barrel, high-speed photography, and a pressure gauge located on the primer to estimate a chamber pressure curve including the effects of the primer. Figure 4.21 is adapted from [10]. This curve, derived from early bullet motion, indicates a significant pressure pulse in the first 0.05 milliseconds. Based on a combination of the pressure histories represented in Figures 4.20 and 4.21, a curve incorporating a primer-induced pressure pulse was modeled (Figure 4.22). Note that the initial slope of the primer pulse is steeper than the initial slope of the base pressure curve, meaning that the curve accounting for primer effects should induce more high frequency vibration in the model.

Initial models (those run prior to experimental testing) did not include

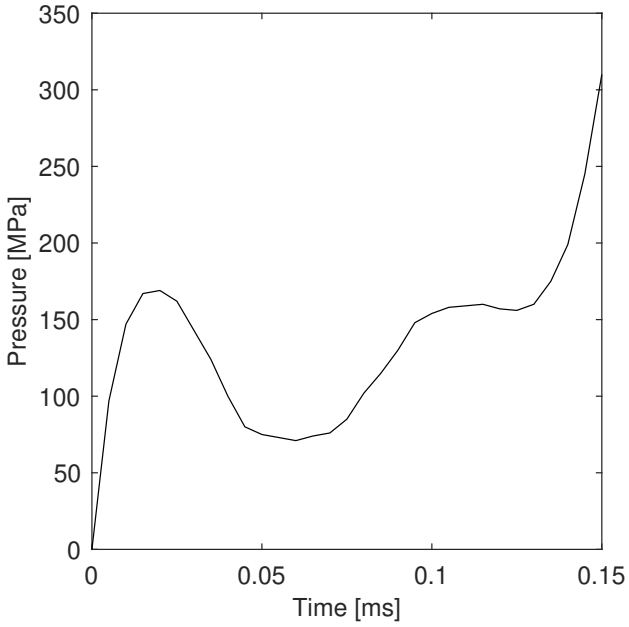

Figure 4.21: Effective pressure curve adapted from [10]. Curve represents a blending of the primer pressure impulse with pressure generated by burning propellant.

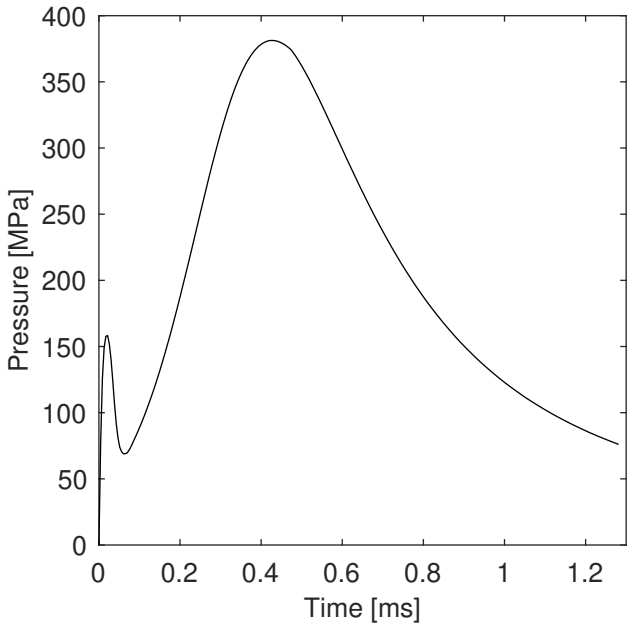

Figure 4.22: Breech pressure curve including simulated primer pressure pulse.

primer effects, but they were incorporated into later models after experimental evidence suggested it was needed to get better predictions of higher frequency barrel behavior.

4.5 Gravity Loading

There are no kinematic boundary conditions applied to the model. In this model the boundary conditions supporting the rifle assembly are based on the assumption that during realistic firing of a rifle, the motion of the firearm against the supports (hands, shoulder) is small during the in-bore transient. The in-bore time is on the order of 2 milliseconds and involves an axial recoil distance of approximately 2-3 millimeters. Changes in support forces during this time are assumed small and the effect on the barrel motion negligible.

The barrel and receiver are attached together with a threaded connection. Modeling of threaded connections is complex, and the simplifying assumption was made that the joint between the barrel and receiver could be approximated using tie constraints that create a rigid connection.

Gun tubes droop under the transverse loading of gravity. While less pronounced than for large guns with barrel lengths measured in meters, this static deflection is still present in small arms. Any amount of droop introduces an asymmetry into the system and causes the bullet to follow a curved path. This contributes to projectile-barrel interaction and barrel vibrations. Furthermore, the pressure behind the projectile acts to attempt to straighten a curved bore, a phenomenon known as the Bourdon Effect. Therefore, correctly predicting barrel behavior during the firing cycle requires including the effects of gravity in the model.

Direct implementation of static gravity loading in an explicit dynamic analysis is problematic. Seen by the explicit solver as a time dependent application of load, the transient response is calculated, and the static state can only be achieved at high computational cost. This was overcome through the coupling

of two analyses. A quasi-static implicit analysis returns the drooped geometry and static equilibrium reaction forces. The solved equilibrium state is then imported into the explicit analysis as an initial condition, eliminating the transient dynamic response normally required to reach steady state. This includes drooped coordinates for all nodes in the model, the associated strains, and the reaction forces generated at constraints in the implicit model (placed on the bottom of the pillars) as required for static equilibrium.

4.6 Factors Not Included

An effort has been made to account for the most obvious and significant sources of loading that the firearm experiences during the in-bore period. However, it should be noted that the model intentionally neglects some sources of loading that can be present in real-world small arms use.

As created, the model makes no attempt to account for the influence of the shooter. Possible examples include body motion due to breathing and heartbeat, trigger pull, twisting of the firearm grip, or firing while the firearm is in motion. While a trained and experienced user will mitigate these factors to the best of their ability, they will still be present to some extent. The purpose of the model is to simulate and assess purely the mechanical abilities of the system, therefore it was deemed acceptable to neglect the human influence.

The model also neglects the potential energy associated with the firing pin spring and the related force caused by using that energy to accelerate the firing pin. As will be discussed in Chapter 5, this assumption is likely invalid in terms of correctly modeling barrel motion during the in-bore period.

The cartridge case is omitted from the model, a common assumption for small arms and large gun modeling alike. This likely has a small amount of influence on high frequency behavior, but negligible influence on larger scale barrel dynamics.

4.7 Modeled Configurations

This section describes notable model configurations that were run during the course of this research. These include a group of models run prior to experimental testing, more detailed models run during the model validation effort, and a series of models run to examine the effect of non-ideal centerline inclusion.

4.7.1 Exploratory Models

During the initial modeling phase four models were developed to show, qualitatively, the effect of increasing asymmetry on barrel vibration. Each subsequent model includes the entirety of the models before it, augmented with additional features.

Designated Model 1, the first model considered contained a barrel and projectile only. Pressure was applied to the chamber, barrel interior, and projectile base. No additional loading or boundary conditions were applied. The model did not include a breech, and consequently has no way to capture the recoil force. Contact between barrel and projectile was modeled as frictionless.

Designated Model 2, the second model added the simplified RPR receiver geometry (without additional masses). This introduced two important features to the model: asymmetry and a breech-face. The asymmetry is critical as a source of lateral vibration. The breech-face is equally important, as it is the surface through which the recoil force is transmitted. Loading remained nearly the same as the previous case, with the addition of the application of the chamber pressure to the breech-face.

Designated Model 3, the third model introduced representative masses to simulate an approximate representation of the full firearm geometry. These masses were included as pillars in the location of the action screws. Loading was identical to Model 2. The purpose of this model was to investigate the effects of the offset of the center-of-mass from the line of action of the recoil

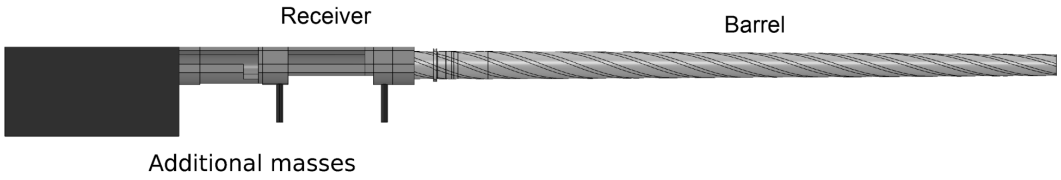

Figure 4.23: Full model geometry used in this investigation. Receiver, barrel, and additional masses are shown.

force.

Designated Model 4, the fourth model was identical to Model 3, but incorporated the asymmetry of barrel droop due to gravity loading.

4.7.2 Enhanced Models

These models were somewhat similar to the 'Model 4' configuration described above. Key differences include a change to the receiver version with three masses and experimentally measured center-of-mass and implementation of the user subroutine-based pressure application. The first model using these enhancements did not include the previously described primer impulse while the second model did. A representation of the full model is shown in Figure 4.23. This model configuration was also used to assess the validity of a potential dispersion calculation, as later in this chapter.

Additionally, due to concerns that the chosen simplified geometry did not adequately represent the structural stiffness of the system, simulations were performed wherein the geometry remained the same but the receiver was artificially stiffened. The addition of secondary masses to the explicitly modeled geometry works well for closely approximating the center-of-mass and rotational inertia, but does not replicate the contributions of the missing components to the overall structural stiffness of the firearm. In this case, two components in particular are of interest: the Picatinny optics rail and the lower receiver. The Picatinny rail is a slotted strip of metal attached to the top of the upper receiver by screws; the lower receiver is attached to the bottom of the upper receiver in a similar manner. In both cases, material is attached to the action

in such a way as to inhibit bending in the vertical plane. Rather than add additional components to the model, the Young's modulus of the receiver material (4140 steel, $E = 205$ GPa) was doubled for the third simulation and tripled for the fourth to assess the effects of higher stiffness representative of a full chassis assembly. Using the increased material stiffness as a proxy for structural stiffness functioned as a proof-of-concept for the purpose of investigating the sensitivity of the system to action stiffness.

4.7.3 Modal Analysis

A straightforward modal analysis was also performed, using the model detailed in the previous subsection. Of primary interest were the vertical bending modes, as this is the predominate barrel deformation during firing. The projectile was removed from the assembly during modal analysis.

4.7.4 Warped Centerline Models

Models were also run in order to investigate two aspects of bore curvature in terms of their effect on projectile exit conditions. The first set of models were run to allow comparison of the effects of five experimentally measured centerlines. As shown in Figure 4.14 above, general curve shapes were similar in the vertical plane, primarily varying in amplitude. Centerlines were rotated to the same orientation (maximizing curvature in the vertical plane, concave downwards) to provide a more direct comparison. The second set of models featuring a warped centerline involved a single centerline rotated around the nominal bore axis, with the dominant warp curvature oriented at 0°, 90°, 180°, and 270°. This allowed investigation into whether indexing the barrel during installation has any potential effect on barrel dynamics.

This group consisted of nine total models: one baseline model without curvature, one model for each measured centerline, and three models incorporating some degree of centerline rotation. These were similar to the above "high-fidelity" models, with the exception of a change to the fine-meshed pro-

jectile.

4.8 Data Processing

This section briefly describes methods of extracting useful data from the previously described models. In general, a Python script was used to access the Abaqus output database files and write the relevant data to text files which were then processed using MATLAB.

4.8.1 Data Extraction

The dynamic state of the barrel muzzle and projectile at the time of projectile exit are of primary interest. The muzzle exit is not a discrete event, but rather a transition during which the projectile contact area with the bore gradually reduces to zero. The time of last contact was defined as the exit time for the purposes of this research. Furthermore, the muzzle motion is defined by motion of the FE nodes on the muzzle face. The quantities of interest for the muzzle are lateral velocity, pitch, and yaw. Projectile quantities of interest include the aforementioned, as well as axial velocity, pitch rate, and yaw rate.

The muzzle kinematic values were calculated using data from all nodes on the muzzle face. Velocity components were calculated using the average of all muzzle nodes. Pitch and yaw values were obtained by fitting a plane to the muzzle nodes and calculating the normal vector. Pitch is defined here as the angle of the projectile axis in the vertical (X-Z) plane, with positive upwards. Yaw is defined as the angle of the projectile axis in the horizontal (Y-Z) plane, with positive to the right when viewing the system from above.

Projectile quantities were calculated using either the location of the projectile center-of-mass, for translations, or a line of nodes located on the projectile centerline, for rotations. The projectile center-of-mass is calculated internally by Abaqus, using information from all projectile elements. This center of mass position versus time is then used to calculate all three velocity components.

Pitch and yaw, along with their corresponding rates, were calculated using a line obtained by fitting a straight line to coordinate data for all nodes on the projectile centerline. Raw data for the projectile exhibited excessive noise that was smoothed through application of a 10-point moving average filter [70] on data output at 11.4 MHz. Note that this rate far exceeded that of the experimental equipment used (392 kHz). This output rate was chosen because it was sufficient to capture the fastest theoretical stress wave propagating axially along the barrel. It is far in excess of the rate needed to capture the larger scale motion of the barrel.

4.8.2 Jump Calculation

The models are capable of providing projectile-related ballistic quantities of interest: three velocity components, pitch, yaw, pitch rate, and yaw rate. Transverse velocities, pitch, and yaw are also available for the muzzle. While direct comparisons can be made between these values for the different centerlines, the quantitative comparisons are difficult to parse directly in terms of their effect on projectile trajectory. To attribute relative significance to the output variables it is useful to estimate each of their contributions to "jump".

Jump is defined here as the difference in angle between the nominal bore axis for a non-warped, non-drooped barrel prior to firing, i.e., the line-of-sight (LOS), and the free-flight bullet trajectory. For the purposes of this paper, 6 components are considered, 5 of which are described by Celmins [48]. These components can be used to plot a jump diagram. An example is shown in Figure 4.24 to illustrate qualitatively typical contributions to jump as defined below.

- **Warp Pointing Angle (WPA):** A novel component of this analysis, the warp pointing angle is defined as the static angle of the bore centerline at the location of the muzzle, relative to a line normal to the muzzle face. This is defined by the curve-fit equation used to smooth the experimental data and define warp in the model.

- **Static Pointing Angle (SPA):** The static pointing angle is defined as the angle between the LOS and a vector normal to the idealized muzzle face prior to firing. In terms of this simulation, this jump component accounts for the application of gravity droop to the barrel and is taken from the muzzle pitch and yaw values prior to firing.

- **Dynamic Pointing Angle (DPA):** The dynamic pointing angle is defined as the angle between the LOS and a vector normal to the muzzle face at the time of projectile exit. This accounts for barrel dynamics during the firing event and is calculated using the muzzle pitch and yaw values at the time of projectile exit.

- **Muzzle Crossing Velocity (MCV):** Muzzle crossing velocity is defined as the jump induced by lateral movement of the muzzle at the time of projectile exit. This is calculated as the arc tangent of the ratio of the transverse muzzle velocity to the projectile axial exit velocity.

- **Center of Gravity (CG) Jump:** Total CG jump is defined as the angle of the initial projectile trajectory relative to the initial LOS. Equation 4.3, based on the work of McCoy [71], may be used to estimate the total CG jump components (CG_X, CG_Y). Projectile axial, vertical, and horizontal velocities are denoted as V, $\dot{Y}$, and $\dot{X}$. This includes the effects of the four previous jump components, therefore it is beneficial to define the *relative CG jump* as the portion of total CG jump not accounted for by pointing angles or muzzle crossing velocity. Per the definition, relative CG jump is calculated by subtracting the MCV, DPA, SPA, and WPA from the total CG jump given by Equation 4.3. Hereafter, the term CG jump should be taken to refer to the relative quantity, unless otherwise noted.

$$\begin{Bmatrix} CG_Y \\ CG_X \end{Bmatrix} = tan^{-1}\left(\frac{1}{V}\begin{Bmatrix} \dot{Y} \\ \dot{X} \end{Bmatrix}\right) \tag{4.3}$$

- **Aerodynamic Jump:** The aerodynamic jump is the difference between the initial projectile trajectory and the downrange trajectory. Driven by aerodynamic forces acting upon the projectile, this can be estimated using projectile pitch/yaw behavior. Equation 4.4, also based on the work of McCoy [71], may be used to estimate the aerodynamic jump (A_X, A_Y). Pitch and yaw angles are given as α and β and have associated pitch and yaw rates $\dot{\alpha}$ and $\dot{\beta}$. System variables are barrel twist (L) and projectile mass (m), diameter (d), parallel (I_1) and transverse (I_2) mass moments of inertia, and coefficients of lift force ($C_{L\alpha}$) and overturning moment ($C_{M\alpha}$). Measurement of the two aerodynamics coefficients is difficult, leading to limited availability of data for most projectiles. Therefore, the coefficients used were taken from a similar projectile, believed to be representative of the modeled projectile.

$$\begin{Bmatrix} A_Y \\ A_X \end{Bmatrix} = \frac{C_{L\alpha}}{C_{M\alpha}} \frac{2\pi I_1}{Lmd} \begin{Bmatrix} -\beta \\ \alpha \end{Bmatrix} - \frac{C_{L\alpha}}{C_{M\alpha}} \frac{I_2}{Vmd} \begin{Bmatrix} \dot{\alpha} \\ \dot{\beta} \end{Bmatrix} \tag{4.4}$$

It is convenient to divide these six jump components into two categories, static jump and dynamic jump. The warp pointing angle and the static pointing angle are combined to define the static jump. The dynamic jump is defined as the combination of aerodynamic jump, relative CG jump, muzzle crossing velocity, and dynamic pointing angle.

4.9 Dispersion Calculation

Dispersion in impact location is a quantity of interest for all direct fire weapons. The ability to predict dispersion for different firearm configurations would represent a valuable capability. Although trajectory is most accurately calculated using a six degree-of-freedom model involving the iterative solution of partial differential equations, it is possible to approximate impact locations using the jump equation detailed in the previous subsection. Ignoring the effect of grav-

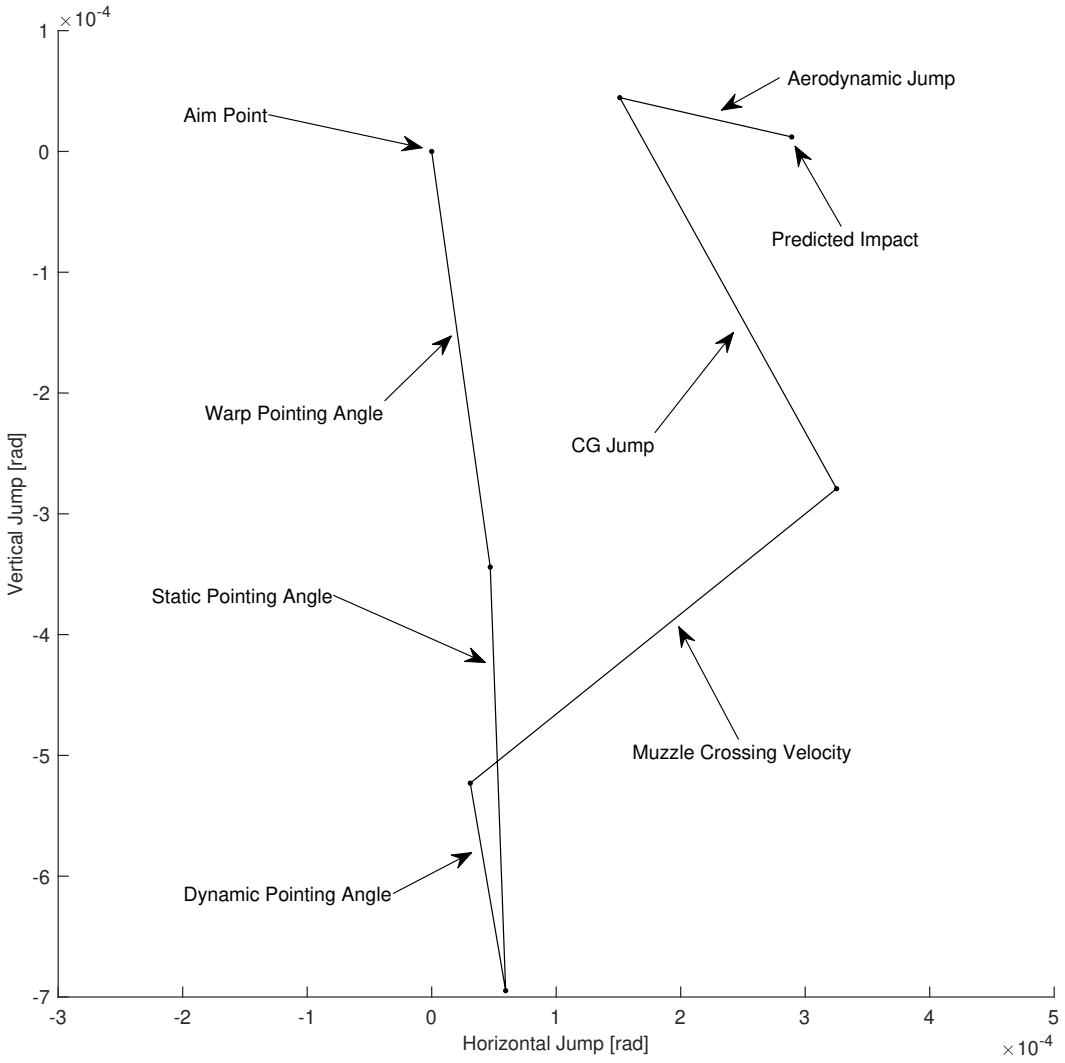

Figure 4.24: Example jump diagram showing the six individual components.

ity and assuming small angles, projectile impact locations can be predicted by multiplying the estimated jump by the distance to the hypothetical target.

An obvious approach exists wherein model input parameters are varied, the model is run, and jump is calculated for each variation. Aggregation of the impacts would then allow calculation of measures of dispersion. However, two problems are immediately evident. The first is that appropriate variation of the input parameters requires data about the underlying distribution for each varied parameter. These quantities could be estimated, or statistically significant samples obtained experimentally. The second is that computational expense is extremely high, requiring hundreds of hours of runtime per variable tested using the current model.

A method proposed by Dutschke et al. [46] was tested as a possible alternative to a brute-force approach. The method is based on the assumption that small variations in input conditions may be approximated by a small change in exit time, having a negligible impact on barrel dynamics. A number of exit times are chosen in the vicinity of the predicted exit time and the corresponding ballistic quantities for each time point are used to estimate an equivalent number of impact locations. Thus, a simulated shot group can be generated from a single run of the model.

This method was implemented in MATLAB, using the Abaqus output files as input information. Dutschke et al. did not provide the details of how the additional data points were chosen, therefore several methods were examined. There were three aspects considered when choosing the additional exit times: location of the additional data points relative to the predicted exit time, the total amount of time covered by the additional data points, and the spacing/distribution of those data points.

4.9.1 Artificial Exit Time Selection

When considering the location of the points relative to the model-predicted exit time it is attractive to consider an array of exit times centered about the

predicted exit time. Intuitively, random variations in input parameters would be as likely to cause an increase as to cause a decrease in in-bore time. However, this approach is flawed when considering the way in which loading is applied to the model. Prior to the predicted exit time the chamber, bore, breech, and projectile base are all subjected to pressure loading and the bore and projectile are interacting in contact. After the predicted exit time all of these inputs are removed, meaning that the behavior of the barrel and projectile after predicted exit are dissimilar to the behavior before. Note that it could be argued that the system response to the changes in loading is slow enough that data points immediately after exit could still provide useful information. This leads directly to the second consideration: what neighborhood of exit times should be considered?

More than one approach exists to choosing of the exit time neighborhood. One approach could be to make a semi-arbitrary choice based on time history plots of the exit parameters. Recalling the discussion above, it may be that only a certain number of data points after the exit time appear to be valid. A different approach is to choose based on experimental data. Ammunition quality is sometimes quantified through measurement of the extreme spread in muzzle velocities when fired. An expected muzzle velocity along with a measured or assumed extreme spread could be used with an internal ballistics program to calculate the spread in exit times required to produce that variation in muzzle velocities.

Finally, the number and distribution of data points must be considered. A primary factor is the frequency of data output from the finite element model. While interpolation can be used to obtain additional data for artificial exit times located between data points, the resolution of the underlying data should be considered. The intention in generating the data should also be taken into account. If the intent is to compare the response of a barrel to two different inputs, the distribution of the data points is largely irrelevant (as long as it is consistent between the two models). If the intent is to generate as realistic

a shot group as possible, then the data points should be distributed normally about the predicted exit time, with a standard deviation either assumed or obtained experimentally. Note that this approach ties back to the first consideration of whether the data points taken after projectile exit may be considered valid.

For the purposes of this thesis it was decided to only consider artificial exit times that occurred prior to the predicted exit time, the neighborhood size was calculated from an assumed velocity extreme spread, and the distribution of points within that neighborhood was uniform. These parameters were then used to attempt to validate the proposed theory. The assumed velocity spread (9.1 m/s) was based on personal experience in chronographing both factory and handloaded rifle ammunition. The uniform distribution was used to address the concerns outlined above concerning random generation of points occurring after exit time.

4.9.2 Validation of Proposed Dispersion Estimation Technique

Recall that the crux of the proposed theory is that small variations in input can be approximated as a small change in exit time, with no appreciable change in barrel dynamics. This was not feasible to validate experimentally, as exit time data could not be captured with the available experimental configuration. Therefore, an alternative method using simulation was proposed. Two models would be generated and run, with the only difference between them being a slight change in the pressure curve, such that the predicted exit times would vary slightly. Processing of the model results using the method described above would yield two dispersion plots which can then be compared using standard measures of dispersion. Two different degrees of validation were proposed. The highest degree of validation would be that for any given artificial exit time, the predicted point-of-impact would be the same (within a tolerance) between the two dispersion plots. A lower degree of validation would be that, even if

the predicted points-of-impact did not align, that dispersion characteristics for the two dispersion plots would be the same (again within a tolerance).

4.9.3 Measures of Dispersion

Two measures of group dispersion are commonly used for quantifying firearm precision: group extreme spread and mean radius (also known as average-to-center). Extreme spread (ES) is defined at the maximum straight-line distance between any two impact locations. ES is easy to measure on a physical target. However, since the extreme spread, by definition, only contains data from two points in the group, it is a relatively weak statistical tool. Average-to-center (ATC) is defined as the average distance from the mathematical center of the group to each impact location. Since the ATC values contains information from all shots in a group, it is a stronger statistical indicator of precision.

Chapter 5

Results and Discussion

This chapter presents and discusses results from throughout the course of this research effort for both experimental and numerical efforts. The first results presented are those published in Leonhardt and Garnich [72]. These results were important in developing an understanding of the importance of detailed model geometry and guided subsequent model development. Next, the results from the effort to validate the improved finite element model are presented, a combination of experimental and finite element results. In this case there is not a clear separation between model and experiment as findings from both are used to enhance findings from the other. This is followed by a discussion on the effects of bore centerline curvature, as modeled using the validated model. Finally, results of the attempt to validate a method for dispersion calculation are presented and discussed.

5.1 Effect of Model Fidelity on Barrel Dynamics

As described in Chapter 4, initial modeling was focused on discovering the degree of model detail required to obtain acceptable results. Prior to obtaining experimental data, "acceptable" was based on qualitative comparison of results from models with increasing levels of complexity. It is also true that the

increase in model complexity was necessarily accompanied by associated assumptions. However, attempts were made to either justify those assumptions, or limit them to a scope previously examined in the literature.

The premise of the qualitative comparison was that the addition of a critical model feature would noticeably change the behavior of the model. If the addition of features failed to change predicted barrel behavior it would suggest that an acceptable level of detail had been reached, regardless of quantitative values. This shouldn't be taken to mean that if the addition of a single feature failed to produce a result that no other features would be tested; it was expected that different features would have different levels of impact. However, a weakness of this early approach is that it would not necessarily capture instances were two or more features would have a combined influence, only noticeably affecting results when all were present. In an attempt to mitigate such this, the early comparison only included large steps in model fidelity, i.e. a change from only the barrel to including the barrel and receiver.

Ideally, this comparative approach would be unnecessary, as model results would be compared directly to experimental data. The qualitative comparison was put into place as a temporary approach. However, when experimental data became available, it was obtained for an incompatible set of boundary conditions.

For the qualitative comparisons, select model outputs were chosen to illustrate the effects of asymmetric geometry and off-axis mass. Due to the direct relation to projectile exit conditions, outputs were taken at the location of the muzzle. Muzzle values were preferred to values taken directly from the projectile because they were the outputs that would be used for subsequent experimental validation. Time-histories plotted in this section were calculated by averaging values across all nodes directly on the muzzle face. Outputs were normalized relative to their initial configurations in order to allow comparison between motion predicted for the model incorporating gravity and that of the others. Where indicated, results were subjected to a low-pass filter with a

cut-off frequency of 10 kHz. Projectile exit occurs at 1.33 milliseconds.

5.1.1 Transverse Muzzle Displacements

Muzzle displacements as a function of time are shown in Figures 5.1 and 5.2 for the vertical and horizontal planes, respectively.

The vertical results show the importance of asymmetric features in relation to transverse motion of the muzzle. Model 1, the barrel only model, behaved as expected. The model, apart from the rifling, is axisymmetric and an idealization of a perfect barrel. Pressure and projectile loading alone have minimal impact on the displacement of the muzzle for balanced projectiles, evidenced by the minimal deflection of Model 1. The very small displacements that are present are likely due to numerical noise arising from small asymmetries in the mesh and the non-linear contact between the barrel and projectile. The lack of barrel movement increases confidence in both the geometry and loading.

Notable displacements appear with the addition of a breech face and asymmetric geometry in Model 2. These additions cause significant upward deflection of the muzzle at projectile exit, a trend opposite that of the models incorporating additional off-axis mass. The addition of barrel droop does not significantly impact the vertical motion of the muzzle. However, the static deflection is significant and Model 4 data has been shifted vertically by 194 microns to remove the effect of gravity and allow direct comparison of the dynamic deflections.

When considering the horizontal plane, deflection is again minimal in the barrel-only configuration. Compared to the vertical deflection, where the pillars fundamentally altered the response, Models 2-4 display qualitatively similar behavior. This indicates that the most important consideration for horizontal vibration is receiver asymmetry. Note that the vertical deflections are an order of magnitude larger than the horizontal deflections, a result that again reinforces the importance of center-of-mass location relative to the line of action of the recoil force.

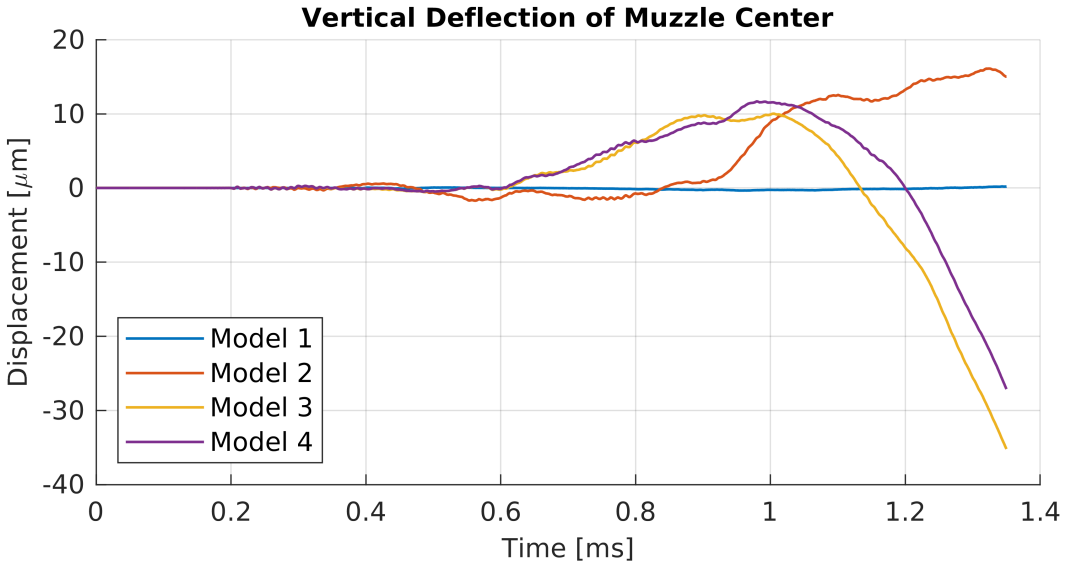

Figure 5.1: Time history of muzzle deflections in the vertical plane.

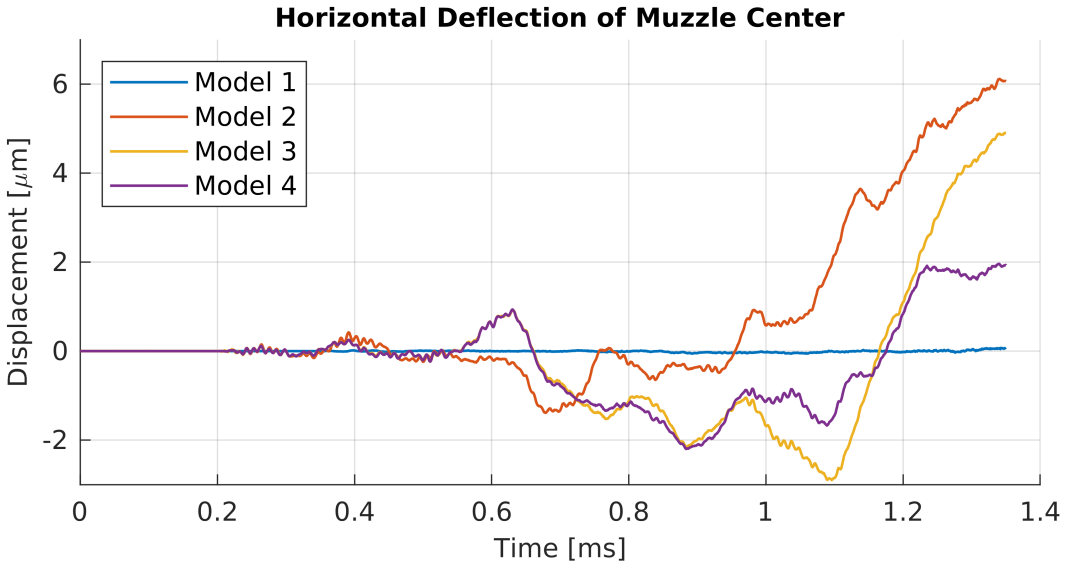

Figure 5.2: Time history of muzzle deflections in the horizontal plane.

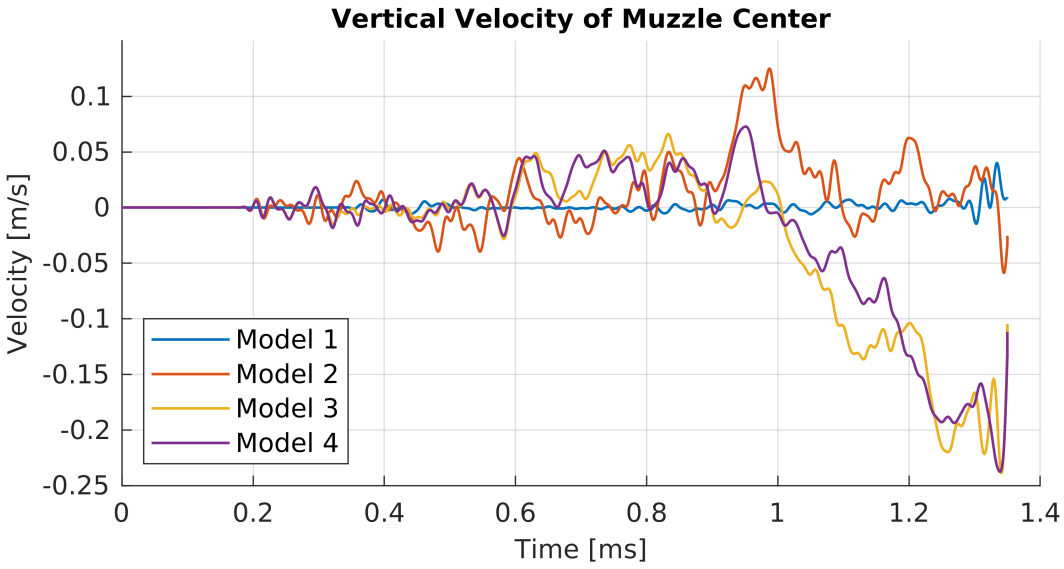

Figure 5.3: Time history of lateral barrel tip velocity in the vertical plane.

5.1.2 Transverse Muzzle Velocities

The exit condition of the bullet is most directly related to the orientation and transverse velocity of the barrel muzzle. Transverse muzzle velocity results exhibited significant high frequency content and was subjected to a low-pass filter with a cutoff frequency of 10 kHz to facilitate examination of general trends. Velocity of the muzzle in the vertical and horizontal directions is shown in Figures 5.3 and 5.4, respectively. Trends in the velocity results are very similar to those in the deflection data. That is, response in the barrel-only model is small relative to the other simulations (as expected) and in this instance the presence of off-axis mass is the most relevant predictor of greater barrel motion. When considering the vertical results this is present for Model 2 (receiver only) and dominated by the added pillars for Models 3-4. As later seen, details of the structural stiffness also have a non-trivial influence on the magnitude of barrel motion, but it is small compared to the change from the models with no off-set mass to those with. The horizontal results for Models 2-4 are also affected by geometric asymmetry and its associated small mass imbalance.

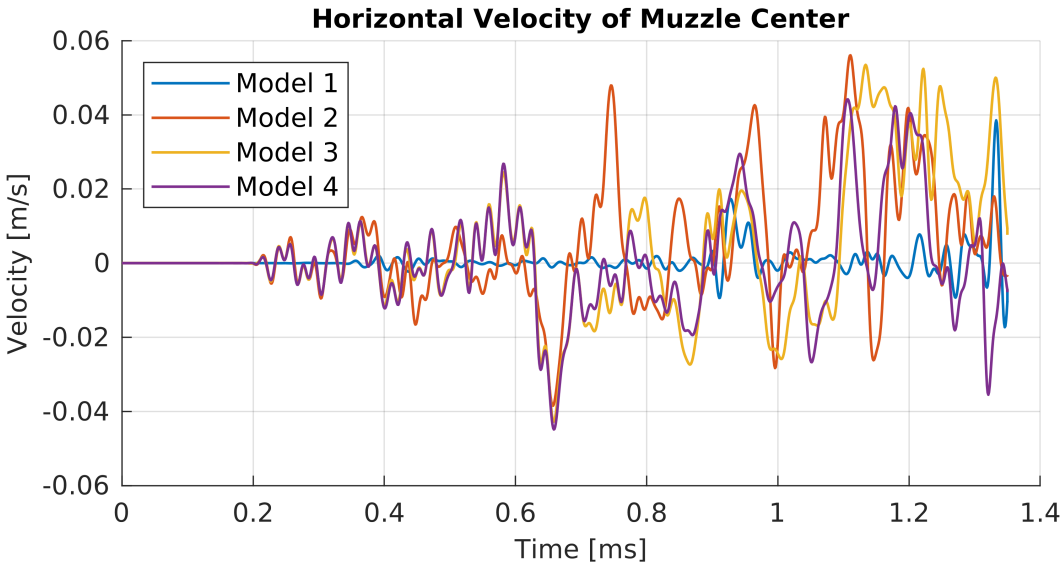

Figure 5.4: Time history of lateral barrel tip velocity in the horizontal plane.

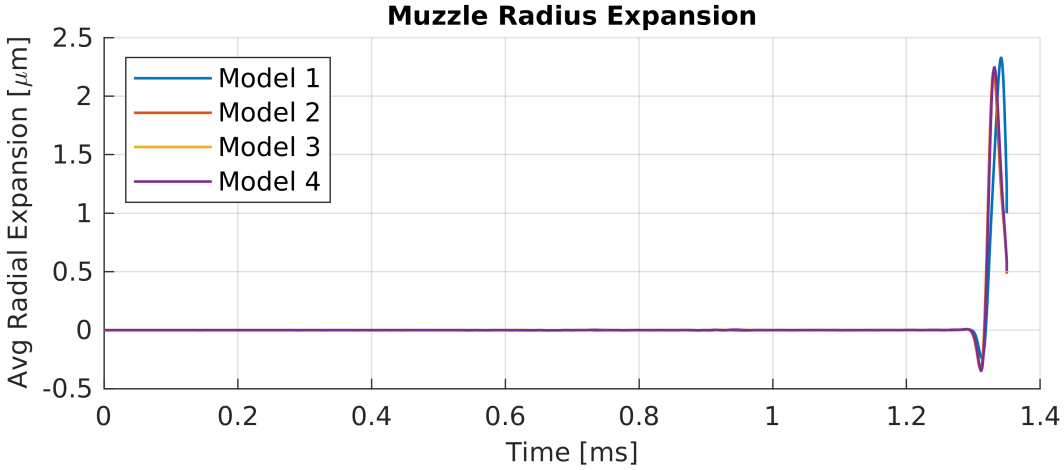

Figure 5.5: Time history of the change in muzzle radius.

5.1.3 Muzzle Expansion

Radial expansion of the muzzle is shown in Figure 5.5. This value was calculated using the average radial coordinate for all muzzle nodes at each output time. As with the lateral velocities, this output was subjected to low-pass filtering at 10 kHz. No significant difference in radial expansion exists between the four models, with the defining feature being a contraction preceding the projectile followed by an expansion directly coincident with the bullet. As expected, radial expansion is independent of external masses and geometries. This qualitatively provided a small amount of validation to the model.

5.1.4 Muzzle Rotations

Considering data from all nodes on the muzzle face allows calculation of muzzle rotations, with pitch and yaw shown in Figures 5.6 and 5.7, respectively. Model 1 exhibits minimal pitching and yawing motion. This was expected, as with muzzle deflections; nothing exists to induce lateral (vertical or horizontal) vibration. The recoil force on the breech-face, in combination with mass asymmetries, has the largest influence on overall pitch behavior. However, results for Model 2 differ from those of Models 3 and 4. In this case, the recoil couple induced by the presence of off-axis masses is enough to drive a substantial difference in vibratory behavior. Models 3 and 4 have a similar pitch response, but differ in value at projectile exit. The difference in final values is thought to be caused by the straightening effect of projectile and pressure acting counter to gravity-induced barrel droop (Bourdon effect). The same effect is present when considering vertical deflections. The Model 4 pitch data has been shifted 0.398 milliradians upwards to remove the static rotation due to droop. Differences in yaw behavior for Models 2-4 (those containing off-axis mass) are small relative to those for pitch. This again is an expected behavior, the amount of mass asymmetry in the horizontal plane does not change between the three models. Therefore, any visible difference is driven by a coupling with an effect acting in the vertical plane.

5.2 Modal Analysis

A simple modal analysis was run to obtain mode shapes and natural frequencies for barrel vibrations in the vertical plane. When including the full model geometry, the first, second, and third modes occurred at frequencies of 122 Hz, 345 Hz, and 668 Hz, respectively. The corresponding deflected shapes are shown in Figures 5.8, 5.9, and 5.10. These frequencies are reasonable, being somewhat lower than those discussed by Vaughn (third mode of 1250 Hz) who used a much lighter rifle and barrel [65].

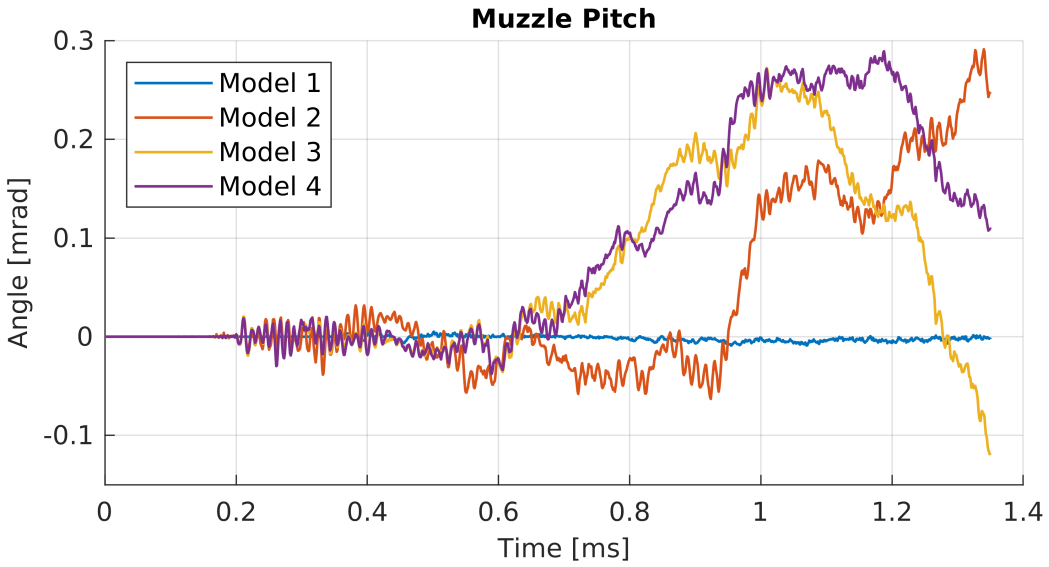

Figure 5.6: Time history of muzzle angle in the vertical plane (pitch).

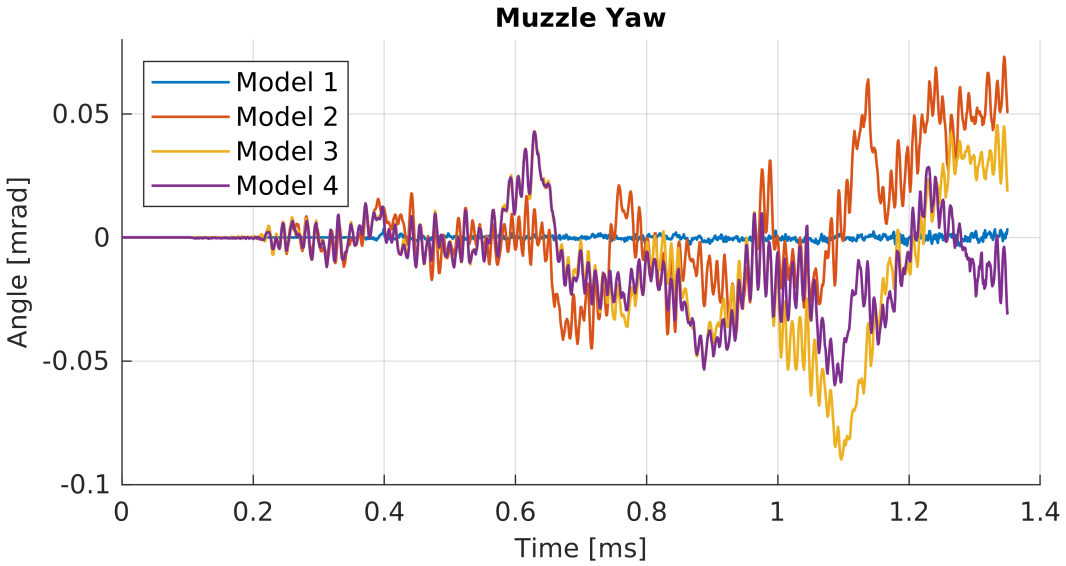

Figure 5.7: Time history of muzzle angle in the horizontal plane (yaw).

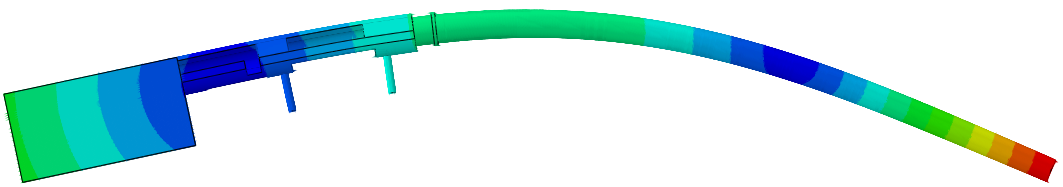

Figure 5.8: First vertical bending mode, occurring at 122 Hz.

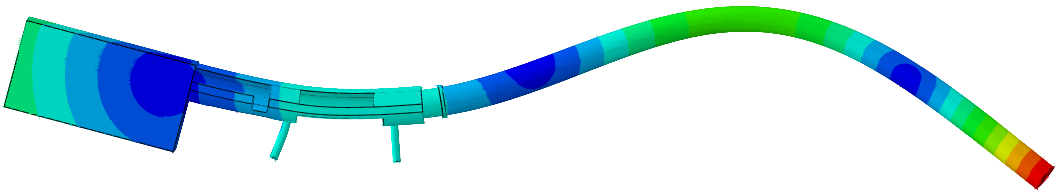

Figure 5.9: Second vertical bending mode, occurring at 345 Hz.

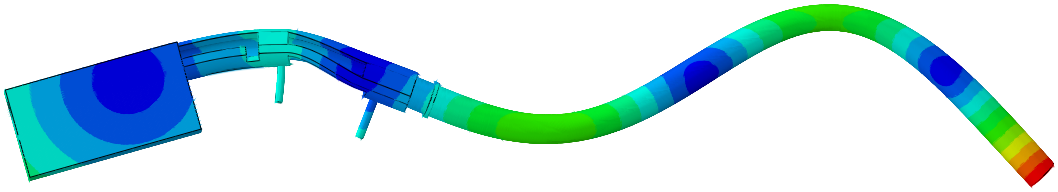

Figure 5.10: Third vertical bending mode, occurring at 668 Hz.

5.3 Vibration Measurement and Modeling

This section focuses on the more detailed model detailed in Chapter 4 along with the experimental validation efforts.

Recall that the breech pressure was calculated using QuickLOAD and the pressure gradient from there to the base of the projectile is determined based upon the Lagrange approximation. The results show a discrepancy between projectile motion predicted by QuickLOAD and that predicted by the FE model. The comparison of projectile displacement and velocity predictions is shown in Figure 5.11. It appears that the resistance to motion caused by engraving causes the FE model predicted velocity (807 m/s) and position to lag slightly behind that predicted by QuickLOAD (817 m/s). Experimentally measured average muzzle velocity for five shots was 825 meters per second.

5.3.1 Baseline Results

Vertical barrel deflection near the barrel tip was chosen as the primary object of this study, as the larger displacements, compared to horizontal motion, are more easily measured. Attempts to capture horizontal motion experimentally were largely unsuccessful, as discussed in Chapter 3. The limited data that was gathered is included below. Deformed barrel geometry is shown in Figures

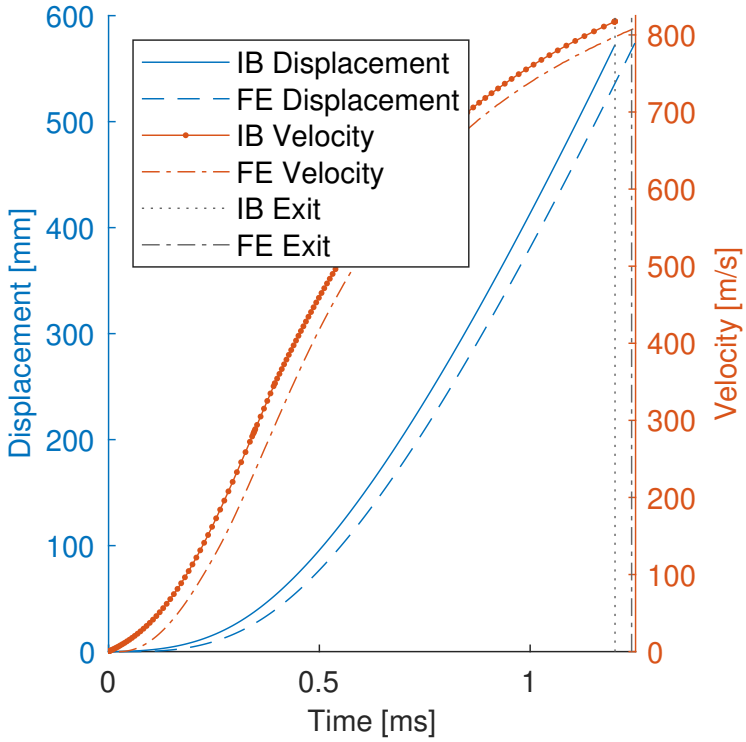

Figure 5.11: Comparison of projectile displacement and velocity curves for internal ballistic prediction and FE model outputs.

Figure 5.12: Gravity deformed initial barrel shape.

5.12, 5.13, 5.15, and 5.14 for four different points during the in-bore period. All deformations shown are scaled by a factor of 100.

Model data was extracted from a point corresponding to that measured in the experiment, in this case 50 mm behind the muzzle. All experimental results have been subjected to smoothing via moving neighborhood averaging with a window of 8 data points (≈ 20 μs) in order to remove high frequency noise from the data. Figure 5.16 illustrates the effectiveness of this approach, accurately capturing the time history while removing excess noise.

Figure 5.13: Deformed barrel shape at 0.7011 milliseconds.

Figure 5.14: Deformed barrel shape at 1.168 milliseconds.

Figure 5.15: Deformed barrel shape at time of exit.

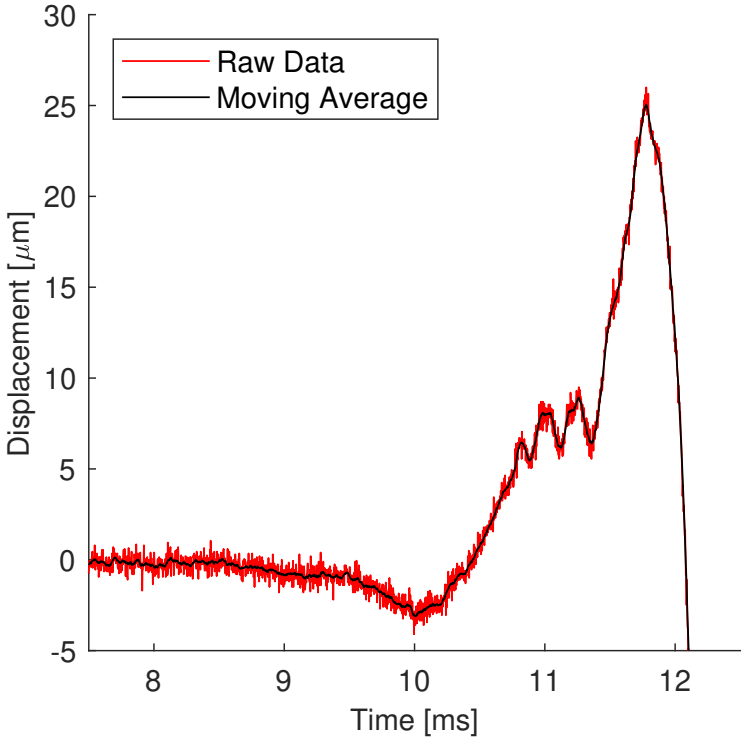

Figure 5.16: Example of the moving average smoothing applied to vertical barrel motion.

Predicted transverse displacements in the vertical plane are shown alongside experimentally measured values in Figure 5.17. Pressure is applied beginning at time 0, with projectile exit occurring at 1.24 milliseconds. Note that no movement is visible until roughly 0.25 ms after the application of pressure. As a pressure wave only transmits axial deflections, a shear wave is required to generate transverse deflections measured by the vibrometers. Barrel length and Equation 5.1 [73], with c_{shear} representing shear wave speed, G representing the shear modulus and ρ representing density, allow calculation of the time for a shear wave to reach the muzzle. Thus, transverse displacements at the muzzle can be estimated to be delayed by about 0.2 ms from the time of an excitation force near the breech. The additional <0.1 ms delay before measurable output is due to the wave needing to be of sufficient transverse amplitude to be detected.

$$c_{shear} = \sqrt{\frac{G}{\rho}} \tag{5.1}$$

In addition to the model predicted results, Figure 5.17 shows experimental results from three different test firings. The experimental configuration did not include a mechanism to capture either ignition time or projectile exit time, therefore the curves were positioned based on defining characteristics (high frequency content near the 11 millisecond mark). The repeatability of the curve features gives some confidence that they are correctly aligned. The results in Figure 5.17 are positioned relative to one another based on the main peak seen at 1.4 milliseconds. Time zero is defined by the initial application of pressure in the model. The curves exhibit several similarities in features. The main displacement pulse in the 1.0-1.5 millisecond range is of similar frequency and amplitude. There is a higher frequency, smaller amplitude contribution that begins at about 0.3-0.4 milliseconds and is present in both the experimental data and the model results. However, the frequency is >10% different ($\approx$ 3.7 kHz for the model, $\approx$ 4.2 kHz for the experiment), and the peaks and troughs do not align temporally. Additionally, there appear to

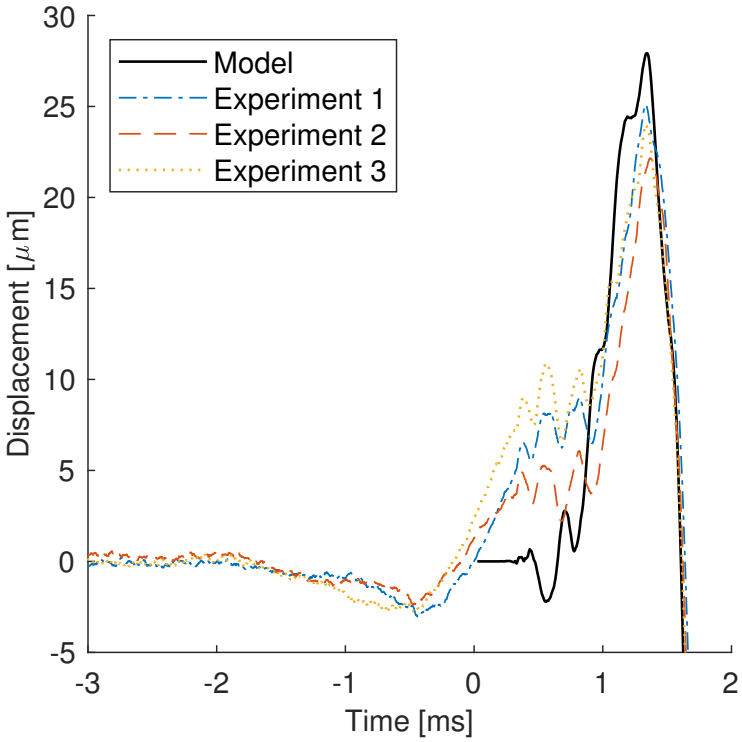

Figure 5.17: Comparison of predicted vertical displacement to experimentally measured results obtained 50.4 mm behind the muzzle.

be some early contributions to motion that are not captured by the model. If the model data and the experimental data in Figure 5.17 are correctly aligned temporally then it is clear that motion begins prior to time zero in the model. Since the model assumes nothing happens prior to ignition of the main charge, it suggests looking to earlier events that could contribute to barrel motion.

Figure 5.18 shows two horizontal traces compared to model predicted horizontal motion. Both acquired using the modified (polymer nut) method previously described, these represent the only successful captures of horizontal movement. The experimental data and model predictions agree in only the most general sense, with the model greatly over-predicting the amplitude of movement. It is not immediately obvious to what degree this should be attributed to model error over measurement error.

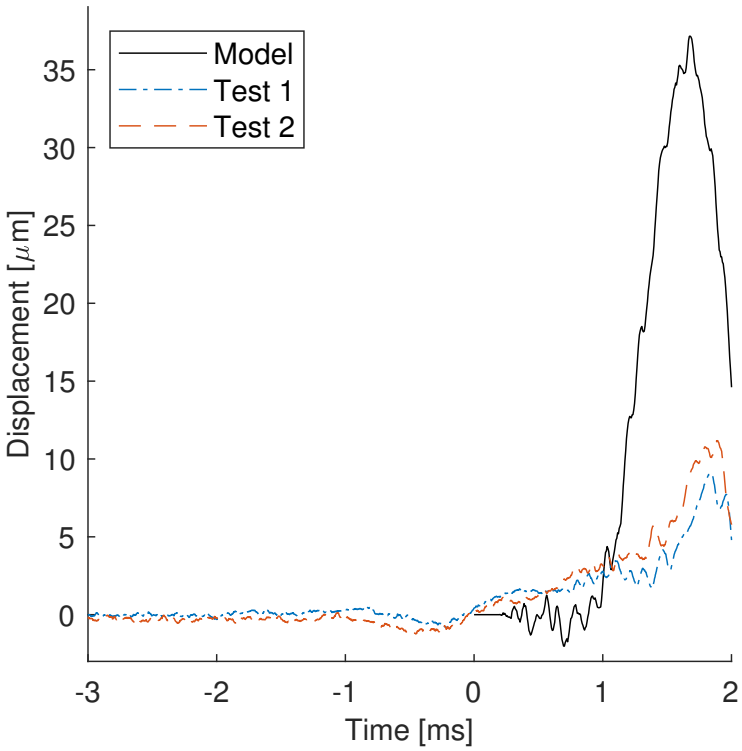

Figure 5.18: Comparison of model predicted horizontal displacement and two experimental measurements.

5.3.2 Effect of Pneumatic Bladder Inflation

Inflation of the bladder used for trigger actuation caused minimal drift over the 1.5 second sampling window (Figure 5.19). Over this period the total drift is roughly 25% of barrel displacement expected during the in-bore period, but this takes place over a period of time three orders of magnitude larger. During the shorter in-bore period (approximately 1.5 ms) a very small amount of positive slope is almost overwhelmed by noise in the measurement. The drift can be assumed linear and is compensated for based on the principle of superposition and the slope of the data immediately prior to the period of interest. Illustrating this principle, Figure 5.20 shows a 1.5 ms period taken from the steepest sloping portion of Figure 5.19. Ignoring the noise, the overall trend is linear.

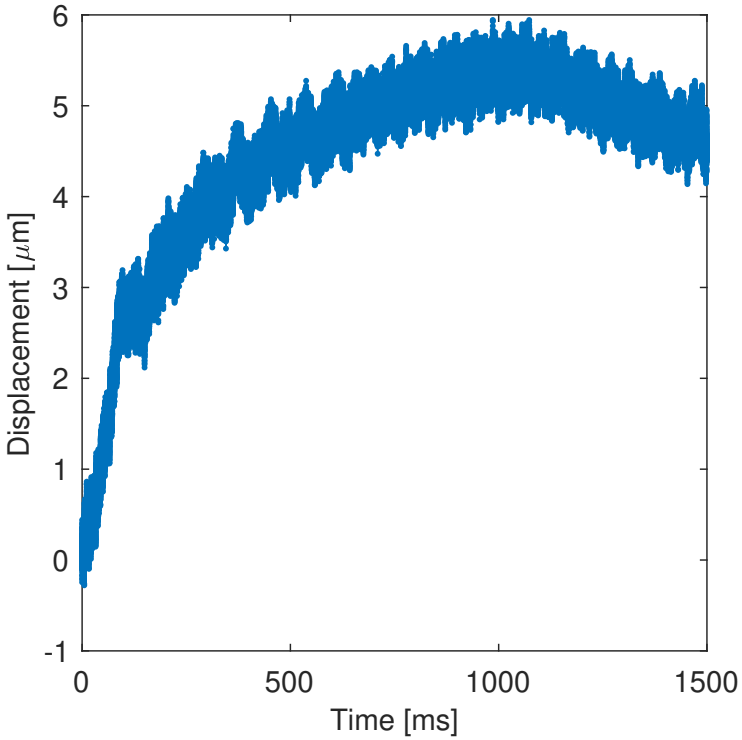

Figure 5.19: Vertical displacement as a result of the trigger actuation mechanism over a long 1.5 second period.

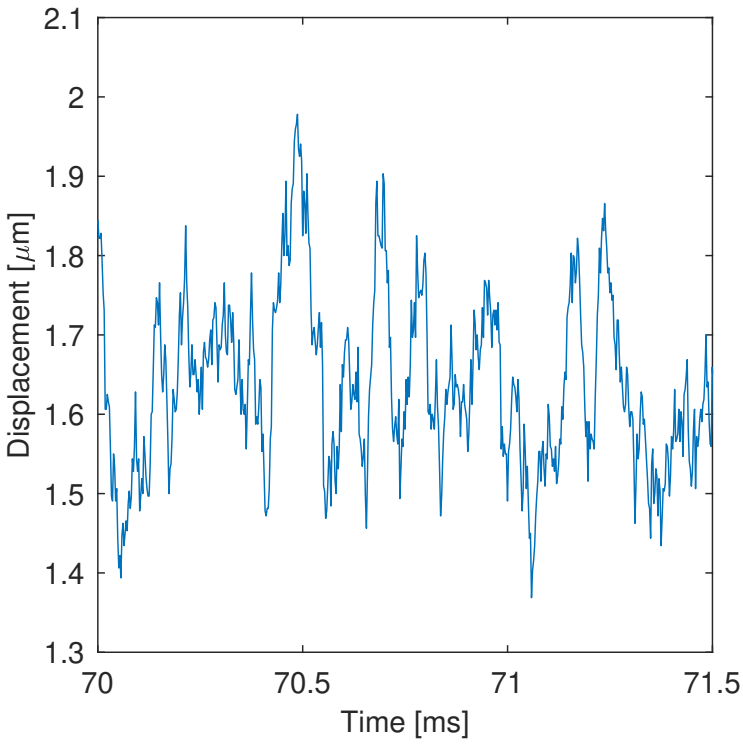

Figure 5.20: Vertical displacement as a result of the trigger actuation mechanism over a short 1.5 millisecond period.

5.3.3 Effect of Primer Impulse

Troubleshooting of the model during development had revealed that the presence of higher frequency content in barrel displacement was related to the initial slope of the pressure curve. If taken directly from QuickLOAD, the breech pressure curve begins with a non-zero value. Seen by the model as an essentially infinite acceleration, this excited higher frequencies that a more realistic pressure curve beginning at zero did not. Indeed, a more gradual rise in pressure would result in little or no higher frequency content in the transverse vibration. Therefore, the breech pressure curve was adjusted to start at zero while maintaining the same area under the curve. This prior experience indicated that the sharp spike of a primer impulse is a possible driver for higher frequency vibration modes.

As discussed in Chapter 2, research by others [10] has been conducted on the interaction between the primer, the propellant bed, and the projectile. While it is not feasible to conduct a firing experiment where this interaction is absent, this is the situation that was initially modeled. Comparison can be made between the results of a model with a primer impulse and one without. Shown in Figure 5.21 is a comparison of predicted barrel movement for the different input pressure curves discussed in Section 2. Seen in the 0.2 to 0.45 millisecond timeframe, the addition of the primer impulse causes high frequency vibrations to appear sooner and at a time consistent with the result from Equation 5.1. Additionally the vibrations appear to be of higher frequency, although apparent destructive interference in the 0.5-0.6 region complicates calculation of the exact change in frequency.

When results for the model including the primer pulse are overlaid with experimental data (Figure 5.22), the predicted displacements are a qualitatively better fit to the experimental data relative to the comparison in Figure 5.17. In particular, some of the destructive interference of different frequencies appears as in the experimental data. Here, the term “better fit” is used relative to higher frequency content, as opposed to the overall shape of the curves.

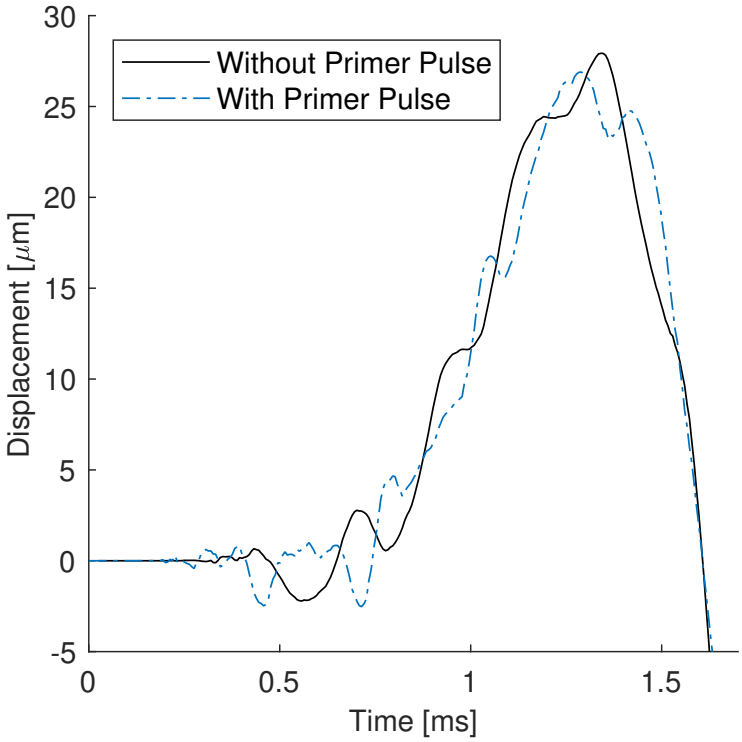

Figure 5.21: Comparison for predicted vertical displacement with and without primer pulse.

Focusing on response in the 0.1-0.9 ms timeframe, both the experimental data and the model with primer exhibit similar frequency. While not conclusive, these results suggest that high-fidelity prediction of barrel movement requires accounting for the primer impulse.

5.3.4 Effect of Firing Pin

While the primer impulse occurs prior to the ignition of the main charge, it does not occur soon enough to cause the early motion discussed in Section 5.3.1. The possible influence of the firing mechanism on barrel dynamics has been largely neglected in the scientific literature but was investigated as a cause of barrel vibration by Vaughn [65]. Shown in Figure 5.23 are displacement measurements taken during dryfire (firing pin dropped on an empty chamber), measured at the same location as for the previous figures. Both the qualitative and quantitative repeatability are good.

Figure 5.24 shows results from similar tests performed with primed cases

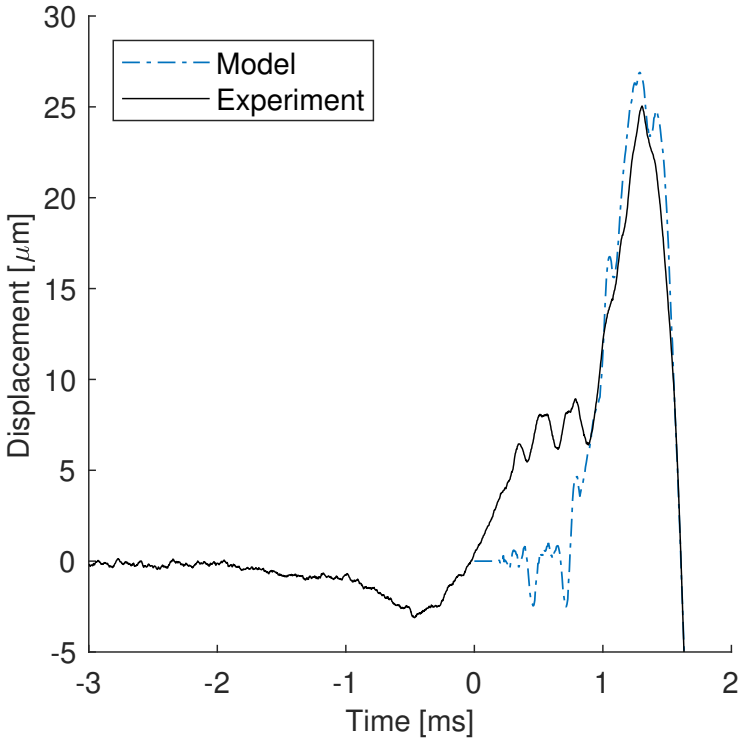

Figure 5.22: Comparison of the FEA results incorporating the primer pulse with the experimental data (Test 1).

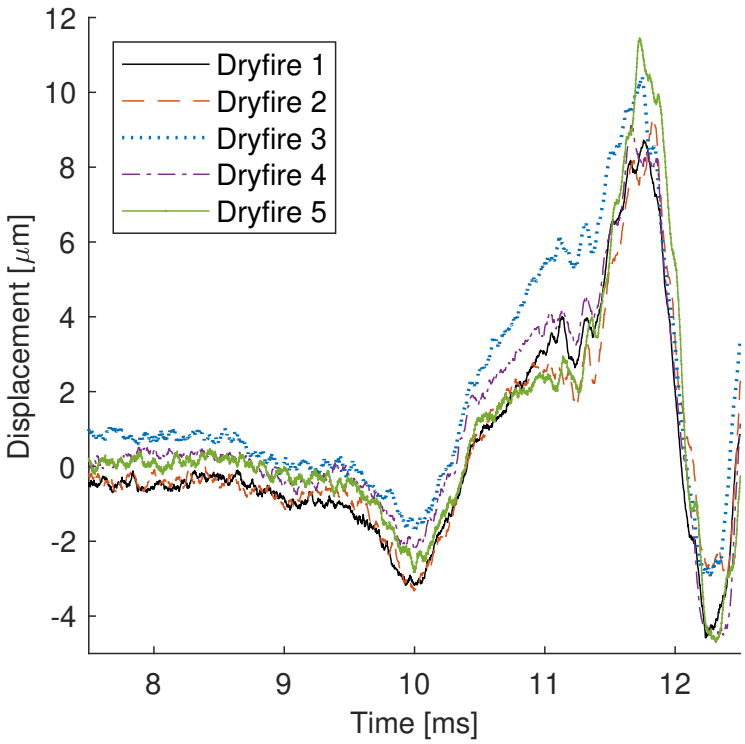

Figure 5.23: Experimentally measured vertical displacement due to dryfire, 50.4 mm behind muzzle.

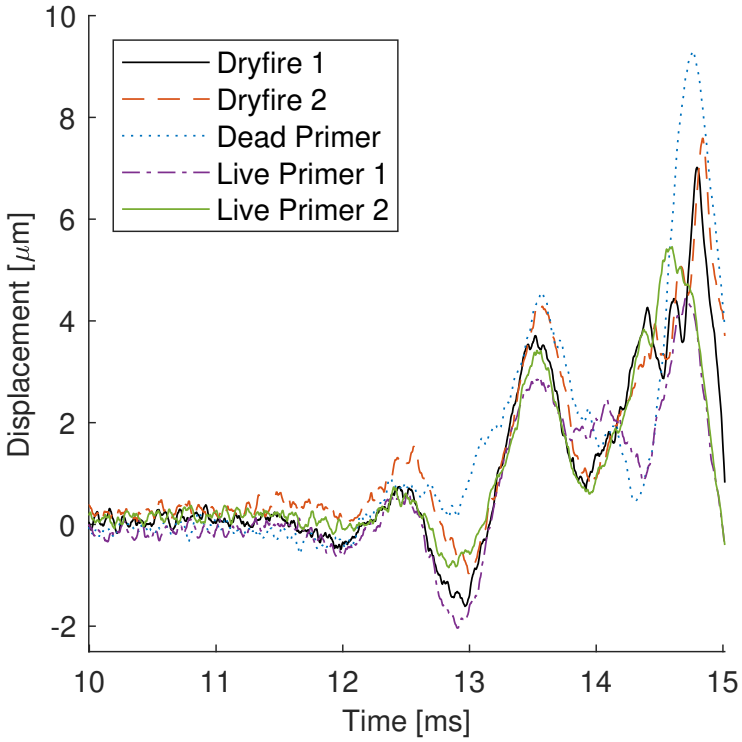

Figure 5.24: Experimentally measured vertical displacements for dry-fire on an empty chamber, on a dead primer, and on a live primer.

(both live and dead) in the chamber. In this instance all measurements were taken at a location 150 millimeters from the muzzle. The results of these tests were not significantly different from the empty chamber results, especially early in the time history. For reasons that aren't clear, the dead primer exhibited the largest deviation in behavior from the other data series. Overall, these findings suggest that the impact on the primer itself does not contribute significantly to barrel vibrations, rather the firing pin itself. A likely explanation for this behavior is that the energy of the firing pin travel is absorbed primarily through impact with the bolt, not through indentation of the primer.

Figure 5.25 shows a representative dryfire curve (Dryfire 1) overlaid on both the model predicted results and a representative livefire curve. It is apparent that the early movement seen in the experimental data but not visible in the model results matches almost exactly with the early portion of the dryfire curve (7 to 10.5 milliseconds). This indicates that the trigger/firing pin mechanism is responsible for movement early in the firing cycle that the model is currently

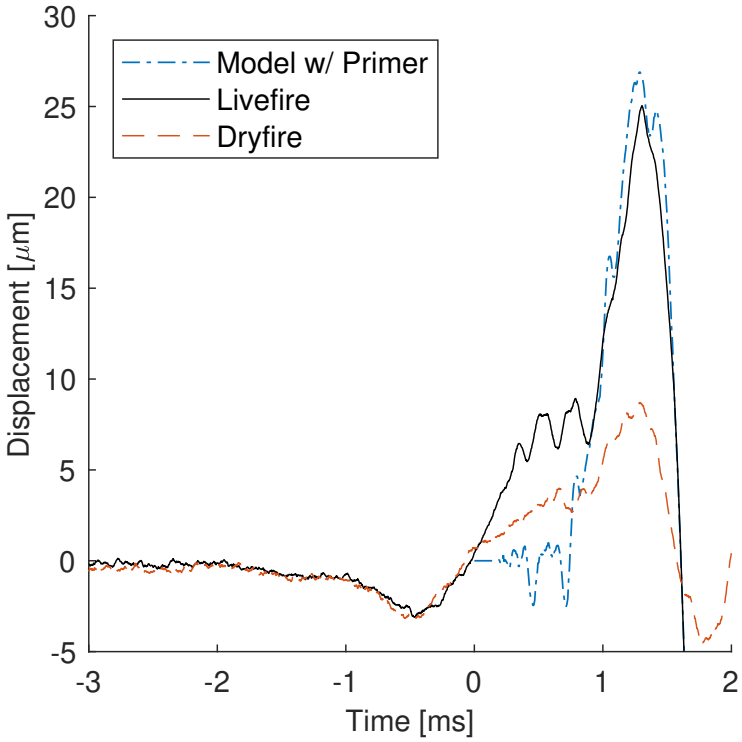

Figure 5.25: Comparison of vertical displacements for the model incorporating the primer pulse, livefire data (Test 1), and dryfire data (Dryfire 1).

not capable of accounting for. Furthermore, the relative magnitudes of the remainder of the curves suggests that the firing pin impact alone is responsible for a significant portion of the vertical barrel displacement seen during the in-bore period.

Figure 5.25 also contains results from the finite element model. In this case the model was run with the pressure curve incorporating primer effects. A simple summation of the model data with the dryfire curve would yield a curve closer to the experimental data than either alone, but would still underpredict the livefire data from 0.1-0.9 ms and overpredict beyond that point. This either indicates that the relationship between the response to the firing pin impact and the response to gas pressure/projectile is more complex than originally thought (such that simple superposition is not valid), or one or more other factors are yet to be accounted for.

A second possible effect of firing pin motion is visible in Figure 5.25, from approximately 8.5 ms to 10 ms. Prior to that time barrel motion is minimal; 8.5

ms marks the beginning of a decreasing slope. Recalling the method detailed in Chapter 3 for estimation of lock time, the RPR is estimated to have a lock time of 2.4 milliseconds. Recognizing that the firing pin spring will convert stored potential energy into kinetic energy over the course of that period, not in a infinite impulse, it seems likely that the slope in the 8.5-10ms regime is a direct result of the firing pin acceleration.

5.3.5 Effect of Stiffened Receiver

Two variants of the model included an artificially high receiver modulus in order to ascertain whether or not omission of certain assembly components, such as the scope rail and lower receiver, had the potential to noticeably impact barrel displacements. The Picatinny scope rail is a strip of aluminum affixed to the top of the receiver using screws. The lower receiver is fitted to the bottom of the action/upper receiver and is also attached with screws. Beyond performing their intended functions, both components also act to structurally stiffen the upper receiver. An increase in the modulus was chosen as a proxy for this stiffening effect.

Figure 5.26 compares four curves: an experimental livefire data curve, the standard (steel) stiffness model result summed with a dryfire curve, a double stiffness model summed with a dryfire curve and a triple stiffness model summed with a dryfire curve. This summation uses the model prediction with primer pulse shown in Figure 5.21, which was spliced and summed with the dryfire data from Dryfire 1 (Figure 5.23) for each iteration. The double and triple values were not meant to directly represent either of the missing components, but to act as a proof-of-concept in investigating the importance of the receiver stiffness.

For the standard stiffness this is the same as a direct summation of the "Model w/Primer" and "Dryfire" time histories shown in Figure 5.25. This was repeated for versions of the model where the receiver modulus was increased. The artificial stiffness causes a reduced amplitude of the main peak of the

curve and affects the high frequency response. The alignment of curves during superposition also changes the apparent high-frequency response. Note that changing the receiver material stiffness has effects beyond increasing the overall resistance to bending. It also increases the speed of sound in the material, affecting both the minimum time step for those elements and high frequency vibrations. With that in mind, the time-history plots are obtained roughly 600 millimeters from the receiver and the magnitude of the primary peak was the quantity of interest in this exercise. In terms of overall amplitude, the two stiffened model results bracket the main impulse in the experimental data when attempting to account for the effects of the firing mechanism. This suggests that the level of detail currently present in the model is not sufficient to accurately predict barrel dynamics during firing. Additional components of the rifle assembly should be included to correctly capture the overall structural stiffness. Consideration should also be given to the rotational inertia of the model, though the relative importance of the two values was not investigated.

5.3.6 Validation Summary

Of note, no other published work appears to show this level of agreement between model and experiment for transverse barrel displacements during the in-bore transient. This instilled confidence that the model could be used for further parametric study of gun barrel dynamics. Furthermore, it suggested that enhancement of the model to include movement of the firing pin could achieve unprecedented quality in gun barrel dynamics prediction. However, the ad-hoc accounting for the primer impulse (splicing together of experimental and modeling data), firing pin impact, and structural stiffness shows there are still notable differences between the model and experiment in the 0 to 0.8 millisecond timeframe. This suggests that some additional factor may still be unaccounted for. It is also possible that the principle of superposition does not apply in this situation.

The comparison between modeling and experimental results is based on

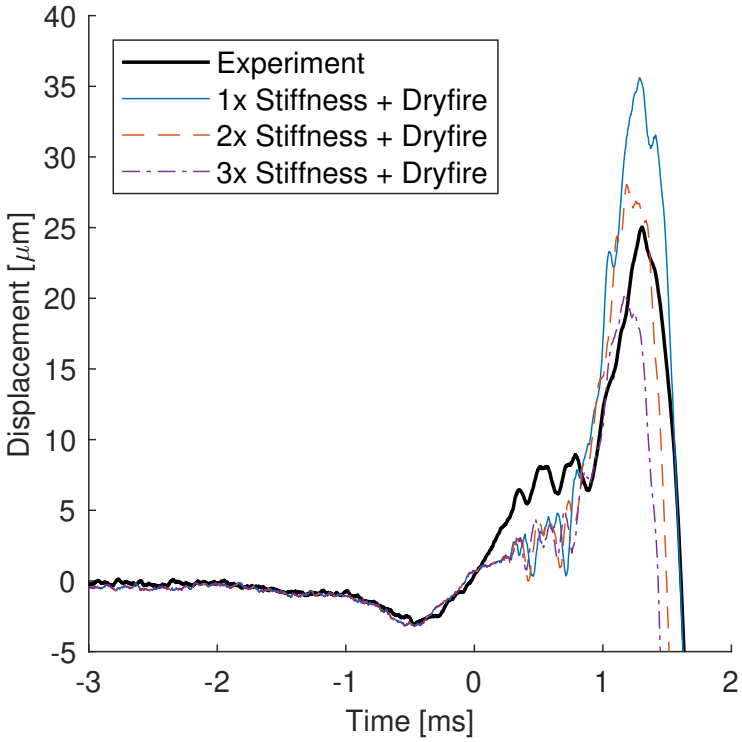

Figure 5.26: Comparison of artificially stiffened action with action using real properties. Both data sets are augmented with a firing pin impulse and overlaid with experimental data (Test 1).

the assumption that the gun supports in the experiment are not significantly affecting the measured transverse barrel displacements during the short time before the projectile exits the bore. Or, put another way, that the change in external forces at the supports during the in-bore period is small compared to the internal and inertial forces acting on the system. The good agreement between model and experiment suggests this assumption is reasonable. However, the model predicts that in the absence of external resistance the gun will recoil approximately 2 mm during the in-bore transient. In the model, only inertial forces resist motion of the gun while in the experiment there are two locations of external support that can generate horizontal friction forces and vertical normal forces in response to recoil motion. Soft foam padding was used to help keep the firearm upright during firing, which could also have a minor influence. Further investigation of the validity of this assumption could include modifying the experiment to include innovative supports that

further minimize external resistance to gun rigid body motion. Alternatively, the model could be modified to more realistically represent the physical supports employed in the experiment and the evolution of contact forces. These changes could facilitate comparison of results for lengths of time greater than the in-bore period.

Prior to the addition of droop displacements, the present model assumed a perfectly straight bore centerline. It is known [44] that high velocity projectiles forced to follow a curved centerline will generate lateral forces. This was another potential source of discrepancy between model and experimental results and led to further research.

5.4 Centerline Curvature

This section addresses the model results produced when including the various warped centerlines in the model. Multiple possible approaches exist to analyzing the impact of warp on simulation results. One approach is to examine direct changes to various model outputs such as muzzle deflection. However, it is not immediately obvious what these changes in output mean in terms of projectile behavior down-range, or how changes in different outputs interact. A second approach is to combine the various outputs using the jump equations to yield outputs that are more easily compared between centerlines. Stated differently, this is a method of converting kinematic variables whose relative importance is difficult to assess, into individual contributions to jump which is a metric of general interest and provides a means of assessing the relative importance of different variables.

5.4.1 Barrel Dynamics

Barrel motion due to interior ballistics is caused by two factors. Primarily, barrel dynamics are driven by internal pressure that radially expands the barrel while accelerating the combustion gases and projectile, with an equal and

opposite reaction accelerating the rifle rearward. This recoil force is eccentric to the mass center of the firearm, causing a recoil moment that flexes the barrel into transverse vibration modes. This aspect of barrel motion is nominally the same for each simulation reported here. The second contribution to barrel motion is due to interaction forces with the balloting projectile. The ratio of barrel to projectile mass is approximately 200:1 and barrels are generally straight, with angular deviation generally less than 1 milliradian. This results in balloting forces having a relatively small contribution to barrel motion.

Consequently, it is expected that the angle of the warp at the muzzle will affect the projectile jump but not affect barrel dynamics. This is because the angle of warp at exit directly affects the pitch and yaw of the projectile. However, the angle of the warp at the muzzle cannot affect barrel dynamics during the in-bore transient because neither the projectile or the high-pressure propellant gases interact with that portion of the barrel until the time of exit. Muzzle displacements for a range of time close to muzzle exit for both the vertical and horizontal planes are shown in Figures 5.27 and 5.28, respectively. These results show small changes in both planes, with changes in the vertical being more pronounced.

Due to the complexity of barrel dynamics, it is not necessarily expected that a clear correlation should exist between the overall centerline deviation and the muzzle exit condition. In the vertical plane, all warped centerlines produced a smaller positive displacement compared to the baseline. The relative changes in vertical displacement do not correspond with the relative degree of warp present in each centerline. Referencing Figure 4.14, Centerline 1 exhibits the largest degree of warp, followed by Centerline 2, with the remaining three centerlines more closely clustered. Referencing Figure 5.27, Centerline 1 does exhibit the largest deviation from the baseline behavior, but Centerline 2 shows the least deviation at time of exit and a tightly clustered intermediate deviation with the other three. Overall, it seems to be question of why Centerline 1 deviates from the other 4 centerlines to the degree seen. One possiblity is that

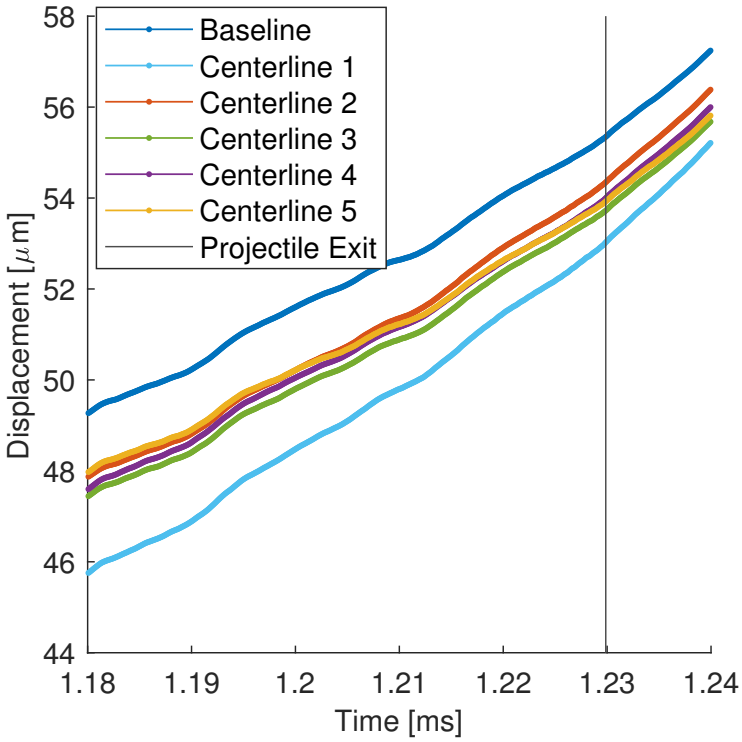

Figure 5.27: Vertical muzzle displacement near projectile exit.

Centerline 1 deviates to such a degree that some threshold is reached, triggering some change in dynamic behavior. As implemented, Centerlines 1 and 2 have similar initial and final slopes as well as overall degree of deformation. It is important to keep in mind that these centerlines were obtained from match-grade barrels, all five centerlines are relatively straight, and the deviations seen in Figure 5.27 are so small that they are within the measurement resolution of the experimental equipment used in this thesis.

Deviation from the baseline is so small as to be negligible in the horizontal plane. However it can be noted that centerlines 2, 3, and 5 start positive in warp angle (pointing to the shooter's left) and go negative (pointing to the shooter's right) in the second half of the barrel while centerlines 1 and 4 have the opposite trend. These groupings can be seen in Figure 5.28 at the time of muzzle exit.

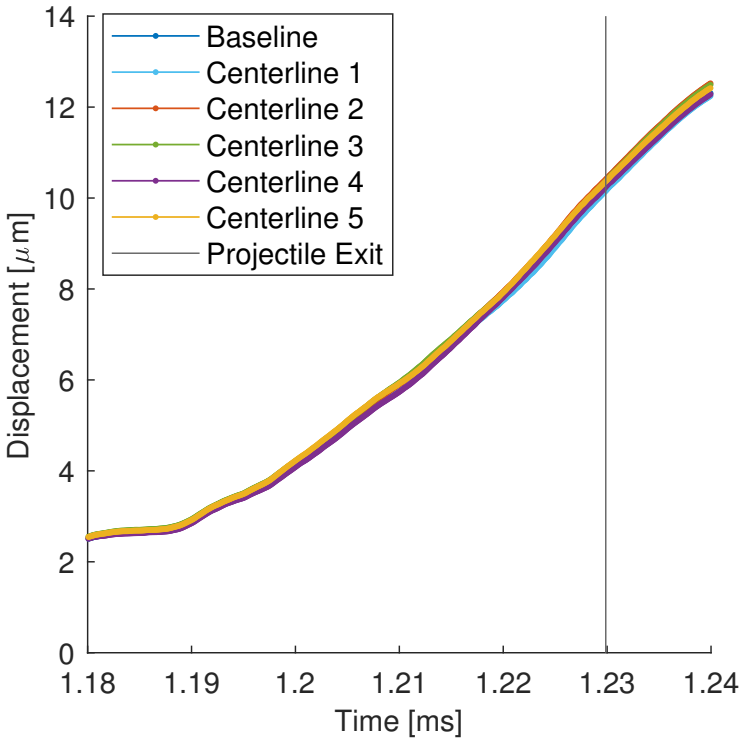

Figure 5.28: Horizontal muzzle displacement near projectile exit.

5.4.2 Jump Associated with Assorted Centerlines

Figure 5.29 shows the calculated jump components for six simulated barrels: a control barrel with no warp, denoted *Baseline*, and five barrels incorporating the measured centerlines, denoted *Centerlines 1-5*. All centerlines were rotated such that maximum curvature occurred in the vertical plane, concave downwards. Note that all barrels, including the baseline, are subject to gravity droop.

The bore curvature, which is predominately in the vertical plane, leads to vertical spread in the overall jump. Although somewhat difficult to distinguish from the static pointing angle for some centerlines, the warp pointing angle is one of the largest individual jump components for most centerlines and features the most variation between barrels. Variation is also visible in other components, notably the aerodynamic jump. This is a finding of interest, as it indicates that centerline warp influences barrel dynamics in such a way as to affect other jump components. The exception is the static pointing angle (due to gravity loading) which is, of course, nearly identical for all barrels by

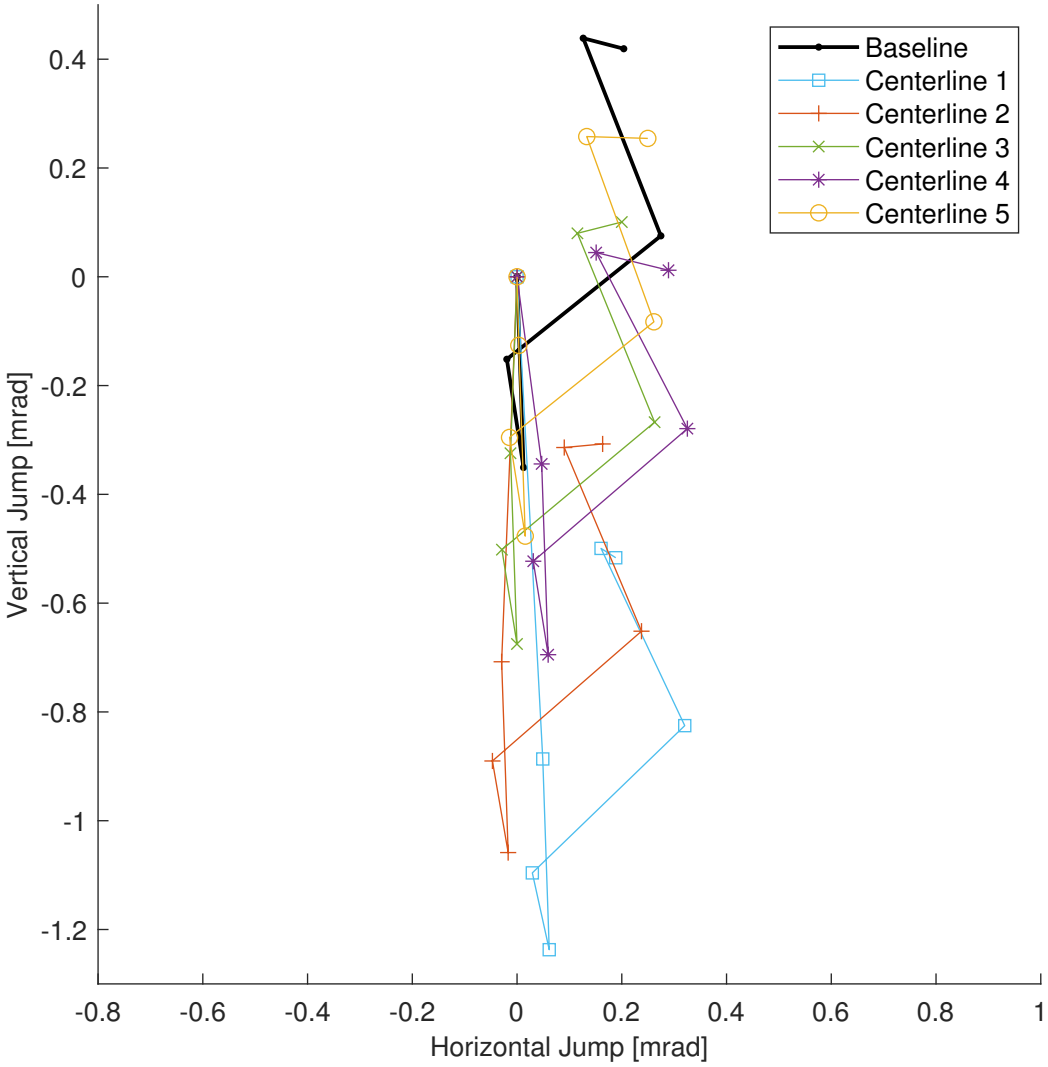

Figure 5.29: Jump comparison for the baseline barrel and five measured centerlines.

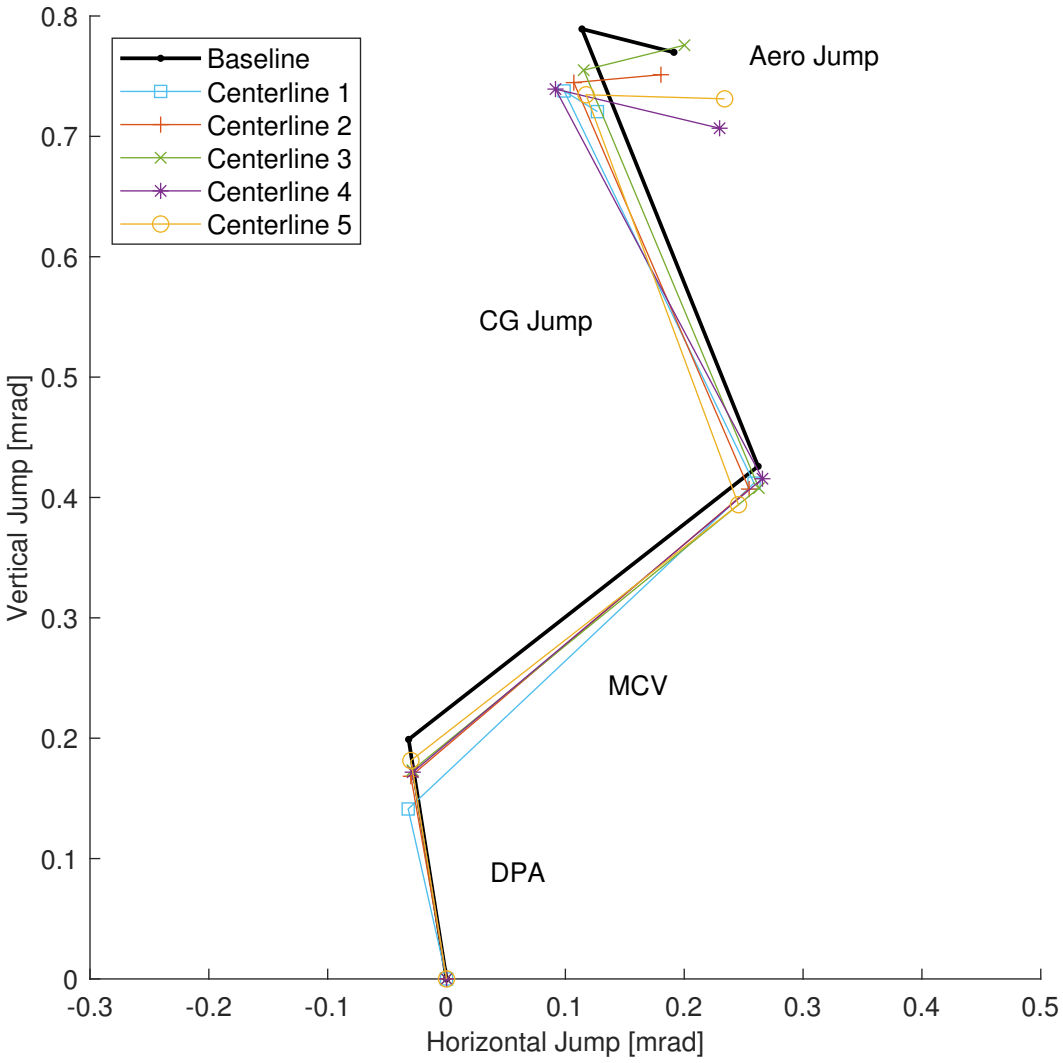

Figure 5.30: Jump comparison for the baseline barrel and five measured barrels with static jump components removed.

virtue of having the same mass and virtually identical geometric properties with respect to static beam deflection analysis. Removing the static jump components results in the jump diagram shown in Figure 5.30, exposing more clearly the differences in dynamic response of the barrel/projectile systems.

Table 5.1 shows both component values and total dynamic jump in each plane in milliradians. These results give a sense for the relative magnitude of each jump component as well as the associated variability. For context it is useful to note that 0.1 milliradians of jump equates to a lateral deviation of 1 centimeter at a distance of 100 meters. Furthermore, 0.1 milliradians is the unit of sight adjustment on many sighting devices in common use.

Considering total dynamic jump, the horizontal plane exhibits a standard deviation 1.6 times larger than the vertical despite the average horizontal jump value being roughly one quarter that of the vertical. Considering individual components, the aerodynamic jump stands out as exhibiting relatively high standard deviations in both planes, rivaled only by the vertical muzzle crossing velocity. Recall, the aerodynamic jump is related to projectile yaw and pitch behavior. It is important to note that these deviations are so small that they do not exceed the resolution of the adjustments on the sighting device. That is to say, all other sources of dispersion being eliminated, if each barrel was installed on a rifle in turn and the known/measured static jump accounted for, the resulting group could not be improved by adjusting the sighting device for the dynamic portion of the individual barrel characteristics.

Table 5.1: Dynamic jump components and associated standard deviations compared to baseline values for assorted centerlines. Values are given in milliradians.

	DPA		**MCV**		**CG Jump**		**Aero Jump**		**D. Jump**	
	Horz.	Vert.	Horz.	Vert.	Horz.	Vert.	Horz.	Vert.	Horz.	Vert.
Baseline	-0.032	0.199	0.294	0.227	-0.148	0.363	0.077	-0.019	0.191	0.770
Centerline 1	-0.032	0.141	0.291	0.271	-0.160	0.326	0.028	-0.017	0.127	0.721
Centerline 2	-0.030	0.168	0.285	0.239	-0.147	0.338	0.073	0.007	0.180	0.751
Centerline 3	-0.029	0.173	0.292	0.234	-0.147	0.347	0.085	0.021	0.200	0.776
Centerline 4	-0.028	0.172	0.294	0.244	-0.174	0.324	0.138	-0.033	0.230	0.707
Centerline 5	-0.030	0.181	0.276	0.213	-0.128	0.341	0.117	-0.003	0.234	0.731
Std. Dev.	0.002	0.015	0.007	0.021	0.017	0.010	0.042	0.021	0.044	0.027

5.4.3 Jump Associated with Rotated Centerline

Previously results from warped barrel simulations were presented where the dominant warp was in the vertical plane. In real firearms the same result can be achieved through indexing of the barrel, but this is unlikely to be the case

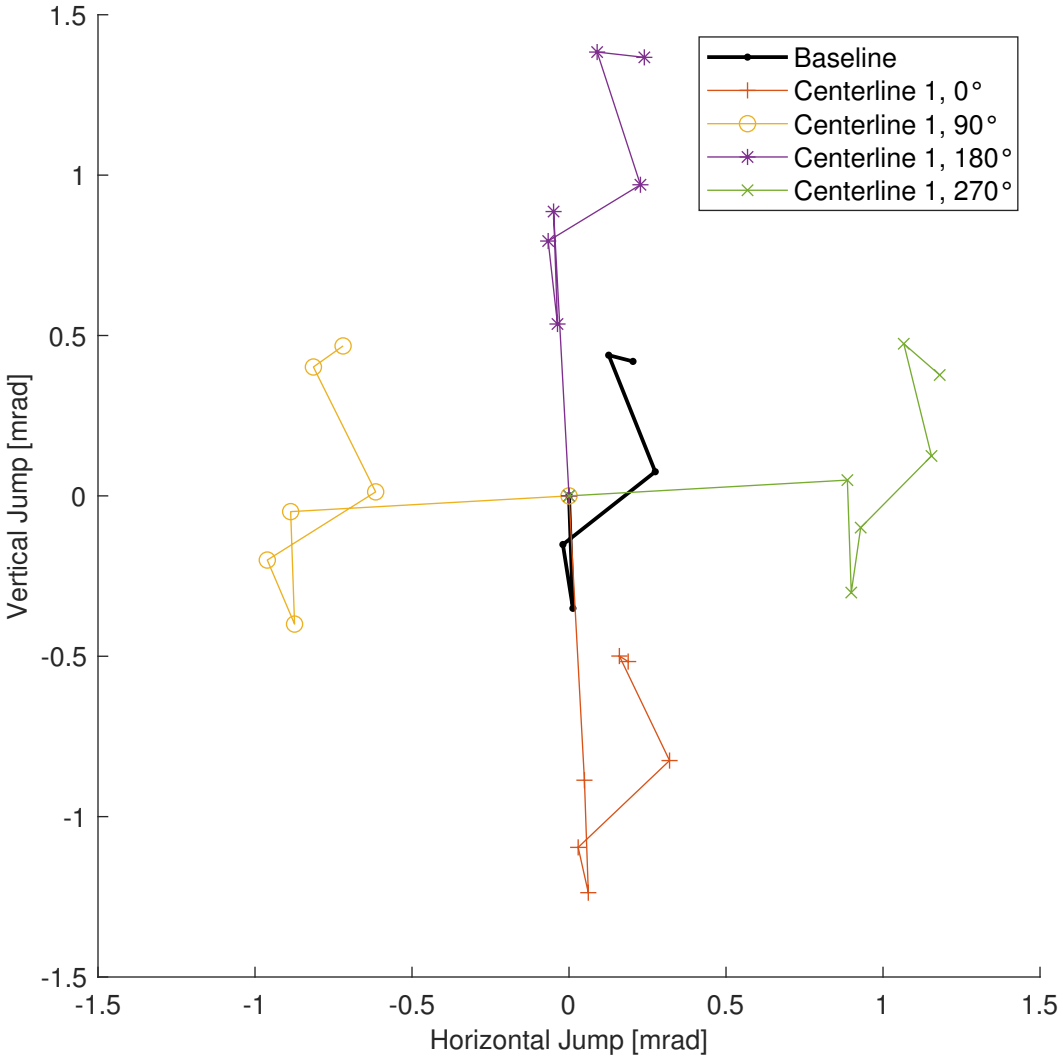

Figure 5.31: Jump comparison for the baseline barrel and Centerline 1 rotated to four positions.

for mass-produced factory rifles. Therefore, the dominant warp will be at some random orientation relative to the rest of the firearm. Here, in an attempt to isolate the effects of warp orientation, the results of a single centerline rotated to multiple positions is shown. Figure 5.31 shows calculated jump components for a comparison between the baseline model and a single measured centerline (Centerline 1) in four different orientations. The 0° orientation corresponds to the concave downward configuration considered previously. Centerline 1 was chosen as it exhibited the highest degree of warp among the measured centerlines, with the intention that orientation related effects would be more easily noted.

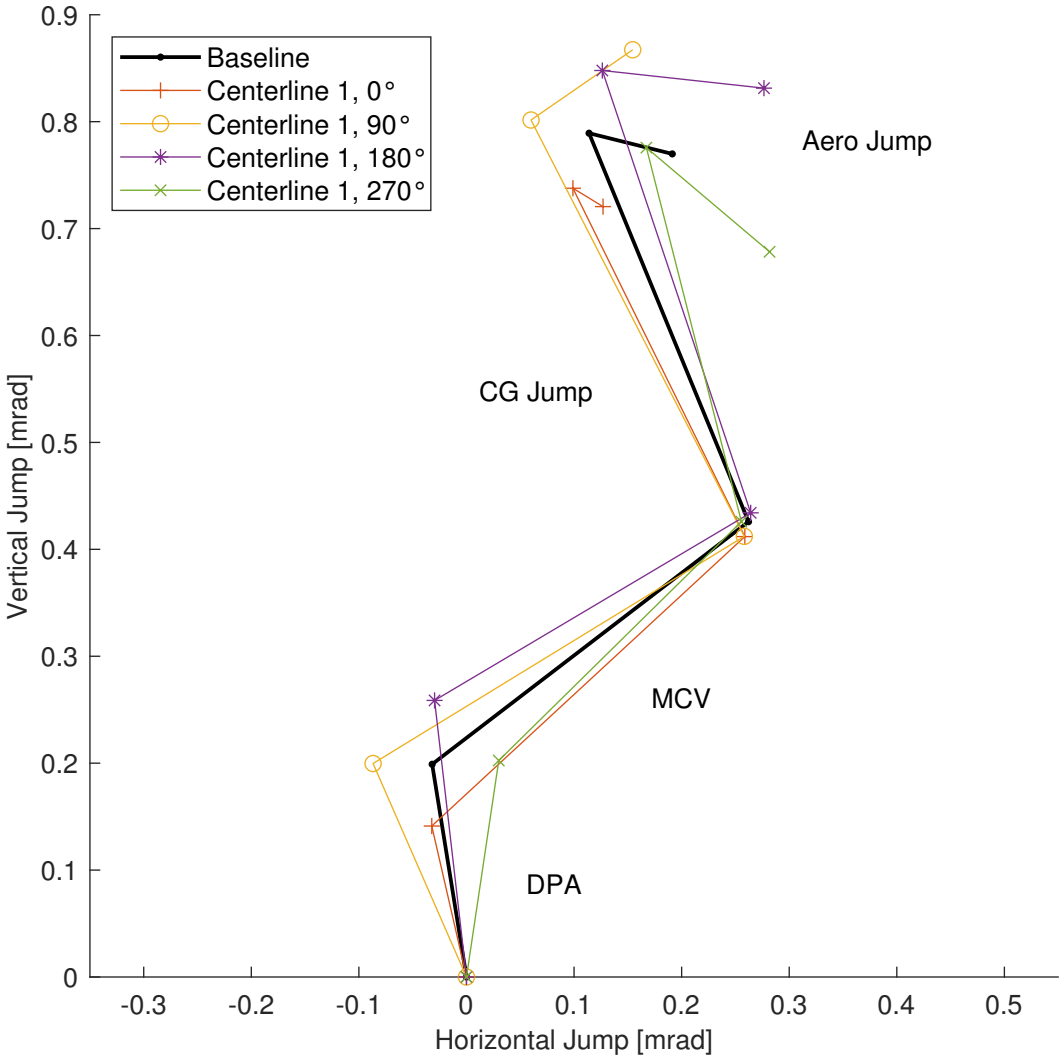

Figure 5.32: Jump comparison for the baseline barrel and Centerline 1 rotated to four positions with static jump components removed.

The centerline warp is rotated with the barrel. This results in the warp pointing angle, and its contribution to jump, to simply rotate with the barrel. The other five jump components retain behavior similar to the baseline, with some visible variability. As before, the static jump components may be removed to clarify the variability (Figure 5.32). It is interesting to note a strong correlation between the variation in dynamic pointing angle and the barrel orientation. Furthermore, the muzzle crossing velocity component appears to compensate for the variation seen in the dynamic pointing angle component. This is likely due to a kinematic relationship between the muzzle angle and velocity, associated with transverse vibrations of the barrel.

Dynamic jump totals and components for the rotated centerlines are given, alongside baseline comparison values, in Table 5.2. Here the overall dynamic jump standard deviation is nearly equal in the vertical and horizontal planes, and is roughly double the largest deviation calculated for the assorted centerlines (which were aligned). The aerodynamic jump again exhibits the largest standard deviation of the individual components, although by a smaller margin. These deviations are of a scale that approaches the resolution of sighting device adjustment.

Table 5.2: Dynamic jump components and associated standard deviations compared to baseline values for rotated centerline. Values are given in mrad.

	DPA		**MCV**		**CG Jump**		**Aero Jump**		**D. Jump**	
	Horz.	Vert.	Horz.	Vert.	Horz.	Vert.	Horz.	Vert.	Horz.	Vert.
Baseline	-0.032	0.199	0.294	0.227	-0.148	0.363	0.077	-0.019	0.191	0.770
0°	-0.032	0.141	0.291	0.271	-0.160	0.326	0.028	-0.017	0.127	0.721
90°	-0.087	0.200	0.345	0.213	-0.198	0.389	0.095	0.066	0.155	0.867
180°	-0.030	0.259	0.294	0.175	-0.138	0.414	0.150	-0.017	0.277	0.831
270°	0.030	0.202	0.226	0.223	-0.088	0.350	0.114	-0.097	0.282	0.678
Std. Dev.	0.048	0.048	0.049	0.039	0.046	0.039	0.051	0.067	0.081	0.089

5.5 Dispersion Simulation Validation

Chapter 4 included a description of a method designed to allow prediction of group dispersion from a single finite element simulation. This section contains model results and a discussion of this validation attempt. Figure 5.33 shows comparisons of projectile parameters for a baseline model and a second model with the pressure curve slightly perturbed such that it exhibits a slightly earlier bullet exit time.

Recall that a central contention of the theory being tested was that small perturbations in loading would affect exit time without a significant impact on

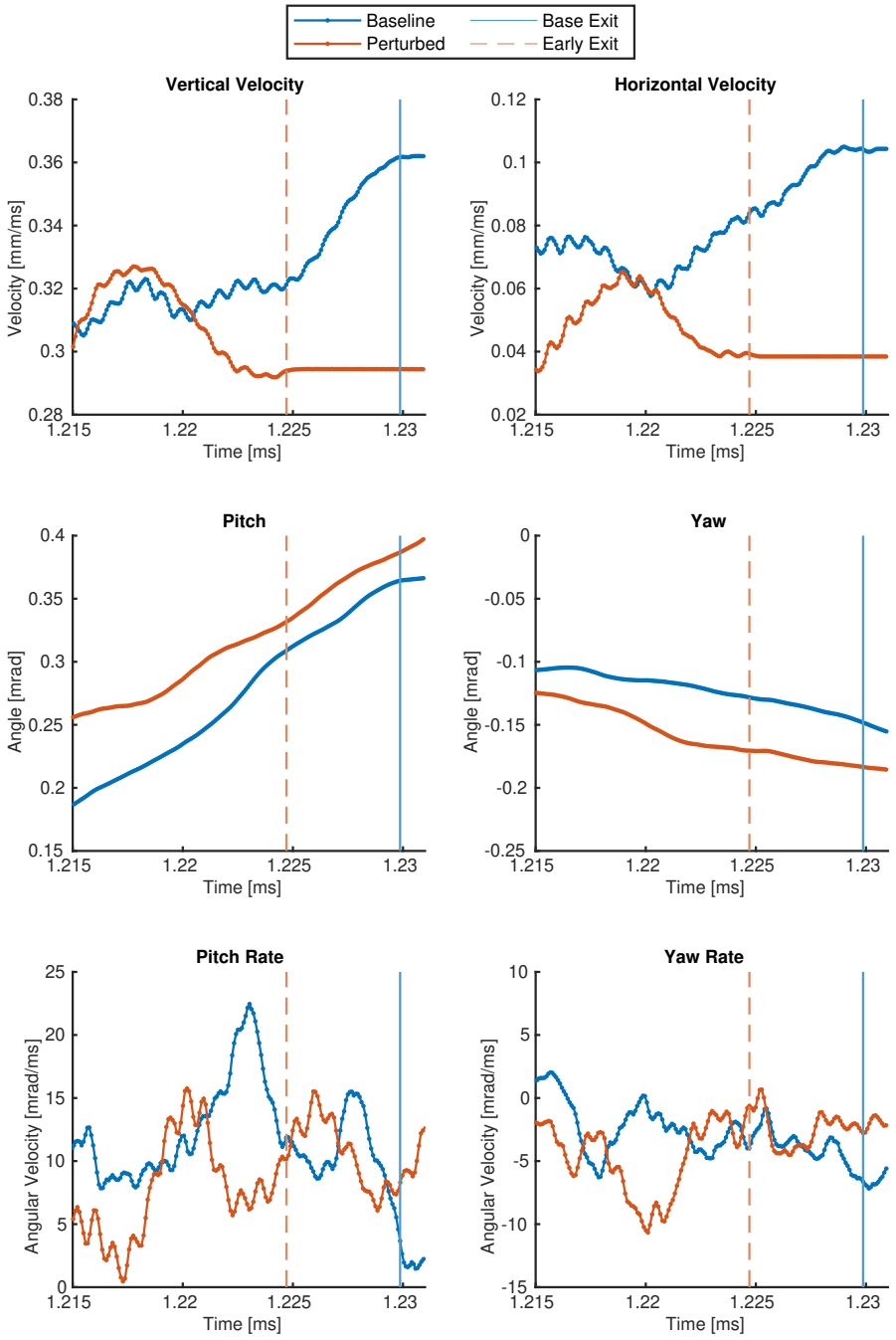

Figure 5.33: Comparisons for six projectile outputs of interest. Exit times are denoted by vertical lines.

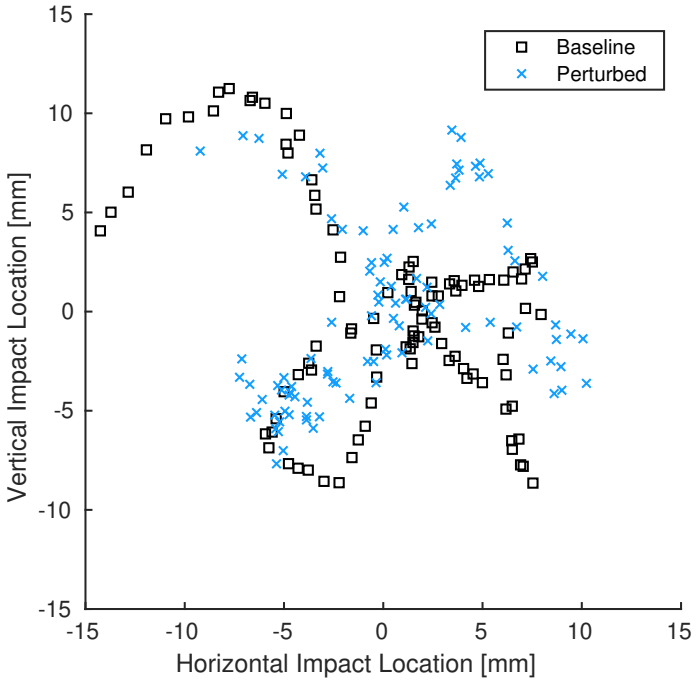

Figure 5.34: Dispersion plot comparing 100 simulated impacts for each model. Data had been shifted to center the baseline group on the origin.

projectile or barrel dynamics. While "significant" is somewhat subjective in this context, only two of the six variables (pitch and yaw) appear to follow similar trends between models. Indeed, in the case of the other four variables, the two models often exhibit slopes of opposite sign. This indicates that simulated groups are unlikely to be similar between the two models.

A dispersion plot with 100 simulated shots for each model is shown in Figure 5.34. It is immediately clear that, despite identical arrays of synthetic exit times being used for the two models, the simulated impact locations do not align. Similarities exist, such as the "tail" of impacts curving to the upper left from the center of the group, but the groups are different enough that this method fails to meet the strictest level of validation outlined previously.

A second, lower, level of validation was also proposed, in which group dispersion statistics, not exact locations, would be compared. Table 5.3 contains the relative group center locations along with extreme spread and average-to-center measurements for both models. Examination of the values leads to

two immediate conclusions. The first is that the group center did not shift appreciably between models. Second is that there is an approximately 13% difference in ES and approximately 8% difference in ATC for the simulated impacts. In this case it is more difficult to make a clear decision on whether the standard of validation is met. In all likelihood it is dependent on the exact situation. That is, if this method was to be used to establish whether or not a given change in geometry or input condition caused a significant change in expected precision, the change in dispersion would have to be greater than the changes shown here to be considered a results. Put another way, this method is not suited to quantify sub-10% changes in precision.

Table 5.3: Group center locations and measures of dispersion for both models.

	Horizontal [mm]	**Vertical[mm]**	**ES [mm]**	**ATC [mm]**
Baseline	0.0	0.0	26.1	6.42
Perturbed	-0.1	0.0	22.7	5.91

Chapter 6

Conclusions

This chapter summarizes the most important findings of the research and suggests possible avenues for future work.

6.1 Summary

Results of a combined experimental and FE modeling study of gun barrel vibration have been presented. To the knowledge of the authors, the quality of agreement between measured transverse barrel displacements and model predictions is unprecedented. This is true even when considering the identified weaknesses of the current approach. Comparisons are limited to the period of projectile in-bore travel. This time period is of primary interest due to the relation to accuracy and precision. The various observations in comparing the modeling and experimental data have resulted in the following conclusions.

- Vibrations of the barrel are sensitive to structural details of the complete gun structure. Of particular importance are the structural stiffness of the receiver and the firearm center-of-mass. Consequently, the present model would be improved by including representations of the main components of the complete chassis assembly.

- More rapid rates of pressure change will excite higher frequency modes of barrel vibration. It is important to accurately represent the initial

pressure transient, including the presence of a pressure contribution from the primer that precedes pressure due to the main charge of propellant.

- Movement of the firing pin contributes significantly to the total vibration response of the barrel during the in-bore transient. The present model would be significantly improved by including a representation of firing pin dynamics.

- Impact of the firing pin on the primer appears to have a negligible effect on barrel dynamics compared to a dry-fire impact with no primer.

- The order of the warp pointing angle contribution to total jump is equal to or greater than the order of magnitude of any other jump component. The effect of this centerline deviation acts mainly to shift projectile impact location in a manner exactly correlated to the angle of the centerline relative to the muzzle face, acting as a static shift.

- Beyond its influence as a static contributor to overall jump, warp affects barrel dynamics in such a way as to influence other jump components. This holds true for the rotation of a single centerline as well.

- While warp does affect barrel dynamics and the associated jump, the standard deviation in the dynamic jump is small enough that it exists within common sighting device adjustment resolution.

- A proposed method for calculation of shot dispersion from a single simulation was not strongly validated.

6.2 Future Work

Given the complexity of the ballistic process, numerous possibilities for future work exist. Building upon the existing code would be possible, as would taking the lessons learned in order to create a more specialized model from the ground up. Some especially promising research possibilities are detailed here.

Increased Model Fidelity The importance of sufficient model fidelity has been previously discussed, along with the associated computational limits. As computational capabilities increase, investigation using more detailed geometries coupled with the explicit modeling of additional components could be explored.

Parametric investigation could also be made into the effect of a simulated primer pulse, with variation in pulse amplitude and wavelength being considered. Development of a primer model and integration with a more sophisticated IB solver would be another improvement to the existing model.

Additionally, results suggest that accurate representations of more components attached to the receiver would likely improve barrel displacement predictions. This could take the form of adding lower receiver and scope rail geometry. The RPR is an assembly of >50 individual parts. It is not practical to include all possible geometric details, but the level of detail required is dependent upon desired model outputs.

Firing Pin Modeling Detailed modeling of the bolt/firing pin assembly would give valuable insight into the earliest detectable barrel movement and is required to better match experimentally measured barrel movement. There are several ways in which this problem could be approached. For example, the firing pin assembly could be integrated directly into the model described in this thesis, or it could be developed as a stand-alone model with the results being used to apply equivalent loading to the current model.

Depending on the degree of detail included, the first suggested approach would be computationally expensive. This is especially true for the case in which the firing pin and its travel is modeled explicitly. Given the lock time calculated in Chapter 3, including the full travel of the firing pin would roughly double the duration of time modeled. However, this approach has the benefit of most directly capturing the physics of the interaction. Acceleration of the firing pin during travel and impact on the primer would both be accounted

for.

A stand-alone firing pin simulation offers computational benefits, as the model could be run once for a given geometry and the results applied to the barrel dynamics model. Implemented correctly, this should offer the same level of accuracy as the first approach. This method may not be viable however, as gravity loading is already imported as the model initial state.

Finally, a loading replicating the final state of a stand-alone firing pin model could be applied to the barrel dynamics model. This would come at some cost in accuracy, but would not interfere with importation of the gravity initial state.

Parametric Variation of Loading Parameters In the context of firearms, one of the most attractive reasons to employ modeling over experimentation is the ability to isolate individual variables in a way that is difficult or impossible to accomplish in live-fire testing. This is especially true for attempts to elucidate which input factors have the most influence on precision. Unfortunately, the inability to validate a method for calculating shot dispersions from a single model run means that parametric variation of a single input parameter could require hundreds of hours of computation.

With that caveat, an in-depth investigation into various loading parameters (charge weight, seating depth, etc) could yield valuable insight into which variables are most critical to changes in barrel vibration behavior. If data was somehow acquired regarding the underlying distributions for the variability in each input, dispersion calculations could be performed (at substantial computational cost).

Alternative Barrel Construction An original motivator for this project, baseline capabilities for non-homogeneous barrel structures are already in place. Prototyping of composite barrels is costly, and the ability to model these structures represents a valuable capability. Future work in this area could include implementing support for anisotropic material properties as well

as accounting for changes in wrap angle for fiber-wrapped barrels.

Thermal Effects Originally envisioned as within the scope of this project, thermal effects where excluded from consideration as the complexity of the underlying vibration problem became more apparent. Future efforts in this area would expand the basic thermal capabilities present in the code. This could involve a tightly-coupled thermo-mechanical formulation but the benefits would be minimal and the computational cost high. Such an approach would only be useful if the model was to be used to explore bullet frictional heating or a similar highly transient situation.

It is more likely that the object of interest would be possible differences in dynamic barrel response at elevated temperatures. In this situation it would be most feasible to couple separate thermal and mechanical models. This is due to the large differences in time scale (roughly five orders of magnitude) between the firing event and the subsequent thermal effects. Under this methodology the thermal model would be run for the desired number of firing cycles and the final predicted temperature distribution could be imported into the mechanical model as an initial condition. These enhancements to the model would need to be coupled with experimental validation using a combination of vibrometers and thermal measurement.

References

[1] Corner, J., 1950. *Theory of the Interior Ballistics of Guns.* John Wiley & Sons, Inc., New York.

[2] Miner, R., 2013. "Computational interior ballistics modeling". Master's Thesis, University of New Mexico.

[3] Anderson, R. D., and Fickie, K., 1987. IBHVG2 (Interior Ballistics of High Velocity Guns, Version 2)–A User's Guide. Tech. rep., Ballistic Research Laboratories.

[4] Micković, D. D., Jaramaz, S., Elek, P., Jaramaz, D., and Micković, D. D., 2013. "Determination of pressure profiles behind projectiles during interior ballistic cycle". *Journal of Applied Mechanics,* **80**(3), Apr., p. 31402.

[5] Bougamra, A., and Lu, H., 2015. "Interior ballistics two-phase reactive flow model applied to small caliber projectile-gun system". *Propellants, Explosives, Pyrotechnics,* **40**(5), Oct., pp. 720–728.

[6] Newill, J. F., Nusca, M. J., and Horst, A. W., 2004. "Advances in Coupled Projectile-Dynamics/Interior-Ballistics Simulations: Coupling the DYNA3D Code and the ARL-NGEN3 Code". In 21st International Symposium on Ballistics.

[7] Broemel, H. G., 1995. QuickLOAD Interior Ballistics Program.

[8] Langlotz, W., Leroch, H., and Stein, W., 1989. "Initial Stages of Projectile Motion of Automatic Gun Ammunition". In 11th International Symposium on Ballistics, pp. 141–150.

[9] Williams, A. W., Brant, A. L., Kaste, P. J., and Colburn, J. W., 2006. Experimental Studies of the No. 41 Primer and Ignition of 5.56-mm Ammunition. Tech. Rep. ARL-TR-3922, Army Research Laboratory.

[10] Minnicino, M. A., and Ritter, J. J., 2016. "Simulation of Asymmetric Shot Start in Small Caliber Ammunition". In 29th International Symposium on Ballistics, pp. 811–818.

[11] Ritter, J. J., 2014. "Barrel Leade Effects on 5.56-mm Interior Ballistics". In 28th International Symposium on Ballistics, pp. 428–433.

[12] Ritter, J. J., and Beyer, R. A., 2015. Primer Output and Initial Projectile Motion for 5.56- and 7.62-mm Ammunition. Tech. rep., US Army Research Laboratory.

[13] Schmidt, J. R., and Nusca, M. J., 2008. Investigation of Small-Caliber Primer Function Using a Multiphase Computational Model. Tech. Rep. ARL-TR-4514, Army Research Laboratory, Aberdeen Proving Ground, MA.

[14] Tawfik, M., 2008. "Dynamics and Stability of Stepped Gun-Barrels with Moving Bullets". *Advances in Acoustics and Vibration,* **2008**, Mar., pp. 1–6.

[15] Esen, İ., and Koç, M. A., 2013. "Dynamics of 35mm Anti-Aircraft Cannon Barrel During Firing". In 3rd International Symposium on Computing in Science & Engineering, pp. 252–257.

[16] Hua, H., Qiu, M., and Liao, Z., 2017. "Dynamic analysis of an axially moving beam subject to inner pressure using finite element method". *Journal of Mechanical Science and Technology,* **31**(6), pp. 2663–2670.

[17] Esen, I., and Koç, M. A., 2015. "Dynamic response of a 120 mm smoothbore tank barrel during horizontal and inclined firing positions". *Latin American Journal of Solids and Structures,* **12**(8), June, pp. 1462–1486.

[18] Zhao, Y., Zhou, Q., and Yue, P., 2017. "Research on vibration characteristics of gun barrel based on contact model". *AIP Conference Proceedings,* **101**(10), pp. 20017–20031.

[19] Ruzzene, M., and Baz, A., 2006. "Response of periodically stiffened shells to a moving projectile propelled by an internal pressure wave". *Mechanics of Advanced Materials and Structures,* **13**(3), May, pp. 267–284.

[20] Bulman, D. N., 1995. "Simulation of Gun Dynamics to Improve Accuracy and Consistency". In 15th International Symposium on Ballistics, pp. 249–256.

[21] Koç, M. A., Esen, I., and Çay, Y., 2016. "Tip Deflection Determination of a Barrel for the Effect of an Accelerating Projectile Before Firing Using Finite Element and Artificial Neural Network Combined Algorithm". *Latin American Journal of Solids and Structures,* **13**(10), pp. 1968–1995.

[22] Koç, M. A., Esen, I., and Çay, Y., 2018. "Dynamic Analysis of Gun Barrel Vibrations Due to Effect of an Unbalanced Projectile Considering 2-D Transverse Displacements of Barrel Tip Using a 3-D Element Technique". *Latin American Journal of Solids and Structures,* **15**(9), Apr.

[23] Hopkins, A., 1991. Predicting dynamic strain amplification by coupling a finite element structural analysis code with a gun interior ballistic code. Tech. rep., U.S. Army Ballistic Research Laboratory, Aberdeen Proving Ground, MA.

[24] Wilkerson, S. A., and Hopkins, D. A., 1994. Analysis of a Balanced Breech System for the M1A1 Main Gun System Using Finite Element Techniques. Tech. rep., U.S. Army Research Laboratory, Aberdeen Proving Ground, MA.

[25] Wilkerson, S., 1995. The Effect of Initial and Gun Mount Conditions on the Accuracy of Kinetic Energy (KE) Projectiles. Tech. rep., U.S. Army Research Laboratory, Aberdeen Proving Ground, MA.

[26] Tzeng, J., and Hopkins, D., 1996. "Dynamic Response of Composite Cylinders Subjected to a Moving Internal Pressure". *Journal of Reinforced Plastics and Composites,* **15**, pp. 1088–1105.

[27] Laughlin, K. D., 2008. "Characterization of the Parameters that Affect Projectile Balloting Using Finite Element Analysis". Doctoral Dissertation, University of Oklahoma.

[28] Randrianangaly, I., Renard, J., Campion, B., and Petitpas, E., 2001. "Propagation of longitudinal waves in a gun barrel". In 10th U.S. Army Gun Dynamics Symposium Proceedings, GIAT Industries, pp. 80–91.

[29] Ahmed, N., Brown, R. D., and Hameed, A., 2008. "Finite Element Modelling and Simulation of Gun Dynamics Using 'ANSYS"'. In Proceedings - UKSim 10th International Conference on Computer Modelling and Simulation, EUROSIM/UKSim2008, pp. 18–22.

[30] Ahmed, N., Brown, R. D., and Hetherington, J. G., 2009. "Modeling of Dynamic Interaction Between Gun System Components During the Recoil Motion of the Gun". In International Design Engineering Technical Conferences & Computers and Information in Engineering Conference, ASME International, pp. 733–738.

[31] Alexander, J. E., 2012. "Advanced Gun System Gun and Projectile Dynamic Model Results and Correlation to Test Data". *Journal of Pressure Vessel Technology,* **134**(4), July.

[32] Kumar, P., Nayak, S., Dater, A. M., and Bhushan, G., 2014. "Analysis of transverse vibration modes of a gun barrel subjected to recoil". *Applied Mechanics and Materials,* **592-594**, pp. 2011–2015.

[33] Ding, C., Liu, N., and Zhang, X., 2017. "A mesh generation method for worn gun barrel and its application in projectile-barrel interaction analysis". *Finite Elements in Analysis and Design,* **124**, Feb., pp. 22–32.

[34] Yu, Q., Yang, G., and Sun, Q., 2018. "Dynamics analysis on barrel considering the temporal and spatial distribution of propellant gas by numerical simulation". *Journal of Vibroengineering,* **20**(4), pp. 1588–1602.

[35] Yu, Q., and Yang, G., 2019. "Dynamic Stress Analysis on Barrel Considering the Radial Effect of Propellant Gas Flow". *Journal of Pressure Vessel Technology.*

[36] Chevalier, O., Liennard, M., Langlet, A., Guilmard, Y., Mansion, M., and Bailly, P., 2017. "Dynamic of Tubes Crossed by High Speed Projectiles, Influence of Tube and Weapon Geometry on Accuracy and Dispersion". In 30th International Symposium On Ballistics, pp. 950–960.

[37] Burns, B. P., Newill, J. F., and Wilkerson, S. A., 1998. "In-Bore Projectile-Gun Dynamics". In 17th International Symposium on Ballistics, pp. 63–70.

[38] Eches, N., Cosson, D., Lambert, Q., and Langlet, A., 2011. "Modelling of the Dynamics of a 40 Mm Gun and Ammunition System During Firing". In 26th International Symposium on Ballistics, pp. 1026–1037.

[39] Vitek, R., 2008. "Influence of the Small Arm Barrel Bore Length on the Angle of Jump Dispersion". In Proceedings of the 7th WSEAS International Conference on System Science and Simulation in Engineering, pp. 114–118.

[40] Vitek, R., 2009. "The generally unbalanced projectile load on the sporting rifle barrel". In Proceedings of the 8th WSEAS Internation Conference on System Science and Simulation in Engineering, pp. 164–169.

[41] Deng, S., Sun, H., and Chiu, C.-J., 2012. "Rifles In-Bore Finite Element Transient Analysis". In International Conference on Mechanical, Production and Materials Engineering, pp. 58–62.

[42] Deng, S., Sun, H. K., Chiu, C.-J., and Chen, K.-C., 2014. "Transient Finite Element for In-Bore Analysis of 9 mm Pistols". *Applied Mathematical Modelling,* **38**, pp. 2673–2688.

[43] Štiavnický, M., and Lisý, P., 2013. "Influence of Barrel Vibration on the Barrel Muzzle Position at the Moment when Bullet Exits Barrel". *AiMT Advances in Military Technology,* **8**(1), pp. 89–102.

[44] Chen, M. M., 2010. "High Fidelity In-Bore Pressure Modeling". In 11th International LS-DYNA Users Conference.

[45] Eichhorst, C., Hopkins, D. A., Drysdale, W. H., and Minnicino, M., 2011. "Inclusion of Rifling and Variable Centerline for Enhanced Modeling of Launch Dynamics". In 26th International Symposium on Ballistics, pp. 966–975.

[46] Dutschke, B., Hunzinger, M., and Sattler, A., 2019. "A Numerical Analysis of the In-Bore Motion of Small Caliber Projectiles". In 31st International Symposium on Ballistics, V. Saraswat, G. S. Reddy, and C. Woodley, eds., pp. 1027–1039.

[47] Sava, A.-C., Piticari, I.-L., Nistoran, D.-G., and Moldoveanu, C.-E., 2015. "The Analysis of the Vibratory Movement of the Gun Barrel and Its Influence on the Firing Accuracy". In Knowledge-Based Organization, pp. 883–887.

[48] Celmins, I., 2011. "5.56mm M855 Accuracy and Jump Measurements". In 26th International Symposium on Ballistics, pp. 987–998.

[49] Paxton, K., Oberlin, G., Puckett, T., and Cashen, D., 2017. "AR-15 Barrel Motion as a Function of Weapon Mount Configuration". In 30th International Symposium On Ballistics, pp. 342–354.

[50] Bulman, D. N., 1986. "The Effects of Barrel Droop on Gun Barrel Response". In 9th International Symposium on Ballistics, pp. 325–329.

[51] Critchley, R., and MacMahon, J., 1996. "Computer Modelling of the 155mm 52 Calibre Extended Range Ordnance Using the DYNA Suite of Finite Element Codes". In 16th International Symposium on Ballistics, pp. 517–526.

[52] Chen, M. M., 2007. "Sensitivity of Projectile Muzzle Responses to Gun Barrel Centerline Variations". In 23rd International Symposium on Ballistics, pp. 465–474.

[53] Chen, M. M., 2010. "Projectile Balloting Attributable to Gun Tube Curvature". *Shock and Vibration,* **17**(1), pp. 39–53.

[54] Gur, Y., Gringaus, M., and Siegman, S., 2004. "The Effect of Tube Curvature on Jump Error in Tank Firing, an Empirical and Numerical Approach". In 21st International Symposium on Ballistics.

[55] Gur, Y., Azulay, I., Touati, D., and Arad, M., 2007. "Jump Error & Gun Dynamics: A Comparison Between Two Types of 120mm Smooth-Bore Tank Guns". In 23rd International Symposium on Ballistics, pp. 565–572.

[56] Wilkerson, S., 1993. "Modeling of Gun Dynamics Using Three-Dimensional Finite Element (FE) Techniques". In 14th International Symposium on Ballistics, pp. 547–559.

[57] Lee, H.-L., Yang, Y.-C., Chang, W.-J., and Wu, T.-S., 2009. "Estimation of heat flux and thermal stresses in multilayer gun barrel with thermal contact resistance". *Applied Mathematics and Computation,* **209**, pp. 211–221.

[58] Hill, R. D., and Conner, J. M., 2012. "Transient heat transfer model of machine gun barrels". *Materials and Manufacturing Processes,* **27**(8), pp. 840–845.

[59] Akcay, M., and Yukselen, M. A., 2013. "Unsteady thermal studies of gun barrels during the interior ballistic cycle with non-homogenous gun barrel material". *Journal of Thermal Science and Technology,* **34**(2), pp. 75–81.

[60] Qu, P., Li, Q., and Yang, S. F., 2014. "Temperature field and thermal stress analysis of large caliber gun barrel". *Applied Mechanics and Materials,* **518**, pp. 150–154.

[61] Sun, Y., and Zhang, X., 2016. "Parameter Analysis of Two Dimensional Heat Transfer of Gun Barrel". In 29th International Symposium on Ballistics, pp. 858–867.

[62] Isik, H., and Göktas, F., 2017. "Cook-off analysis of a propellant in a 7.62 mm barrel by experimental and numerical methods". *Applied Thermal Engineering,* **112**, pp. 484–496.

[63] Chang-Wei, W., Yong-Hai, W., and Qin-Man, F., 2013. "Analysis of temperature and stress of a thin-walled cylinder based on FEM". *Applied Mechanics and Materials,* **373-375**, pp. 12–15.

[64] Şentürk, A., Işýk, H., and Evci, C., 2016. "Thermo-mechanically coupled thermal and stress analysis of interior ballistics problem". *International Journal of Thermal Sciences,* **104**, pp. 39–53.

[65] Vaughn, H. R., 1998. *Rifle Accuracy Facts*, 3rd ed. Precision Shooting, Inc., Manchester, CT.

[66] Chaplin, R., and Gubernat, D., 2016. "Factors Affecting Bore Resistance in the Structural Analysis of Interior Ballistics". In 29th International Symposium On Ballistics, pp. 906–916.

[67] Blot, A., and Chaplin, R., 2014. "Coupling of a Lumped Mass Interior Ballistic Code with the Structural Finite Element Code Abaqus". In 28th International Symposium on Ballistics, pp. 521–531.

[68] Hu, C., and Zhang, X., 2016. "Influence of Gun Bore Structure on the Performance of Interior Ballistic Process". In 29th International Symposium on Ballistics, pp. 868–879.

[69] Carlucci, D. E., and Jacobson, S. S., 2014. *Ballistics: Theory and Design of Guns and Ammunition*, second ed. CRC Press, Boca Raton.

[70] Smith, S. W., 1997. *The Scientist and Engineer's Guide to Digital Signal Processing*, 1st ed. California Technical Publishing, San Diego.

[71] McCoy, R. L., 2012. *Modern Exterior Ballistics: The Launch and Flight Dynamics of Symmetric Projectiles*, second ed. Schiffer Publishing Ltd., Atglen, PA.

[72] Leonhardt, D., and Garnich, M., 2019. "A Finite Element Model to Predict the Influence of Asymmetries on Barrel Dynamics in Small Arms". In 31st International Symposium on Ballistics, V. Saraswat, G. S. Reddy, and C. Woodley, eds., pp. 1015–1026.

[73] Kinsler, L. E., Frey, A. R., Coppens, A. B., and Sanders, J. V., 1999. *Fundamentals of Acoustics*, fourth ed. John Wiley & Sons, Inc., New York.